

UCSF

UC San Francisco Electronic Theses and Dissertations

Title

Understanding the Mechanisms of Epimorphic Regeneration in the Mammalian Tympanic Membrane

Permalink

<https://escholarship.org/uc/item/62j4w99n>

Author

Scaria, Sonia

Publication Date

2022

Peer reviewed|Thesis/dissertation

Understanding the Mechanisms of Epimorphic Regeneration in the Mammalian
Tympanic Membrane

by
Sonia Scaria

DISSERTATION
Submitted in partial satisfaction of the requirements for degree of
DOCTOR OF PHILOSOPHY

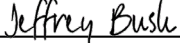
in

Biomedical Sciences

in the


GRADUATE DIVISION
of the
UNIVERSITY OF CALIFORNIA, SAN FRANCISCO

Approved:

DocuSigned by:

367536768C42487... Jeffrey Bush
Chair

DocuSigned by:

Licia Selleri

DocuSigned by:

7D7A13DE0D5746E... Aaron Tward

Committee Members

Copyright 2022
by
Sonia M. Scaria

Dedications and Acknowledgements

The work presented here truly took a village, and I have more people to acknowledge and thank than there is space for. First, I want to thank my PI, Aaron Tward. Without his support, his wild enthusiasm for all things ear, his curiosity, and his encouragement to take on big challenges, this work would not have come to fruition, particularly in light of a global pandemic. Thank you for teaching me that failure is inevitable and that failing early and often is actually the key to doing good science. Aaron opened my eyes to the realities of what it really means to be a basic science researcher and taught me how to captain my own ship, and for that, I am grateful.

I also want to thank my mentors within the Tward Lab, who truly were the glue that held me together throughout this process. In particular, Stacey Frumm was my guiding light through every step of this PhD and is likely the most influential mentor I have had in my career; she answered every email, made countless return trips to lab while being back in medical school to show me new protocols, and she took the time to ask me hard questions and push my scientific thinking. More importantly, she served as a best friend and personal mentor during this time, and there is truly no way I would have been able to accomplish this body of work without her by my side. I've miss her shoulder to cry on deeply this past year. I would also like to thank Vicente Planells-Palop and Celine Mahieu for being by my side these past years, fighting the fight, and for refusing to let my breakdowns persist. They may have been Team Cancer, but we were all Team Tward and in it together. Marta Losa-Llabata, though technically not part of the Tward Lab, deserves many thanks as well- she

made me a better scientist (and person) and sets an example for me to aspire to everyday; For reading my science, for comforting me when I cried- many thanks!

I would also like to thank the collaborators on the TM project – Stacey Frumm, for pioneering the cause of the ear to begin with. Kevin Yu did the initial analysis of the TM perforation scRNA-seq data using CellFindR. Eliah Shamir created our new and improved live-cell imaging protocols and gave countless advice on conducting experiments in the later stages of this project. Amar Sheth optimized scVelo for our data. Ellee Vikram helped with numerous quantifications of our proliferation studies. Jason Park served as a never-ending source of advice and calm throughout this project though only being in the lab for a short time as well. For the many conversations, answers to desperate texts, and coffee chats, thank you thank you! Additionally, I want to thank collaborators outside of the lab, knowing this list is likely not complete: Jordan Briscoe, Pauline Marangoni, Taha Jan, Dylan Chan, Ali May, and Stephanie Rouse.

I would be remiss not to profusely thank my thesis committee members here – Jeff Bush and Licia Selleri. They both were the perfect science parents I needed in this PhD, and I am so grateful they took the time to mentor me. Yes, they gave me numerous hours during thesis committee meetings, but they also allowed me to stop by their doors whenever needed and made me feel heard when I really needed it. Whether it was about science, career, or life, I knew I could always count on them to support and mentor me. They offered me guidance during some of the most difficult times of my graduate career, and I feel extremely lucky to have had them be a part of my scientific journey at UCSF. I'd also like to

thank previous mentors I had before joining the Tward Lab: Marco Jost, with whom I rotated with in the Weissman lab many years ago, Jose Orozco, both an unbelievable mentor and a lifelong friend for whom I worked in the Sabatini Lab, and Lynne Chantranupong, who to this day is still the most prolific, accomplished graduate student I've seen, and who I had the pleasure of working with for 3 years in the Sabatini Lab. The Sabatini Lab (and the amazing mentors I found there) supported me in pursuing this journey, and this PhD would not have happened without them. You all made me believe that science could be fun and gave me the faith in myself to pursue this wild career.

Lastly, I would be remiss to not acknowledge the friends and family that truly were the backbone of this work. I could dedicate pages in this section to my mother. This PhD exists because of her- her example she set years ago getting a PhD of her own, her choice to continue to pick up my phone calls no matter the time and place, her patience with listening to me cry for endless hours, have numerous breakdowns and the times I quite literally had fallen and was refusing to get up, and lastly, for her constant reminders that she loved me no matter how much of a failure my PhD might be. It was her love and faith in me that allowed me to persevere. Thanks to my dad for being the tough love I needed throughout this process and for being the constant reminder that I can do hard things and that the only limiting reagent was myself. I hope I've made you proud. Both of you constantly reminding me to "focus on the journey, not the destination" has been a guiding force over these past 3 years. Thanks to my sisters for going through this crazy mess with me. In particular, thanks to Natasha for being the rock I needed her to be, a distraction

when I didn't want to cry anymore, and my soul mate in life; how lucky am I to have a sister like you.

To my UCSF medical school friends – Zane Hellmann and Ryan Badiee- thank you for not letting my numerous breakdowns drive you away and for coming and sitting through all of those late nights and weekends at lab with me. The PhD can be very isolating, but thanks to you guys, I knew I was never alone. To my running friends – Zach Lipps and Ellen Tsay- thank you for giving me life and for doing hard things with me every week; thanks for making me faster, better, and happier.

Lastly, I dedicate this work to Max Feinstein. Though you didn't get to see the end of this PhD, you were there through some of the toughest moments in the beginning. You made sure I was never alone. Whether it was late nights in lab, trips to Souvla, or sprinting up really big hills, you brought me love and light, and I hope this work makes you proud. Thank you for believing in me and for fighting as hard as you did. I am here and fighting for this dream because of you.

Contributions

Chapter 2 of this dissertation contains reprints of material published in Frumm, S.M., et al., 2021, A Hierarchy of Proliferative and Migratory Keratinocytes Maintains the Tympanic Membrane, *Cell Stem Cell*, 28, 2: 315-330.

Abstract

Understanding the Molecular Mechanisms of Epimorphic Regeneration in the Mammalian Tympanic Membrane

Sonia M. Scaria

The tympanic membrane (TM) is the central component of the conductive apparatus of the ear and is the first major organ sound waves hit in the process of being transmitted to the brain. The TM receives sound from the external auditory ear canal (EAC) and appropriately vibrates to transmit this sound to the middle ear. Notably, the TM has the remarkable ability to rapidly repair itself, with perforations typically closing in days to weeks in all mammalian species studied. However, in a subset of cases, these perforations do not close, and patients present with conductive hearing loss. Though this function of the TM has been known for many decades, lack of understanding of the basic biology of the TM has hindered our ability to explain the pathophysiology of chronic perforations because the cellular and molecular mechanisms underlying this repair ability remain largely unknown. This study looked to thoroughly characterize the repair process of the injured TM as epimorphic regeneration and uncover mechanisms of epithelial regeneration that could serve as future targets for treatments for disorders of the tympanic membrane and be applied broadly to epithelial wound repair.

Table of Contents

| | |
|---|-----------|
| Chapter 1: Wound Healing vs Epimorphic Regeneration | 1 |
| 1.1 Wound Healing Principles | 2 |
| 1.2 Skin: a case study for epithelial wound healing..... | 4 |
| 1.3 Epimorphic Regeneration Principles | 5 |
| 1.4 Axolotls: a case study for epimorphic regeneration | 7 |
| 1.5 Mammalian Epimorphic Regeneration: examples and failures | 8 |
| 1.6 Figures..... | 10 |
| 1.7 References | 12 |
| Chapter 2: Structure, Functions, and Maintenance of the Homeostatic Tympanic | |
| Membrane | 16 |
| 2.1 Anatomy of the Ear | 17 |
| 2.2 Anatomy and Structure of the Tympanic Membrane..... | 18 |
| 2.3 Proliferation and Migration of Cells of the Tympanic Membrane | 20 |
| 2.4 Cellular Identities and Dynamics of the Tympanic Membrane at Homeostasis... | 21 |
| 2.5 Stem Cell and Progenitor Niches of the Tympanic Membrane..... | 23 |
| 2.6 Figures | 25 |
| 2.7 References | 30 |
| Chapter 3: Epimorphic Regeneration in the Mammalian Tympanic Membrane | 35 |
| 3.1 Abstract..... | 36 |
| 3.2 Introduction..... | 36 |
| 3.3 Results..... | 39 |

| | |
|---|------------|
| 3.4 Discussion | 52 |
| 3.5 Figures | 58 |
| 3.6 Methods | 81 |
| 3.7 References | 88 |
| Chapter 4: Effects of Topical Stimulation on the Tympanic Membrane | 101 |
| 4.1 Introduction and Project Goals | 102 |
| 4.2 Results..... | 104 |
| 4.3 Discussion and Future Directions..... | 106 |
| 4.4 Figures | 110 |
| 4.5 References | 113 |
| Chapter 5: Future Directions | 117 |
| 5.1 Overall conclusions of this thesis and next steps | 118 |
| 5.2 Manipulating Regenerative Mechanisms of the Tympanic Membrane for Therapeutic Development..... | 123 |
| 5.3 Single-Cell Resolution of Initiation Steps of Regeneration prior to 24 hours ... | 125 |
| 5.4 Single-Cell Resolution and Validation of Fully Regenerated Tympanic Membranes..... | 127 |
| 5.5 Live-Cell and Live-Animal Imaging of the healing murine Tympanic Membrane..... | 129 |
| 5.6 Figures | 132 |
| 5.7 References | 134 |

List of Figures

| | |
|---|-----------|
| Figure 1.1: The four stages of wound healing | 10 |
| Figure 1.2: Mammals lose the ability to regenerate after embryonic stage | 11 |
| Figure 2.1: Tympanic Membrane Anatomy | 25 |
| Figure 2.2: TM migratory patterns revealed by live-cell imaging..... | 26 |
| Figure 2.3: Single-cell RNA sequencing (scRNA-seq) identifies cell types in the murine TM | 27 |
| Figure 2.4: TM keratinocyte clones arise from distinct stem cell and committed progenitor populations | 28 |
| Figure 3.1: The TM displays a rapid and robust proliferative response to injury macroscopically | 58 |
| Figure 3.2: The TM regenerates without permanent scarring | 60 |
| Figure 3.3: Single-cell RNA sequencing (scRNA-seq) reveals the transcriptional shifts of the regenerating TM | 62 |
| Figure 3.4: A migratory wounded epithelium forms within one day post-injury..... | 64 |
| Figure 3.5: A blastema-like structure with activation of the Egfr pathway arises at the site of injury | 66 |
| Figure 3.6: Egfr is required for the early TM regenerative response..... | 67 |
| Supplementary Figure 3.1: The TM undergoes a rapid, patterned response to injury | 69 |

| | |
|--|------------|
| Supplementary Figure 3.2: Collagen changes in response to wounding dissipate by 2 weeks | 70 |
| Supplementary Figure 3.3: scRNA-seq identifies major populations of cells at each timepoint during the injury response | 71 |
| Supplementary Figure 3.4: Markers of proliferation reveal turnover of all layers of the TM | 72 |
| Supplementary Figure 3.5: Time-course mesenchymal-specific analysis reveals distinct post-injury transitions | 74 |
| Supplementary Figure 3.6: Time-course immune-specific analysis reveals distinct immune populations that arise in response to injury | 76 |
| Supplementary Figure 3.7: Computational analyses of the 1-day post-injury dataset reveal a transcriptional signature for a novel and transient wounded epithelium | 78 |
| Supplementary Figure 3.8: Areg RNA expression identifies activated keratinocytes in response to injury | 79 |
| Figure 4.1: Topical PBS induces proliferation on the tympanic membrane | 110 |
| Figure 4.2: Different forms of topical stimulation all induce proliferation | 111 |
| Figure 4.3: Topical stimulation of the TM induces wounded epithelium markers ... | 112 |
| Figure 5.1: Scanning Electron Microscopy struggles to elucidate the structure of the tympanic membrane | 132 |
| Figure 5.2: Live-cell imaging of the tympanic membrane at homeostasis | 133 |

Chapter 1:
Wound Healing vs. Epimorphic Regeneration

1.1 Wound Healing Principles

When a tissue is injured, a cascade of intermingled biological processes is initiated that ultimately should result in the healing of the injured tissue. However, in a subset of cases, wound healing can lead to a series of complications, resulting in numerous morbidities and mortalities. Moreover, in the case of chronic wounds- wounds that cannot heal- very serious infections and abnormalities can occur in the injured tissue, leaving a high burden for the patient and the provider. Therefore, there has been many in-depth studies into the processes that govern wound healing in an attempt to alleviate this burden on patients and the healthcare system.

The four main stages of wound healing are (1) coagulation and hemostasis, (2) inflammation, (3) proliferation, and (4) remodeling and maturation (**Figure 1.1**) (Velnar, Bailey, and Smrkolj 2009; Broughton, Janis, and Attinger 2006; Wang et al. 2018). These phases must happen sequentially yet with overlapping periods in order for proper wound healing to occur (Wang et al. 2018). Immediately after injury, coagulation and hemostasis have to occur in an instant in order to prevent exsanguination (Velnar, Bailey, and Smrkolj 2009). A combination of vasoconstriction and the clotting cascade brings active bleeding to a stop. The clotting cascade, in turn, initiates phase two of wound healing: the inflammatory phase. In order for proper wound healing to occur, there must be adequate activation and infiltration of inflammatory cells, neutrophils and macrophages into the wound site, which then produce pro-inflammatory cytokines. These cytokines then initiate the activation of

several growth factors and fibroblast-specific growth factors that allow fibroblasts to proliferate and also infiltrate the wound site (Portou et al. 2015). Macrophages are generally thought to be the key cell in orchestrating normal wound healing, and they take about 48 hours to infiltrate the wound site (Gantwerker and Hom 2011a).

Once the immune response has been successfully initiated, the proliferative phase can begin, generally beginning three days after injury and continuing for two more days. The proliferative phase can be broken down into a series of stages itself: (1) fibroblast migration, (2) collagen synthesis, (3) angiogenesis and granulation tissue formation, (4) protrusion, (5) adhesion, (6) traction, and (7) epithelization (Velnar, Bailey, and Smrkolj 2009). Of note, the epithelization phase is thought to begin just a few hours after wounding with cells from the wound edge eventually migrating over the wound site with an increase in proliferation directly over the site. The granulation tissue that forms contains fibroblasts, new blood vessels, and immature collagen (Gantwerker and Hom 2011a). The last phase of wound healing, remodeling, occurs when the new epithelium is fully developed, and final scar tissue is formed. This phase can last from one to two years and sometimes even longer. For this phase to result in a fully resolved wound, there has to be a coordinated balance between degradation and synthesis, particularly with the synthesis and breakdown of collagen (Velnar, Bailey, and Smrkolj 2009). The result is a tissue that grossly resembles that of the original tissue but usually is not identical in structure and function and always contains some remnant scarring.

1.2 Skin: a case study for epithelial wound healing

In studies of wound healing, skin is often used as the model organ due to its canonical stratified epithelial structure and the ease of ability to manipulate the tissue. The skin is separated into three sections: the epidermis, dermis and hypodermis. The epidermis has a stratified structure of 5 levels: (from superficial to deep) the stratum corneum, stratum lucidum, stratum granulosum, stratum spinosum and stratum basale, with further differentiation of cells as the layers move superficially (Gantwerker and Hom 2011a). The epidermis also contains specialized skin structures like hair follicles, sebaceous glands, and sweat glands.

When skin undergoes an injury, the first phase of healing, the hemostatic phase, occurs within seconds to minutes. During this critical window of time, the platelet response- the coagulation cascade- is crucial for the subsequent steps of the healing process. Platelets trigger the necessary cytokine release, which allows for immune cell infiltration. In the inflammatory response in the skin, neutrophils arrive first, and then macrophages and lymphocytes arrive at roughly 48 hours post-injury. Without these inflammatory cells present, the proliferative phase will not begin, and thus skin repair will not occur. The proliferative/epithelization phase involves proliferation and an influx of keratinocytes specifically at the leading edge of the wound with a new basement layer being laid down and subsequent stratification forming. During the fourth and final phase of repair, angiogenesis and collagen remodeling from Collagen III to Collagen I results in the final wound state and a tensile scar (Gantwerker and Hom 2011a).

The skin wound response follows the canonical four phases of wound healing with periods of overlap between the phases. Basal progenitor cells at the wound edge are the primary cells that respond to the injury and proliferate (Gonzales and Fuchs 2017). However, it is unclear how stem cell progenitors at other areas of the tissue not immediately adjacent to the wound respond and to what extent they are necessary for healing. Moreover, in most skin repair, the process will lead to a non-functioning fibrotic mass, a scar, which continues to remodel slowly for years (Gurtner et al. 2008). In particular, the deeper the wound, the poorer job mammals do of repairing it, especially if the wound crosses into the dermis. In this case, scarring is inevitable. Thus, though wound healing will provide a restoration of most function and structure, it does not truly replicate the organ.

1.3 Epimorphic Regeneration Principles

In certain species, injury to a tissue results in, not wound healing, but regeneration of the lost tissue, leading to a replacement organ that is identical in structure and function to the original structure. Generally, the term “regeneration” has been used to refer to the replacement of a lost body part, but it can also be used to refer to the replacement of cells or tissue in response to injury; thus, regeneration can occur at multiple levels of biological organization (Seifert and Muneoka 2018). The focus here in this work was particularly on mammalian epimorphic regeneration, which requires actual cell proliferation in the process of organ replacement, as opposed to the rearrangement of existing cells (Morgan 1901). What particularly separates the processes of epimorphic regeneration from the

processes of disorganized wound healing previously discussed is that regeneration acts through a multi-lineage transient proliferative mass called a blastema (Siefert and Muneoka 2018).

From the literature, seven key components of epimorphic regeneration have emerged. The first is that a specialized wound epidermis must form that serves to attract blastemal cells and maintain cell proliferation (Globus et al 1980). Second is the dependence on innervation and the exposure to nerve secreted factors (Farkas et al 2016). Third is the formation of a pro-regenerative extracellular matrix (Calve et al 2010), and fourth is the activation of major developmental signaling pathways, such as BMP, FGF, or EGFR (Stoick-Cooper et al 2007). Lastly, epimorphic regeneration requires (5) the physical interaction of cells in three-dimensional space (Cook and Siefert 2016), (6) level-specific replacement of the appropriate injured tissue (Siefert and Muneoka 2018), and (7) dependence on macrophages to initiate regeneration (Godwin et al 2013). All of these factors collectively contribute to and support blastema formation

Moreover, in recent years as there has been a resurgence of interest in regenerative biology and trying to harness its powers to create new therapies, the predominant distinguishing trait between canonical wound healing and regeneration has been that wound healing always results in a persisting scar (A. W. Seifert and Maden 2014). While both processes involve inflammation and reepithelization, it is the balance of the processes and the order of operations that determine whether or not there is scarring. The mammalian fetus has been actively documented to be able to undergo scar-free repair (**Figure 1.2**). However,

the adult mammal has been thought to lose this ability entirely, and thus, there does not exist a documented “perfect” model of adult mammalian epimorphic regeneration.

1.4 Axolotls: a case study for epimorphic regeneration

While mammalian adult epimorphic regeneration is still an area of active research, regeneration of amphibians and fish is much better understood. In particular, regeneration in adult axolotls (*Ambystoma Mexicanum*) has been thoroughly characterized and serves as the primary example of perfect limb regeneration. Axolotls are able to repair full-thickness wounds on average by 80 days, including epidermal organs and underlying muscle (A. Seifert et al. 2012). There are a couple of key findings that have been noted that could indicate why axolotls can perform this scar-free repair and most epithelial tissues in mammals cannot: (1) a limited hemostatic response, resulting in only a thin layer of coagulated plasma that is lacking cells, (2) significantly lower numbers of neutrophils in the inflammatory response, (3) faster re-epithelization post-injury, and (4) a delay in deposition of a regenerative extracellular matrix after re-epithelization (A. Seifert et al. 2012). Neutrophils are known to amplify an immune response by recruiting other immune mediators, so by keeping neutrophil levels lower at the wound site, axolotls dampen the inflammation response, which leads to less fibrosis. With a smaller inflammation response, re-epithelization is able to occur much faster, with axolotls reported to be able to re-epithelize 4 mm wounds completely by 18-24 hours post-injury (Durant and Whited 2021).

In axolotl limb regeneration, the wound epidermis (WE) and blastema have also been

studied extensively. The WE has been shown to be required for limb regeneration, and the blastema forms from progenitor cells that aggregate under this wound epidermis (Thornton 1957; Stocum and Dearlove 1972; Mescher 1976). The WE promotes blastema cell proliferation and guides blastema outgrowth (Leigh et al. 2018). Most recently, the individual populations that play integral roles in the axolotl regeneration process have been sequenced and now have comprehensive molecular descriptions, including the basal WE, macrophages, and Pax7+ muscle satellite cells (Leigh et al. 2018).

1.5 Mammalian epimorphic regeneration: examples and failures

It has long perplexed scientists to find a well-matched regenerative example in mammals to the axolotl limb, and it has been difficult to find true parallels. Deer antler regeneration appears to be blastema-mediated, but this is a physiologic process and not in response to injury (Li 2012). Two very specific examples of mammalian epimorphic regeneration in response to injury that have been documented are digit tip and ear pinna regeneration.

Both mouse and human digit tip regeneration have been extensively studied. In a mouse, the digit tip, when injured, is able to restore its original structure and function in a blastema-mediated fashion. Unlike canonical epimorphic regeneration, the digit tip does not, however, undergo rapid re-epithelization, and instead, the epidermis heals first onto the lateral regions of the amputated stump bone, and the blastema eventually arises distal

to this site (Sierfert and Muneoka 2018). A number of major developmental signaling pathways have been implicated in this regenerative response, including BMP (Yu et al 2010), WNT (Lehoczky and Tabin 2015), and VEGF (Yu et al 2014). However, the model of digit tip regeneration is highly dependent on the exact location where the amputation is made. If the amputation is made in the distal third of the distal phalynx, it will regenerate; if the amputation is made anywhere proximal to this distal one third, it results in wound healing (Simkin et al. 2013). Thus, the digit tip regeneration model is an example of regeneration but does not apply universally to the whole organ.

The ear pinna similarly displays some hallmarks of regeneration but comes with a series of limitations. Specifically, in two species of wild African spiny mice (Seifert et al. 2012) and one other mouse species, *Acomys. carihinus* (Gawriluk et al 2016), the external ear pinna can regenerate when a full thickness hole is made. However, wounds made at the edge of the pinna only had the ability to initiate wound repair but not actually regenerate, so like in the case of the digit tip, location has a strong impact on the regenerative nature of the tissue (Seifert and Muneoka 2018). Moreover, it is only these species of mice that have been shown to be able to regenerate these pinna holes, so it is not a universal phenomenon to mammals. However, in the cases where the pinna can regenerate, it does closely follow the tenets of epimorphic regeneration with appropriate neutrophil recruitment, formation of a wound edge that then recruits cells for the blastema, and eventual reparation of the epithelial layer, hair follicles, and cartilaginous matrix (Gawriluk et al 2016). Overall, though ear pinna regeneration is thought to be restricted in mammals, it can provide a useful model for species-specific studies of blastema formation.

Figure 1.1

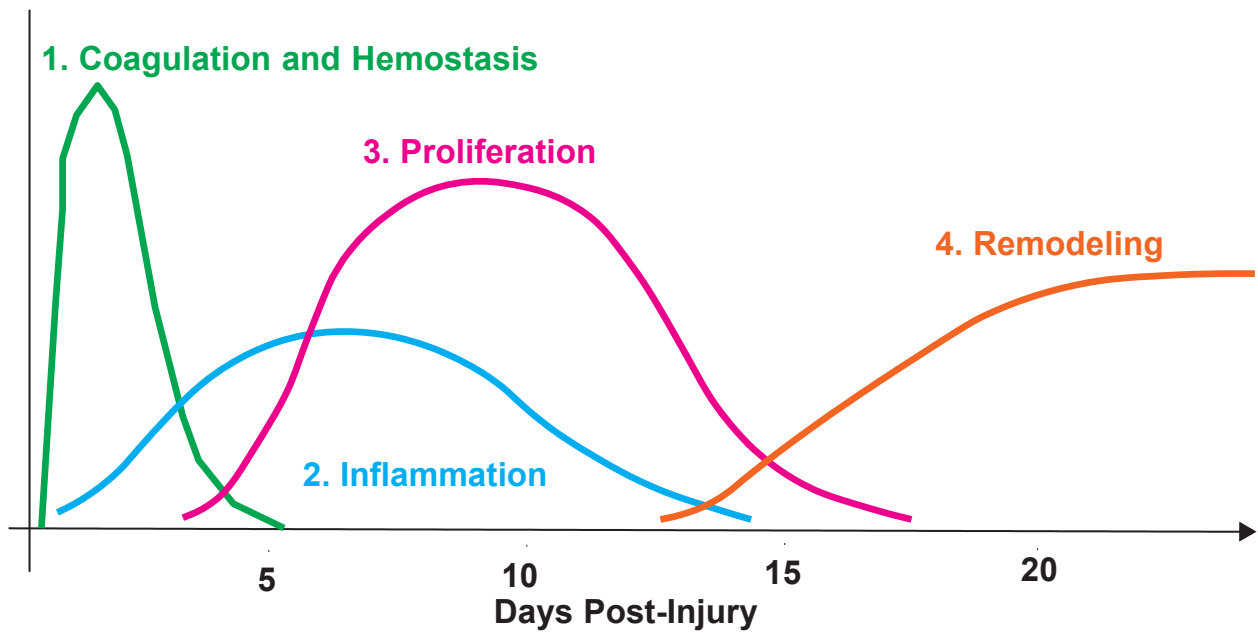


Figure 1.1: The four stages of wound healing. The four stages of wound healing- (1) Coagulation and hemostasis, (2) Inflammation, (3) Proliferation, and (4) Remodeling occur sequentially, but with overlapping periods of time.

Figure 1.2

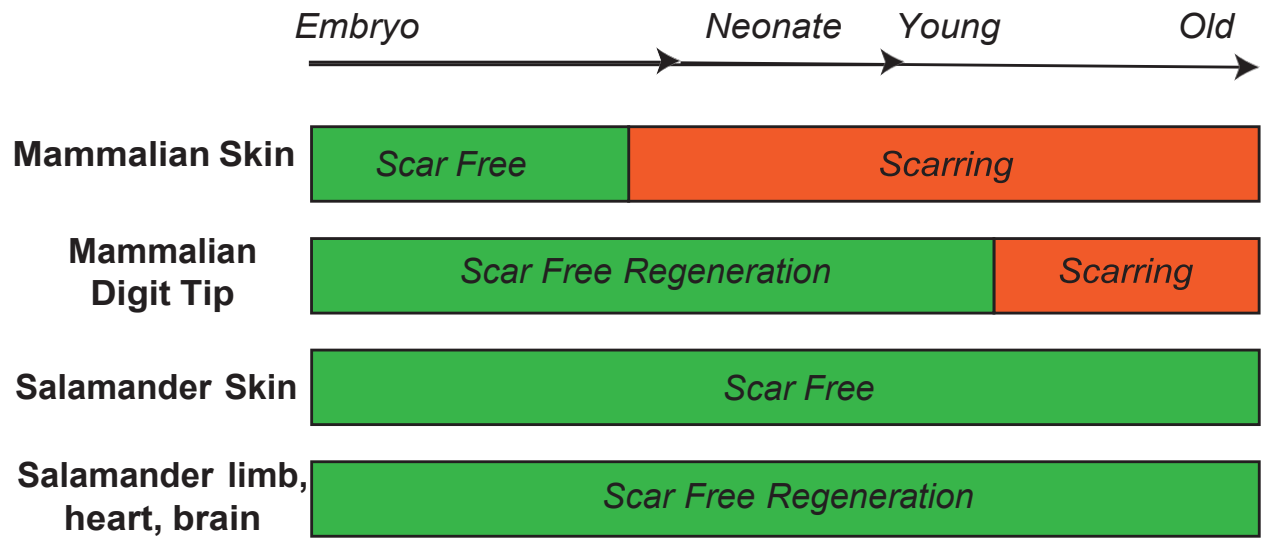


Figure 1.2: Mammals lose the ability to regenerate after embryonic stage. In the fetal stage, mammals can undergo scar-free repair, but soon after birth, this ability is lost. Meanwhile, axolotls are able to regenerate throughout their entire lifespan.

1.6 References

- AW, Seifert, and Muneoka K. 2018. "The Blastema and Epimorphic Regeneration in Mammals." *Developmental Biology* 433 (2): 190–99.
<https://doi.org/10.1016/J.YDBIO.2017.08.007>.
- Broughton, George, Jeffrey E. Janis, and Christopher E. Attinger. 2006. "Wound Healing: An Overview." *Plastic and Reconstructive Surgery* 117 (7 SUPPL.).
<https://doi.org/10.1097/01.PRS.0000222562.60260.F9>.
- Durant, Fallon, and Jessica L. Whited. 2021. "Finding Solutions for Fibrosis: Understanding the Innate Mechanisms Used by Super-Regenerator Vertebrates to Combat Scarring." *Advanced Science* 8 (15). <https://doi.org/10.1002/ADVS.202100407>.
- Gantwerker, Eric A., and David B. Hom. 2011a. "Skin: Histology and Physiology of Wound Healing." *Facial Plastic Surgery Clinics of North America* 19 (3): 441–53.
<https://doi.org/10.1016/J.FSC.2011.06.009>.
- Gantwerker, Eric A, and David B Hom. 2011b. "Skin: Histology and Physiology of Wound Healing Scarring Scars Facial Wounds Healing Skin Histology." *Facial Plast Surg Clin N Am* 19: 441–53. <https://doi.org/10.1016/j.fsc.2011.06.009>.
- Gurtner, Geoffrey C., Sabine Werner, Yann Barrandon, and Michael T. Longaker. 2008.

“Wound Repair and Regeneration.” *Nature* 453 (7193): 314–21.

<https://doi.org/10.1038/NATURE07039>.

KAU, Gonzales, and Fuchs E. 2017. “Skin and Its Regenerative Powers: An Alliance between Stem Cells and Their Niche.” *Developmental Cell* 43 (4): 387–401.

<https://doi.org/10.1016/J.DEVCEL.2017.10.001>.

Leigh, Nicholas D., Garrett S. Dunlap, Kimberly Johnson, Rachelle Mariano, Rachel Oshiro, Alan Y. Wong, Donald M. Bryant, et al. 2018. “Transcriptomic Landscape of the Blastema Niche in Regenerating Adult Axolotl Limbs at Single-Cell Resolution.” *Nature Communications* 2018 9:1 9 (1): 1–14. <https://doi.org/10.1038/s41467-018-07604-0>.

Mescher, Anthony L. 1976. “Effects on Adult Newt Limb Regeneration of Partial and Complete Skin Flaps over the Amputation Surface.” *Journal of Experimental Zoology* 195 (1): 117–27. <https://doi.org/10.1002/JEZ.1401950111>.

Portou, M. J., D. Baker, D. Abraham, and J. Tsui. 2015. “The Innate Immune System, Toll-like Receptors and Dermal Wound Healing: A Review.” *Vascular Pharmacology* 71 (August): 31–36. <https://doi.org/10.1016/J.VPH.2015.02.007>.

Seifert, Ashley, James Monaghan, Randal Voss, and Malcolm Maden. 2012. “Skin Regeneration in Adult Axolotls: A Blueprint for Scar-Free Healing in Vertebrates.” *PLoS ONE* 7 (4). <https://doi.org/10.1371/JOURNAL.PONE.0032875>.

- Seifert, Ashley W., and Malcolm Maden. 2014. "New Insights into Vertebrate Skin Regeneration." *International Review of Cell and Molecular Biology* 310 (January): 129–69. <https://doi.org/10.1016/B978-0-12-800180-6.00004-9>.
- Simkin, Jennifer, Manjong Han, Ling Yu, Mingquan Yan, and Ken Muneoka. 2013. "The Mouse Digit Tip: From Wound Healing to Regeneration." *Methods in Molecular Biology* 1037: 419–35. https://doi.org/10.1007/978-1-62703-505-7_24.
- Stocum, David L., and George E. Dearlove. 1972. "Epidermal-mesodermal Interaction during Morphogenesis of the Limb Regeneration Blastema in Larval Salamanders." *Journal of Experimental Zoology* 181 (1): 49–61. <https://doi.org/10.1002/JEZ.1401810106>.
- Thornton, Charles Stead. 1957. "The Effect of Apical Cap Removal on Limb Regeneration in *Amblystoma* Larvae." *Journal of Experimental Zoology* 134 (2): 357–81. <https://doi.org/10.1002/JEZ.1401340209>.
- Velnar, T, T Bailey, and V Smrkolj. 2009. "The Wound Healing Process: An Overview of the Cellular and Molecular Mechanisms." *The Journal of International Medical Research* 37 (5): 1528.
- Wang, Peng Hui, Ben Shian Huang, Huann Cheng Horng, Chang Ching Yeh, and Yi Jen Chen.

2018. "Wound Healing." *Journal of the Chinese Medical Association* 81 (2): 94–101.

<https://doi.org/10.1016/J.JCMA.2017.11.002>.

Chapter 2:
Structure, Functions, and Maintenance of the Homeostatic Tympanic Membrane

2.1 Anatomy of the Ear

Hearing is a function that mammals rely on in order to perceive their surroundings and appropriately react to them. The process of hearing is highly dependent on the proper functioning of the organ, the ear, and its maintenance of the integrity of its structure. Because the ability to process sound is crucial for mammalian survival, conduction of sound requires the elegant coordination of many different structures within the ear. The ear itself is divided into three main parts: the outer, middle and inner ear. The conductance of sound is divided into two parts: the outer ear, which catches sound and the middle ear, which transduces this sound (P. W. Alberti, n.d.)

The outer ear is composed of all of the structures that are visible outside of the skull. This includes the pinna, which is the cartilage covered by skin that protrudes from the side of the skull, and the external auditory ear canal (EAC), which is lined with skin containing hair, sweat glands and sebaceous glands. These gland secretions are what produce ear wax when mixed with dead epidermal cells (P. W. Alberti, n.d.). At the medial end of the EAC is the tympanic membrane (TM), colloquially known as the eardrum, which separates the outer ear from the middle ear space. The middle ear connects all the way to the back of the nose via the Eustachian tube, a long thin tube lined with mucosal cells. The middle ear space ends with the cochlea, a snail-shaped bony organ that is ultimately responsible for transducing auditory vibrations as neural impulses to the brain. The inner ear consists of the cochlea and the vestibular apparatus, which allows for linear and rotational acceleration to be processed and provide balance to the body.

The path of sound is such that sound waves enter the pinna space and travel down the EAC. When they reach the end of the EAC, they come into contact with the tympanic membrane, which vibrates in response. These vibrations are conducted through the ossicles, or middle ear bones, the first of which, the malleus, is embedded in the surface of the tympanic membrane. The vibrations are passed on from the malleus to the incus and stapes (remaining ossicles) until eventually the vibrations are propagated to the cochlea via the oval window of the inner ear. Once arrived at the cochlea, the sound vibrations are detected by the hair cells within the cochlea. This detection by the hair cells triggers a series of cellular changes, resulting in depolarization of the cells, and corresponding signals being sent to the auditory cortex of the brain. Thus, overall, the tympanic membrane is essential to the conductance of sound since it is the first major organ to come into contact with sound waves and transduce their frequency.

2.2 Anatomy and Structure of the Tympanic Membrane

The tympanic membrane is the main divider between the outer and middle ear. Thus, it is aptly positioned to be the first major organ to encounter sound waves and begin the process of sound conduction. The TM is anatomically broken down into two major regions: the pars tensa and the pars flaccida (**Figure 2.1**). The pars tensa, located superiorly when *in situ*, is a thin epithelial tissue, 1-3 cells thick in the mouse. Unlike many other epithelial tissues, the pars tensa is unique in that it lacks stratification. Interestingly, axolotls, a species with known regenerative capabilities, also lacks a linearly stratified epithelium and

instead only shows patterns of pseudo-stratification (Seifert et al. 2012). Surrounding the pars tensa is the annulus, a ring of thickened fibrous tissue that keeps the pars tensa tethered to the bony ring contiguous with the EAC. This seal allows for the tympanic membrane to be kept taut in order to vibrate when contacted by sound waves.

The pars flaccida, located inferiorly, is a thicker epithelial tissue, usually 3-5 cells thick in the mouse. Unlike the pars tensa, the pars flaccida does display epithelial stratification. The pars flaccida is also not surrounded by the annulus in the same way as the pars tensa, as it does not need to be held taut for sound conduction to occur (Fay, Puria, and Steele 2006).

The TM, though not very thick, has a unique three-layer structure. Facing the EAC is the epithelial layer as previously described, which is contiguous with the EAC epithelium.

Facing the middle ear space is the mucosal layer of cells of the TM, which is usually one cell layer thick and contiguous with the middle ear mucosa. In between these two layers is a fibrous tissue layer that contains mesenchymal cells and an interwoven collagen fiber system. The TM, particularly within the pars tensa, contains two layers of collagen fibers, an inner layer with fibers oriented circularly and an outer layer with fibers oriented radially. The first of the ossicles (middle ear bones), the malleus, is embedded in the fibrous layer, which allows the vibrations from the surface of the TM to be transduced to the middle ear space (Graham, Reams, and Perkins 1978).

2.3 Proliferation and Migration of Cells of the Tympanic Membrane

For decades now, scientists have been observing that anything placed on the surface of the TM would eventually end up removed from the TM and be seen moving down the sides of the EAC (Stinson 1936; Litton 1963; Alberti 1964; Tinling and Chole 2006). From these numerous reports, the authors concluded that the epidermis of the TM must be migrating outwards into the EAC as a protection mechanism for the ear. By removing any debris that gathers on the TM in this way, it prevents a mass from building up in the ear canal, which could lead to conductive hearing loss. In studies involving serial imaging of ink dots placed on the surface of mice, rats, guinea pigs, and human TMs, certain patterns of migration arose. In humans, it appeared that the cells moved out centrifugally from the tip of the malleus, the umbo (Alberti 1964; Michaels and Soucek 1990). Rats and gerbils appeared to show cells moving radially outward from the handle of the malleus. From studies in which mice were dosed with BrdU and TMs were harvested at a variety of time points (Kakoi et al. 1997), three major areas of proliferation emerged: (1) near the annulus, (2) near the handle of the malleus, and (3) in the intermediate zone between the pars tensa and pars flaccida. This was also consistent with findings in human TMs (Kakoi et al. 1997).

To better understand the migratory behavior of TM keratinocytes, we established techniques for time-lapse imaging of TMs cultured as explants, employing the K5-CreERT2 and Ki67-CreERT2 mouse lines paired with the fluorescent reporter mT/mG, in which labeled cells express membrane-localized EGFP, and the reporter R26R-Confetti, in which recombination leads to expression of one of four fluorescent proteins: RFP, YFP, nCFP, or

nGFP (Rock et al. 2009; Muzumdar et al. 2007; Snippert et al. 2010). After tamoxifen-induced recombination in *K5-CreERT2; R26^{mTmG/mTmG}* mice, TMs were harvested and cultured as an explant with serial hourly imaging, which showed that radial movement was seen only on the periphery of the TM, but the predominant direction of migration was over the malleus superiorly-to-inferiorly (**Figure 2.2A**). Live-cell imaging of explants of *Ki67-CreERT2; R26^{mTmG/mTmG}* mice revealed GFP predominantly arising from the pars flaccida and regions of the pars tensa near the malleus and revealed cell movements similar to those seen with the *K5-CreERT2; R26^{mTmG/mTmG}* TM explants (**Figure 2.2B**). We also broke the displacement of cells into directional components, using Imaris software, which showed again that the pars tensa cells predominantly move superior-to-inferiorly (i.e., downward in the y-direction; **Figure 2.4C**). Thus, the basal keratinocytes of the pars tensa exhibit directional lateral migration, and the basal keratinocytes of the pars flaccida do not (**Figure 2.4D**).

2.4 Cellular Identities and Dynamics of the Tympanic Membrane at Homeostasis

Prior studies have defined the basic layers of the TM, but work in the lab initially sought to define the resident stem cell populations of the TM for the first time. Single-cell RNA sequencing (scRNA-seq) of thirty-eight adult murine TMs, pooled and split into two anatomic fractions, epidermal and fibrous/mucosal, generated two corresponding datasets, analyzed with Seurat (Satija et al. 2015) to identify cell clusters (**Figure 2.3A,B**).

In the epidermal fraction, seven cell clusters were identified, including five keratinocyte clusters (numbered 0,1, 2, 3, and 4), mesenchymal (5), and mucosal (6) cells (**Figure 2.3A**). Keratinocytes in cluster 3 are cycling, marked by expression of *Top2a* and *Mki67* (**Figure 2.3C**). The prominent axis of distinction among the other keratinocyte clusters was differentiation state. Clusters 1 and 2 are relatively undifferentiated; they express markers of basal keratinocytes, including *Krt5*, *Krt15*, and *Itga6* (**Figure 2.3C**). Cluster 0 is an intermediate differentiation state; the cells have lost expression of the basal-like markers and gained expression of differentiation-associated genes, including *Krt10* and *Ivl*. Lastly, Cluster 4 are terminally differentiated keratinocytes, expressing markers including *Flg2* and *Hrnr*. Overall, the gene expression profiles obtained among the keratinocytes were similar to those previously observed in other interfollicular epidermal sites (Cheng et al. 2018; Joost et al. 2018; Aragona et al. 2017), providing a level of validation to our scRNA-seq data.

The same approaches were utilized to define the cell populations in the fibrous/mucosal fraction, where 12 clusters were discovered. Among these are multiple *Vimentin+* (*Vim*) mesenchymal populations, including: endothelium (*Pecam1+*), smooth muscle (*Acta2+*), and Schwann cells (*Mbp+*). Four additional clusters of mesenchymal cells were identified, numbered 0 (*Gpx3+*), 2, 3 and 5 (all *Igfbp3+*), marking distinct populations of fibroblasts. Lastly, *Sox2* is a known marker of mucosa and is expressed in both non-ciliated and ciliated mucosal cell clusters (Tucker et al. 2018). Ciliated Mucosa was identified via expression of motor proteins, including *Dnah5* and *Dynlrb2*. The mucosal clusters express *Krt19*, while the keratinocyte clusters do not.

2.5 Stem Cell and Progenitor Niches of the Tympanic Membrane

Prior to studies done in our lab, the clonal architecture of the TM and how it was maintained was very minimally understood. Using a *Ki67-CreERT2;R26R-Confetti* mouse line to visualize individual clones on the TM, mice were given a minimal dose of tamoxifen and clones were visualized two days to two months later (**Figure 2.5A**). From counting the number of cells in each clone at each captured time-point, we found that the distribution of clone sizes was consistent with that of neutral drift dynamics in the stem cell pool (**Figure 2.5B**) (Klein et al. 2010; Mascré et al. 2012; Lopez-Garcia et al. 2010).

At early timepoints, circular clones were found near the umbo of the malleus, which has been characterized as a major site of cell turnover of the TM (Knutsson, Von Unge, and Rask-Andersen 2011). At longer timepoints, there were clones extending supero-inferiorly along the pars tensa that always connected back to the upper border with the pars flaccida, another known proliferative region (**Figure 2.5C**); along with other clones emanating from this region, these data led us to conclude that the junction of the pars flaccida and the pars tensa is the location of the long-term repopulating stem cells of the tissue.

A *K5-CreERT2;R26R-Confetti* mouse model with maximal tamoxifen labeling was used to answer questions surrounding long-term repopulation of the epithelial layer of the TM. At later time points after multiple cycles of complete turnover of the TM, streaks of color formed across the tympanic membrane, consistent with models of stochastic stem cell

turnover (**Figure 2.5D**) (Klein and Simons 2011). Overall, the architecture of the clones from both sets of experiments was consistent with a model in which the long-term repopulating stem cells arise exclusively from the region adjacent to the pars flaccida; the committed progenitors and their progeny then migrate from this stem cell region over the pars tensa and are eventually shed along the sides of the EAC (**Figure 2.5E**).

Figure 2.1

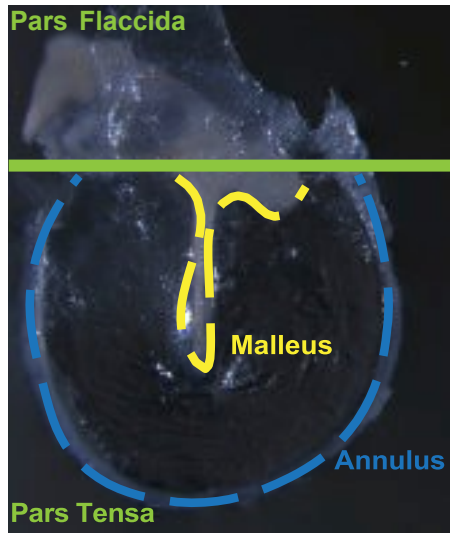


Figure 2.1: Tympanic Membrane Anatomy Image of a tympanic membrane floating in saline. The image is annotated with the two main regions of the TM: the pars flaccida and the pars tensa. The annulus surrounding the pars tensa and the malleus, the first of the middle ear bones, embedded in the pars tensa are also noted.

Figure 2.2

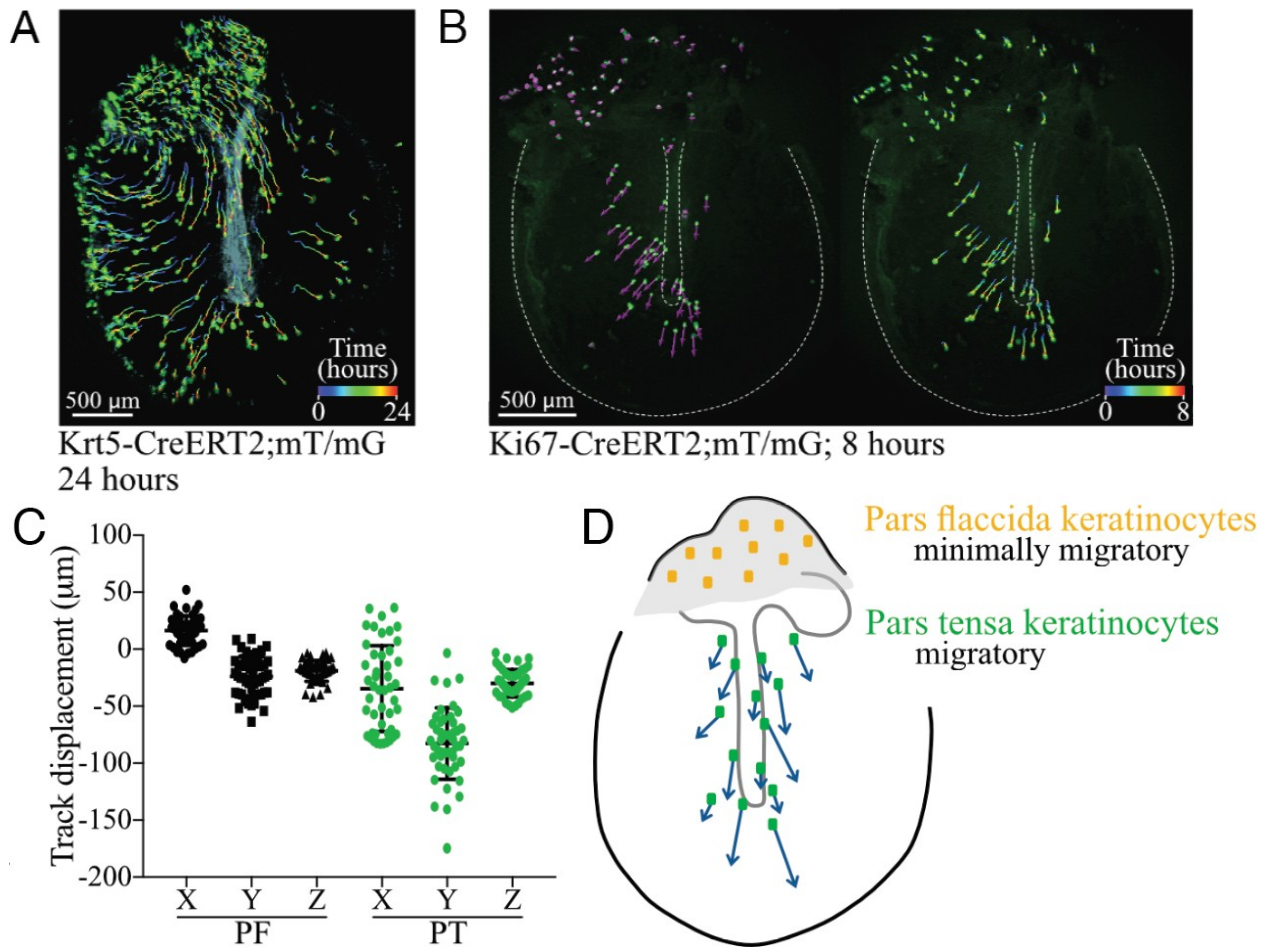


Figure 2.2: TM migratory patterns revealed by live-cell imaging. (A) TM from a *Krt5-CreERT2;R26^{mTmG/mTmG}* mouse serially imaged hourly for 24 hours. Cells were identified and tracked using Imaris. Cells are shown at their final position, with their full track traced from time = 0 hours (purple) to 24 hours (red). (B) Whole-mount TM from a *Ki67-CreERT2;R26^{mTmG/mTmG}* mouse imaged hourly for eight hours. On the left, cells are at their initial positions with vectors showing the directions in which they will move. On the right, cells are at their final positions with tracks showing their paths. (D) X, Y, and Z components of the displacement. (E) Cartoon summarizing findings from the live cell imaging. (Adapted from Frumm et al. 2021)

Figure 2.3

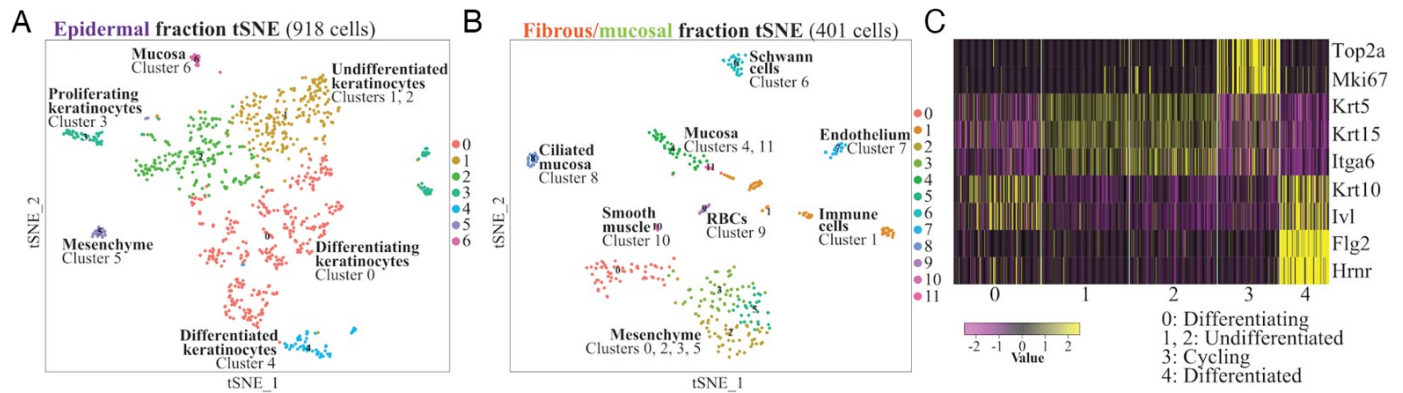


Figure 2.3: Single-cell RNA sequencing (scRNA-Seq) identifies cell types in the murine TM. (A) t-Distributed Stochastic Neighbor Embedding (tSNE) visualization of the cell clusters identified in the epidermal fraction. (E) tSNE visualization of the cell clusters identified in the fibrous/mucosal fraction. (F) Heat-map showing expression of genes associated with keratinocyte differentiation states in keratinocyte clusters 0 - 4. Yellow indicates high expression and violet low expression. Each column is a single cell. (Adapted from Frumm et al. 2021)

Figure 2.4

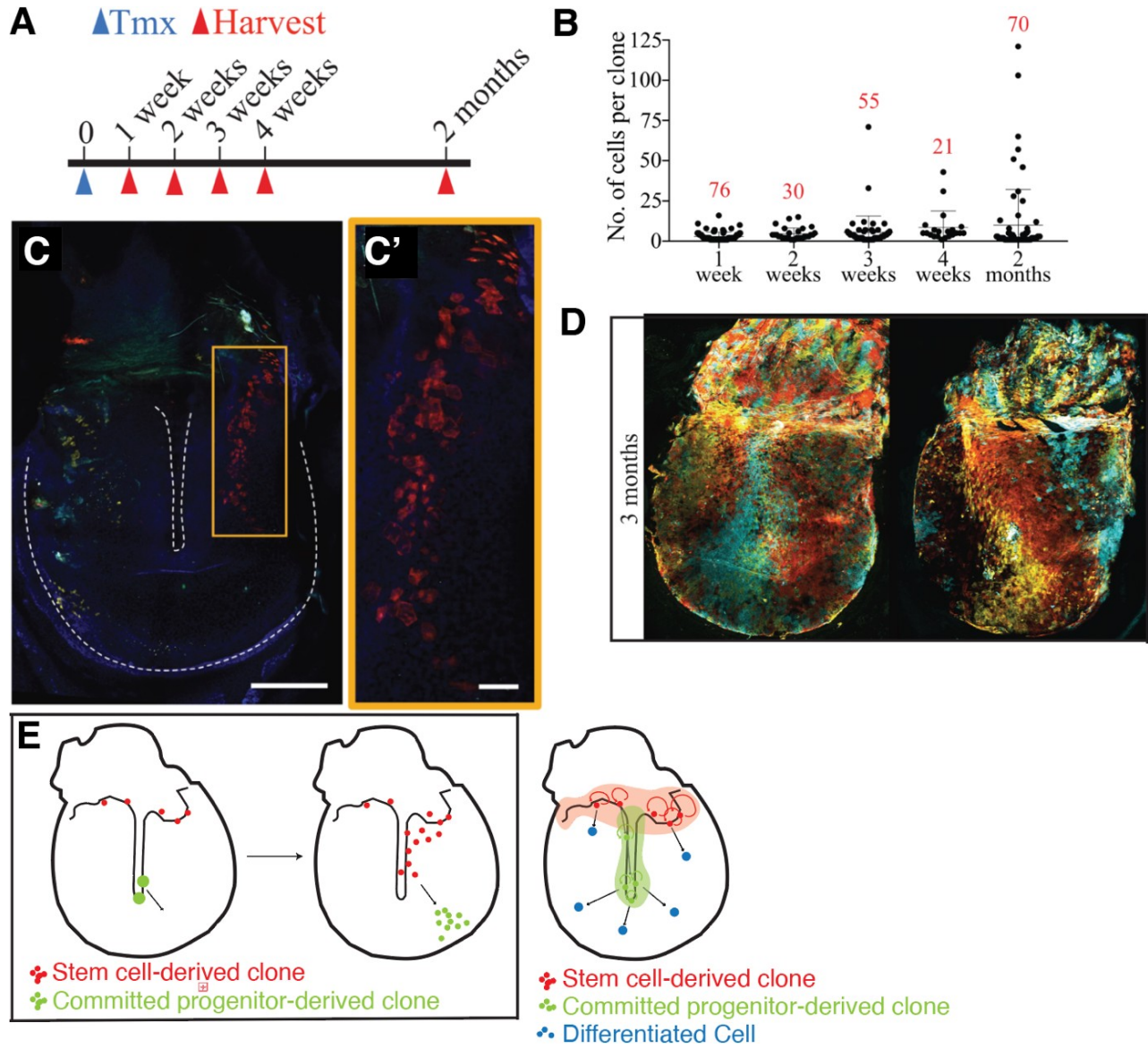


Figure 2.4: TM keratinocyte clones arise from distinct stem cell and committed progenitor populations. (A) Experimental timeline. Mice were injected with 250 mg/kg tamoxifen at day 0 and TMs were harvested weeks to months later. (B) Number of cells per clone identified at each indicated time-point. The total number of clones quantified at each time-point is indicated above the data. (C) Example of clones captured at 2 months. In each pair of images, the entire whole-mount TM is shown on the left with the annulus and malleus outlined by a white dotted line, the magnified area shown with an orange box, and the scale bar indicating 500 μm ; on the right, designated with a prime, are more magnified images of clones, and the scale bar indicates 100 μm . (D) Representative whole-mount TMs from 3 month timepoint from *K5-CreERT2;R26R-Confetti* mice given 5 days of tamoxifen. (E) Cartoon depicting our model for the location of stem cells (SCs) and committed progenitors (CPs) of the murine TM epidermis based on data from *the Ki67-CreERT2;R26R-Confetti* lineage trace. We posit that SCs reside in the superior portion of the pars tensa, near the border with the pars flaccida and that committed progenitors proliferate over the malleus. (Adapted from Frumm et al. 2021)

2.7 References

Alberti, P. W.R.M. 1964. "Epithelial Migration on the Tympanic Membrane*†‡." *The Journal of Laryngology & Otology* 78 (9): 808–30.
<https://doi.org/10.1017/S0022215100062800>.

Alberti, Peter W. n.d. "2 THE ANATOMY AND PHYSIOLOGY OF THE EAR AND HEARING."

Aragona, Mariaceleste, Sophie Dekoninck, Steffen Rulands, Sandrine Lenglez, Guilhem Mascré, Benjamin D. Simons, and Cédric Blanpain. 2017. "Defining Stem Cell Dynamics and Migration during Wound Healing in Mouse Skin Epidermis." *Nature Communications* 2017 8:1 8 (1): 1–14. <https://doi.org/10.1038/ncomms14684>.

Cheng, Jeffrey B., Andrew J. Sedgewick, Alex I. Finnegan, Paymann Harirchian, Jerry Lee, Sunjong Kwon, Marlys S. Fassett, et al. 2018. "Transcriptional Programming of Normal and Inflamed Human Epidermis at Single-Cell Resolution." *Cell Reports* 25 (4): 871–83.
<https://doi.org/10.1016/J.CELREP.2018.09.006>.

Fay, Jonathan P., Sunil Puria, and Charles R. Steele. 2006. "The Discordant Eardrum." *Proceedings of the National Academy of Sciences* 103 (52): 19743–48.
<https://doi.org/10.1073/PNAS.0603898104>.

Graham, M. D., C. Reams, and R. Perkins. 1978. "Human Tympanic Membrane — Malleus Attachment Preliminary Study." *Undefined* 87 (3 I): 426–31.

<https://doi.org/10.1177/000348947808700326>.

Joost, Simon, Tina Jacob, Xiaoyan Sun, Karl Annusver, Gioele La Manno, Inderpreet Sur, and Maria Kasper. 2018. "Single-Cell Transcriptomics of Traced Epidermal and Hair Follicle Stem Cells Reveals Rapid Adaptations during Wound Healing." *Cell Reports* 25 (3): 585-597.e7. <https://doi.org/10.1016/J.CELREP.2018.09.059>.

Kakoi, Hiroyuki, Matti Anniko, Anders Kinnefors, and Helge Rask-Andersen. 1997. "Auditory Epidermal Cell Migration. VII. Antigen Expression of Proliferating Cell Nuclear Antigens, PCNA and Ki-67 in Human Tympanic Membrane and External Auditory Canal." *Acta Oto-Laryngologica* 117 (1): 100-108. <https://doi.org/10.3109/00016489709117999>.

Klein, Allon M., Toshinori Nakagawa, Rie Ichikawa, Shosei Yoshida, and Benjamin D. Simons. 2010. "Mouse Germ Line Stem Cells Undergo Rapid and Stochastic Turnover." *Cell Stem Cell* 7 (2): 214-24. <https://doi.org/10.1016/J.STEM.2010.05.017>.

Klein, Allon M., and Benjamin D. Simons. 2011. "Universal Patterns of Stem Cell Fate in Cycling Adult Tissues." *Development (Cambridge, England)* 138 (15): 3103-11. <https://doi.org/10.1242/DEV.060103>.

Knutsson, Johan, Magnus Von Unge, and Helge Rask-Andersen. 2011. "Localization of Progenitor/Stem Cells in the Human Tympanic Membrane." *Audiology & Neuro-*

Otology 16 (4): 263–69. <https://doi.org/10.1159/000320612>.

LITTON, W. B. 1963. “Epithelial Migration over Tympanic Membrane and External Canal.”

Archives of Otolaryngology (Chicago, Ill. : 1960) 77: 254–57.

<https://doi.org/10.1001/ARCHOTOL.1963.00750010264004>.

Lopez-Garcia, Carlos, Allon M. Klein, Benjamin D. Simons, and Douglas J. Winton. 2010.

“Intestinal Stem Cell Replacement Follows a Pattern of Neutral Drift.” *Science (New York, N.Y.)* 330 (6005): 822–25. <https://doi.org/10.1126/SCIENCE.1196236>.

Mascreé, Guilhem, Sophie Dekoninck, Benjamin Drogat, Khalil Kass Youssef, Sylvain Brohée,

Panagiota A. Sotiropoulou, Benjamin D. Simons, and Cédric Blanpain. 2012. “Distinct Contribution of Stem and Progenitor Cells to Epidermal Maintenance.” *Nature* 489

(7415): 257–62. <https://doi.org/10.1038/NATURE11393>.

Michaels, Leslie, and Sava Soucek. 1990. “Auditory Epithelial Migration on the Human

Tympanic Membrane: II. The Existence of Two Discrete Migratory Pathways and Their Embryologic Correlates.” *The American Journal of Anatomy* 189 (3): 189–200.

<https://doi.org/10.1002/AJA.1001890302>.

Muzumdar, Mandar Deepak, Bosiljka Tasic, Kazunari Miyamichi, Ng Li, and Liqun Luo.

2007. “A Global Double-Fluorescent Cre Reporter Mouse.” *Genesis (New York, N.Y. : 2000)* 45 (9): 593–605. <https://doi.org/10.1002/DVG.20335>.

R, Satija, Farrell JA, Gennert D, Schier AF, and Regev A. 2015. "Spatial Reconstruction of Single-Cell Gene Expression Data." *Nature Biotechnology* 33 (5): 495–502.
<https://doi.org/10.1038/NBT.3192>.

Rock, Jason R., Mark W. Onaitis, Emma L. Rawlins, Yun Lu, Cheryl P. Clark, Yan Xue, Scott H. Randell, and Brigid L.M. Hogan. 2009. "Basal Cells as Stem Cells of the Mouse Trachea and Human Airway Epithelium." *Proceedings of the National Academy of Sciences of the United States of America* 106 (31): 12771–75.
<https://doi.org/10.1073/PNAS.0906850106>.

Seifert, Ashley, James Monaghan, Randal Voss, and Malcolm Maden. 2012. "Skin Regeneration in Adult Axolotls: A Blueprint for Scar-Free Healing in Vertebrates." *PLoS ONE* 7 (4). <https://doi.org/10.1371/JOURNAL.PONE.0032875>.

Snippert, Hugo J., Laurens G. van der Flier, Toshiro Sato, Johan H. van Es, Maaïke van den Born, Carla Kroon-Veenboer, Nick Barker, et al. 2010. "Intestinal Crypt Homeostasis Results from Neutral Competition between Symmetrically Dividing Lgr5 Stem Cells." *Cell* 143 (1): 134–44. <https://doi.org/10.1016/J.CELL.2010.09.016>.

Stinson, W. D. 1936. "REPARATIVE PROCESSES IN THE MEMBRANA TYMPANI: SOME INTERESTING MANIFESTATIONS." *Undefined* 24 (5): 600–605.
<https://doi.org/10.1001/ARCHOTOL.1936.00640050613006>.

Tinling, Steven P., and Richard A. Chole. 2006. "Gerbilline Cholesteatoma Development Part I: Epithelial Migration Pattern and Rate on the Gerbil Tympanic Membrane: Comparisons with Human and Guinea Pig." *Otolaryngology--Head and Neck Surgery : Official Journal of American Academy of Otolaryngology-Head and Neck Surgery* 134 (5): 788–93. <https://doi.org/10.1016/J.OTOHNS.2005.12.022>.

Tucker, Abigail S., Carlene J. Dyer, Juan M.Fons Romero, Tathyane H.N. Teshima, Jennifer C. Fuchs, and Hannah Thompson. 2018. "Mapping the Distribution of Stem/Progenitor Cells across the Mouse Middle Ear during Homeostasis and Inflammation." *Development (Cambridge, England)* 145 (1). <https://doi.org/10.1242/DEV.154393>.

Chapter 3:
Epimorphic Regeneration in the Mammalian Tympanic Membrane

3.1 Abstract

Adult mammals are generally believed to lack the ability to regenerate complex tissues and instead repair wounds by forming scars. In humans and across mammalian species, the tympanic membrane (TM) rapidly repairs perforations without intervention. Using mouse models, we demonstrate that the TM repairs itself through a process that bears the hallmarks of epimorphic regeneration rather than typical wound healing. Following injury, the TM forms a wound epidermis characterized by GFR ligand expression and signaling. After the expansion of the wound epidermis which emerges from known stem cell regions of the TM, a multi-lineage blastema-like cellular mass is recruited. After two weeks, the tissue architecture of the TM is largely restored, but with disorganized collagen. In the months that follow, the organized and patterned collagen framework of the TM is restored resulting in scar-free repair. Finally, we demonstrate that deletion of *EGFR* in the epidermis results in failure to expand the wound epidermis, recruit the blastema-like cells, and regenerate normal TM structure. This work establishes the TM as a model of mammalian complex tissue regeneration and demonstrates that adult mammals appear to retain the capacity for epimorphic regeneration at this site.

3.2 Introduction

Mammals are capable of scar-free injury repair in the embryonic stage; however, after birth, they display increasingly limited capacity to regenerate injured tissues (AW and K 2018). The characteristic stages of wound healing in adult mammals - (1) hemostasis, (2)

inflammation, (3) proliferation, and (4) wound remodeling (V. T, T, and V 2009) - result in tissues that may be functional but do not completely recapitulate the gross morphology and microscopic patterning of the unwounded tissue. In contrast, tetrapods, such as axolotls (*Ambystoma Mexicanum*), are able to regenerate entire complex-tissue limb structures throughout their life-spans (JP and A 2008; Gerber et al., n.d.). The resulting organ resembles the previous unwounded structure in gross morphology, cellular patterning, and full function, with little, if any, remnant of the inflicted injury (scar) (Whited and Tabin 2009). This repair process, termed epimorphic regeneration, is distinguished from mammalian wound healing by a few key features. Epimorphic regeneration is defined by an initial cellular response to wounding, the formation of a cellularly heterogeneous blastema, and subsequent cellular patterning and morphogenesis resulting in scar-free repair of a tissue or organ (AW and K 2018). In the axolotl, the site of the wound is rapidly covered by a specialized epidermis, which then serves as a scaffold for blastema formation and the resulting regeneration of the organ (Leigh et al., n.d.; Chalkley 1954). With rare and species-specific exceptions (TR et al. 2016; K, WF, and SV 1986; U, C, and JS 2009), mammals are believed to lack the ability to regenerate tissues and organs once they develop past the embryonic stage (Seifert and Maden 2014), and epimorphic regeneration has not been described in an adult mammalian organ across species.

The tympanic membrane (TM) or eardrum is a central component of hearing, relaying sound from the environment to the cochlea. Anatomically, it is separated into two major compartments: the larger but thinner pars tensa (PT), and the smaller but thicker pars flaccida (PF). Both regions are composed of three cellular layers: the external epidermis,

the middle fibrous/mesenchymal layer, and the inner mucosal epithelium, which is continuous with the middle ear. In skin elsewhere in the body, the epidermis is stratified, with a basal layer of keratinocytes (KCs) separated from the underlying dermis by a basement membrane. The TM epidermis is a specialized type of skin that is only 3-5 cells thick in humans and 1-3 cells thick in mice and lacks common skin appendages such as hair follicles and sweat glands (Blanpain and Fuchs 2009; KAU and E 2017; CM and A 1999). Within the fibrous layer, the TM has two organized layers of collagen fibers, one radial and one circular. Within the PT, the first sound-transducing bone, the malleus, is embedded within this mesenchymal layer, surrounded by nerves and blood vessels. The junction of the PT and the PF as well as the area over the malleus are thought to be the stem/progenitor niche regions of the organ.

In humans, guinea pigs, mice, rats, dogs, and chinchillas, the TM rapidly and spontaneously repairs following injury (Wang AY et al. 2014; Gao et al. 2017). This process is so robust that in attempting to create models of chronic TM perforation, investigators have struggled to find animal models where this repair is reproducibly prevented (Wang AY et al. 2014; ZC, ZH, and QP 2012). In clinical practice, 750,000 myringotomy procedures are performed in the United States every year, in which a perforation is made in the TM to drain fluid from or relieve pressure in the middle ear space behind the TM (Hall et al. 2010). The vast majority of these surgical perforations successfully heal (Hall et al. 2010). In order to prevent the healing process and keep the perforation patent, metal or plastic tubes are typically inserted into the TM to treat eustachian tube disorders (RM et al. 2013). This robust repair process across adult mammalian species spurred us to characterize the

healing of this organ, the cellular and molecular mechanisms of which repair remain poorly understood.

Here, we demonstrate that the mouse TM displays key features of epimorphic regeneration (M, S, and YC 1980), including the hallmark of scar-free repair. We define a new “wounded” epithelial population of the TM that emerges in response to injury and demonstrate that EGFR is necessary for a robust proliferative response. Taken together, these data provide a cellular roadmap of the TM’s response to injury and for the first time, demonstrate the capacity of an adult mammalian organ to undergo epimorphic regeneration.

3.3 Results

Injury to the TM induces a robust proliferative response

To characterize the TM response to injury, we first assessed gross tissue morphology during the time course of wound repair. We perforated the left TMs of mice in the postero-inferior quadrant of the pars tensa, using the right TMs as unwounded controls (**Figure 3.1A**). We harvested TMs at multiple timepoints during wound healing and imaged whole mounts (**Figure 3.1B**). Macroscopically, there is a large buildup of tissue with thickening of the TM by day 3 post-perforation. This increase in tissue volume persists through day 7. By day 14, the tissue has drastically remodeled and decreased in volume back to the gross appearance of an unwounded TM, without apparent evidence of the prior injury. Across all

experiments, we found that TM perforations observed at day 7 or later (240/240) were closed.

We next sought to characterize the spatial and temporal proliferative response following TM injury. We created perforations as previously described and pulsed the mice with EdU two hours prior to harvesting the TMs (**Figure 3.1C**). Within 18 hours of perforation, there was a detectable increase in proliferation ($p = .0082$) (**Supp. Figure 3.1A,B**). This early increase in EdU-labeled cells is faster than that seen in mammalian wound healing in skin, which typically shows an increase in proliferation only 48 hours following wounding (Aragona et al. 2017). At one day post-injury, there was a marked increase in proliferation in the same regions that are proliferative under homeostasis, the tissue over the malleus and the junction of the pars tensa and pars flaccida (SM et al. 2021) (**Figure 3.1D**). By day 5, we observed the peak in proliferation, with a 5.5-fold increase in EdU+ cells over the whole TM ($p = .0043$) (**Figure 3.1E**). By day 7, the proliferation had substantially decreased, and by day 14, the proliferation pattern resembled that of the unwounded TM.

The proliferative response to wounding in the TM appeared to involve the whole organ rather than just the area around the wound site. Homeostatic turnover of the entire TM epidermis takes approximately 3 weeks (SM et al. 2021). To see how the rate and location of turnover are impacted by wounding, we maximally labeled the TM KCs with EdU supplied via drinking water, then removed the source of EdU upon injury of the TMs and harvested the tissues over the course of four weeks (**Supp. Figure 3.1C**). We observed the loss of the EdU label in the TM epidermis by day 7 rather than the typical 3 weeks seen in

the homeostatic TM (**Supp. Figure 3.1D**). Thus, the robust proliferative response to wounding of the TM accelerates turnover of the TM epidermis throughout the organ.

TM perforation repair restores all layers of the TM

Most skin wounds heal by filling a defect that is bounded by tissue on three sides and results in incomplete reconstitution of pre-existing skin structures (Gantwerker and Hom 2011). In contrast, wounding of the TM creates a full thickness perforation that goes through epidermal, mesenchymal, and mucosal layers (**Figure 3.2A**) and is bound only by tissue along its edges. It also disrupts the organized layers of radial and circular collagen fibers in the TM (**Figure 3.2A-B**). We examined H&E-stained cross-sections of the TM at the area of injury over time (**Figure 3.2C**). At one day following perforation, we began to see some expansion and stratification of the keratinocytes over the malleus and annulus. By day 3, this population had massively expanded, and the TM had thickened substantially. By day 5, the perforation was typically filled by a mass of cells (~16x thicker than the UW TM) including keratinocytes, Pdgfra+ mesenchymal cells (**Figure 3.2E**), and immune cells. At day 7, the TM reached its maximal thickness (~52x thicker than UW), with marked expansion of the epidermis that extended beyond the site of perforation. Notably, we observed keratinization on the epidermis side of the TM with sloughing of keratin debris at day 7 while wild-type TMs do not usually display keratinization. day 14 post-injury, the TM had restored its original thickness and appeared histomorphologically identical to the unwounded TM, with resolution of the multi-lineage disorganized cell mass and with intact mucosal, connective tissue, and epidermal layers. This process resembles the steps of epimorphic regeneration in the axolotl limb, including expansion of a wound epidermis,

formation of a multi-lineage blastema-like structure, and subsequent morphogenesis and resolution (AW and K 2018).

We next investigated the differentiation state of the KCs during the time course of healing. In the initial phases, there is expansion of nucleated, basal-appearing Keratin5+ (K5+) keratinocytes. At later timepoints, we observed heterogeneous labeling for markers of basal KCs (K5), differentiated KCs (Keratin10, Keratin23, Filaggrin(M. T et al. 1990)), and mesenchymal cells (Pdgfra) throughout the thickness of the TM by *in situ* hybridization (ISH) (**Figure 3.2D**) and immunofluorescence (IF) (**Figure 3.2E, F**). Of note, we observed cells positive for both K5 and Keratin10 (**Figure 3.2D**). This disorganized stratification and differentiation was most prominent at day 7 post-injury and resolved by day 14. Taken together with the histological features, we conclude that the keratinocytes within the thickened mass differentiate, keratinize, and form a crust, which is later lost in the external auditory canal, consistent with previous observations in humans and other mammals(ZC, ZH, and QP 2012).

The TM displays scar-free repair

Repair of other mammalian epithelial tissues such as skin generally results in scar formation (Rodrigues et al. 2019), defined as deposition of fibrotic tissue that does not fully recapitulate the original tissue structure and function. We next sought to determine whether repair of the injured TM similarly resulted in a scar by studying the characteristic organization of collagen fibers in the TM (**Figure 3.2B**). The middle mesenchymal layer of the TM is primarily composed of Collagen II (COLII) at homeostasis, with the appearance of

Collagen I (COLI) being associated with injury (Maria et al. 2010). We performed IF for COLII and COLI in the unwounded TM and at multiple timepoints post-injury to visualize the collagen patterning of the injured TM (**Figures 3.2G and Supp. 3.2A**). At 2 weeks following perforation, the TM, though grossly healed, did not display the typical circular and radial COLII fiber patterning, and a small amount of COLI was present localized to the wound site. However, by 2 months, the COLII patterning appeared nearly restored to the pre-injury state (n=15 for Col II), and COLI was minimally present at the site of perforation (n=15). At one year following injury, there was no detectable difference in the appearance of the COLII radial and circular fiber structure (n=3). Thus, the healed TM restores its cellular structure and its highly organized connective tissue layer without evidence of a scar.

TM cell populations undergo transcriptional shifts during healing

We next sought to generate a global transcriptional map of cells during TM perforation repair. We performed single-cell RNA sequencing using the 10x Genomics Single Cell Solution v3 platform on dissociated TM tissues at 4 different timepoints post-injury and compared to unwounded controls (**Figure 3.3A, B**). We selected timepoints at 1, 3, 7, and 14 days after injury based on gross and microscopic changes observed in our prior experiments that indicated that these were key timepoints of wound epidermis response, robust proliferative expansion of cell layers, and morphologic resolution.

Datasets for each timepoint were analyzed with Seurat v3 (R et al. 2015) and the results visualized two-dimensionally using uniform manifold approximation and projection

(UMAP) (**Supp. Figure 3.3**). As we were interested in transcriptional changes over the time-course of repair, we merged the 5 datasets and reanalyzed the combined object with Seurat (**Figure 3.3C-E**). Eight major cell types were identified by their marker gene expression: keratinocytes, non-ciliated mucosa, ciliated mucosa, mesenchyme, immune, red blood cells, adipocytes, and endothelium (Farahani and Xaymardan 2015; Gil-Yarom et al. 2017). In order to identify distinct subpopulations of cells along the time course, we used CellFindR (Yu et al. 2019), an algorithm that incorporates unbiased iterative sub-clustering to identify biologically significant populations. This revealed multiple distinct subpopulations of cells, many of which were specific to distinct stages of TM healing. When the cells were colored by original timepoint in the merged UMAP, cells within each time point occupied a distinct space, indicating that they were dissimilar from cells at other timepoints within the major cell populations of the TM (**Figure 3.3F**). Though the TM tissue structure appeared grossly resolved by day 14 (**Figure 3.1B**), the transcriptional states of the cells did not fully restore to the unwounded state in this time frame. Nevertheless, the general trend over the time course indicated that the cells' transcriptional states were continuing to become increasingly similar to the unwounded state based on RNA velocity vector analysis (**Figure 3.3G, H**).

Single-cell analysis reveals that distinct layers of the TM demonstrate time-dependent transcriptional shifts and turnover following injury

A key feature of epimorphic regeneration is layer-specific and multi-lineage replacement of tissue. Therefore, we sought to investigate the transcriptional shifts over time within each layer of the TM during repair. To separately investigate each layer of the TM, we

subclustered the merged dataset into specific cell types: keratinocytes, mesenchymal cells, immune cells, and mucosal cells (**Figure 3.3I, Supp. Fig 3.4**).

Keratinocytes make a large transcriptional shift almost immediately after perforation; at day 1 after wounding, they occupy an almost entirely separate transcriptional space from that of unwounded keratinocytes (**Figure 3.3I**). There are changes in expression of numerous transcripts, such as *Lgals1*, *Cald1*, *BC100530*, *Odc1*, and *Gpr15L*, some of the highest differentially expressed genes, as well as an increase in inexpression of proliferation-associated genes like *Mki67* and *Ccnd1* in the keratinocytes. This is in line with the rapid proliferative response we observe as early as 18 hours after perforation (**Figure 3.1D, Supp. Figure 3.1B**). In contrast, the other layers of the TM display a more delayed transition transcriptionally, consistent with associated histologically apparent changes (**Figure 3.2**) and prior immunostaining data (DA et al. 2019). In homeostasis, very few cycling cells are seen in the layers of the TM outside of the epidermal layer (SM et al. 2021). However, during TM repair, multiple cell types, including mesenchymal, mucosal, and macrophage populations, express proliferation markers including *Mki67*, *Top2a*, and *Ccnd1*, consistent with a multi-lineage response to injury (**Supp Fig 3.4A-D**). We confirmed the timing of increased proliferation in the keratinocyte and mucosal layers after injury by injecting mice with EdU 2 hours prior to harvesting TMs and co-staining with Krt5 (**Supp. Fig 3.4E**) or Sox2 (**Supp. Fig 3.4F**) antibodies, respectively, to identify cells actively proliferating. Krt5+ cells showed an increase in proliferation (EdU labeling) at one day post-perforation, while Sox2+ cells showed an increase at 3 days post-perforation.

To better understand the populations of mesenchymal cells present during TM wound healing, we computationally isolated the mesenchymal cells from the merged dataset and re-clustered them using CellFindR. We discovered 15 subclusters (**Supp. Figure 3.5A, 3.B**), including several subpopulations specific to the wounded state. Labeling by timepoint revealed a large transcriptional shift at day 3 following injury (**Supp. Figure 3.5C**), with differential expression of multiple genes, including upregulation of *Mt1*, *Mt2*, and *Timp1* amongst the highest expressed genes (**Supp. Figure 3.5D**). Cells in the unwounded state displayed higher expression canonical mesenchymal markers, such as *Vimentin*, *Pdgfra*, *Fibronectin1*, and *Collagen 1a1* and *1a2* (**Supp. Figure 3.5E-I**) (Stone et al. 2016; McDonald et al. 2013). In contrast, in the wounded state, there appeared to be activation and proliferation of an Acta2+ (cluster 1.1.2) subpopulation as well as a distinct Coch+ population (cluster 1.1.4), both of which were detectable as early as day 1 following perforation. RNA velocity analysis revealed transcriptional trajectories that transitioned through wounded states and ultimately returned to a more unwounded like state (**Supp. Figure 3.5M, N**). To corroborate our day 1 findings with our initial analysis that revealed the largest transcriptional shift at day 3 post-injury, we examined the shifts in UMAP space from the unwounded state to day 1 specifically and found that the day 1 wounded and unwounded pars flaccida cells were closely overlapping, indicating that the transcriptional identities immediately post-injury of the mesenchyme still largely resemble that of the unwounded state but more significant transcriptional shifts occur at later timepoints (**Supp. Fig 3.5O, P**). Notably, the unwounded pars tensa cells do not overlap with the day 1 wounded cells, which suggests a transcriptional shift within these cells upon injury. ISH of TM sections revealed Coch+ mesenchymal cells within the blastema of the healing TM

(**Supp. Fig 3.5Q**). Thus, the mesenchyme displays a robust response to wounding, coinciding with blastema formation, but following the induction and expansion of the wound epidermis.

Among immune cells, there are several populations detectable in both the wounded and unwounded states. We identified macrophages, dendritic cells, B cells, T cells, Langerhans Cells, myeloid-derived cells, and monocytes (**Supp. Figure 3.6A, B**). Within these populations, the transcriptomes showed clear differentiators between the wounded and unwounded state with distinct clusters of macrophages, myeloid derived suppressor cells, and T-cells appearing at distinct timepoints after wounding (**Supp. Figure 3.6B, C**). Canonical Markers of the major immune populations were used to identify these sub-clusters (**Supp. Figure 3.6D-H**). In examining the UMAP of immune cells labeled by timepoint, the largest transcriptional changes arise between days 1 and 3 post-injury (**Supp. Figure 3.6C**). Moreover, RNA velocity analysis shows clusters of immune cells that are unique to day 3-14 that do not appear derived from the unwounded timepoints (**Supp. Figure 3.6I**), including a distinct monocyte population, indicating potential immune cell migration into the TM from circulation. ISH for *Cd68*, a marker of macrophages and monocytes (Klinge et al. 2020), revealed an increase in this cell population over the malleus at day 7 post-injury (**Supp. Figure 3.6J**).

Finally, we examined mucosal cells for distinct subpopulations and transcriptional changes in response to injury. Although we identified distinct ciliated and non-ciliated mucosal cells, we did not identify any populations specific to the wounded state.

Injury leads to the development of a specialized wound epidermis

We next sought to more deeply characterize the initial response of keratinocytes following injury. We investigated whether the cells responding to injury were progeny of a pre-existing K5+ population of stem cells in the TM. *Krt5-CreERT2;R26R-Confetti* mice were administered a single dose of 30 mg of tamoxifen to label a minimal subset of resident stem and progenitor cells. The TMs were injured 3 days later and harvested at various timepoints to visualize the K5+ daughter cells (**Figure 3.4A**). In unwounded TMs, we observed rare K5+ cells over the malleus and PF, with little evidence of subsequent expansion or migration. In contrast, in wounded TMs, we observed an expansion of K5+ lineage-traced cells as early as 12 hours following perforation, predominantly over the malleus and at the junction of the PF and PT (**Figure 3.4B**). On days 1-7, there was further expansion of K5+ lineage-traced cells, and their localization shifted to the site of the wound (**Supp Figure 3.7A, B**). This is consistent with rapid expansion of a K5+ population in the stem/progenitor niches of the TM within 24 hours post-injury, with subsequent migration to the site of injury.

Given the rapid proliferative and migratory responses we observed, we next sought to characterize the transcriptional events within the keratinocyte populations. We first investigated the keratinocyte shifts occurring on the first day post-injury by merging and re-clustering the unwounded and day 1 datasets. We found that keratinocytes generally expressed a distinct transcriptional program by one day following wounding (**Supp. Figure 3.7C**). Furthermore, we identified a subpopulation of keratinocytes that expressed genes

distinct from any seen during homeostasis (**Figure 3.4C, Supp Figure 3.7D, E**). We hereafter refer to this novel and transient population as the “wounded epithelium”. In contrast, the other keratinocyte populations had high differential expression of genes that more clearly aligned with markers seen at homeostasis, such as *Fam213a*, *Fcgbp*, *Dst*, and *Apoe*, and likely represent less radically transcriptionally shifted versions of these populations. The wounded epithelium’s highest differentially expressed transcripts were for genes not expressed in unwounded keratinocytes, such as *BC100530*, *Odc1*, and *Gpr15L* (**Figure 3.4C**). There were 167 genes that separated this population from all other keratinocyte populations at day 1, when filtered for at least a two-fold change in average differential expression. This wounded epithelium persisted through day 7 but had largely dissipated by day 14, with top markers of the wounded epithelium no longer detectable (**Figure 3.4D-E**). We used ISH for *Gpr15L*, one of the top three differentially expressed genes in this population, to identify the spatial localization of this population through the time course of repair (**Figure 3.4G**). Cells positive for *Gpr15L* first appeared over the malleus on day 1 post-injury and then around the wound site at later timepoints (**Figure 3.4G, H**). This localization is consistent with the expansion and migration of the K5+ lineage-traced population that we had observed earlier.

The wounded epithelium activates Egfr signaling

Among the top upregulated genes within the wounded population were *Amphiregulin* (*Areg*), *Epigen* (*Epgn*), *Heparin-binding Egf* (*Hbegf*), *Epiregulin* (*Ereg*), and *Tgfa*, all ligands of Egfr (B, G, and R) (2016) (**Figure 3.4C**). *Areg* expression appeared to closely overlap with *Gpr15L* expression in the keratinocyte populations (**Figure 3.5A**). Thus, we hypothesized

that the wounded epithelium may be activating signaling through the Egfr pathway and that activation of this pathway may be required for TM regeneration.

To test whether the increase in *Areg* expression was specific to the post-injury state of the TM, we queried the merged dataset of keratinocytes from all timepoints. We found that *Areg* was maximally expressed in day 3 keratinocytes (**Figure 3.5B**). Using IF, we observed that *Areg* was present in keratinocytes from day 1 to day 7, initially localized to the malleus and shifting to keratinocytes around the wound site at day 3 (**Figure 3.5C**). This expression pattern was consistent with levels and localization of *Areg* mRNA detected via ISH (**Supp Figure 3.8A-C**). This spatial and temporal distribution matched that seen previously in the wounded epithelium (**Figure 3.4B, H**).

We next sought to decipher whether *Areg* was acting in an EGFR-independent (Stoll et al. 2016) or dependent fashion, as both mechanisms had been reported to drive keratinocyte proliferation. Using IF, we stained for pEGFR at various timepoints post-injury and found a robust increase in pEGFR signal (**Figure 3.5D**). The spatial localization of pEGFR and *Areg* was consistent with the pattern of EGFR expression over the malleus and at the wound site on day 3 (**Figure 3.5E-G**) and corresponded to the localization of *Areg* RNA (**Figure 3.5H, I**). We next co-stained for pEGFR and *Gpr15L* RNA and identified a subset of *Gpr15L*⁺ cells that were positive for pEGFR (**Supp. Fig 3.8H, I**). Thus, EGFR signaling appears to be activated in an autocrine fashion within the wounded epithelium.

Deletion of *Egfr* abrogates the TM's rapid proliferative response to injury

To test whether EGFR signaling was required for TM regeneration, we generated a genetically engineered mouse model that allowed for conditional deletion of *Egfr* in keratinocytes (*K5-CreERT2;Egfr^{fl/fl}:R26^{mTmG/mTmG}*) (**Figure 6A**). We also utilized the *mT/mG* Cre reporter, in which cells heritably convert from tdTomato⁺ to EGFP⁺ in response to Cre recombinase expression (Muzumdar et al. 2007). With this mouse model, cells in which *Egfr* is deleted will thus express EGFP. We administer tamoxifen for 5 sequential days to induce Cre activity and then perforated TMs 24 to 48 hours after the last injection to ensure complete degradation of EGFR protein, which has a half-life of 6-24 hours (Ray et al. 2016; Greig et al. 2015) (**Figure 3.6B**). IF staining for EGFR confirmed the absence of EGFR protein in the TM (**Supp. Figure 3.8J-K**). Macroscopically, TMs with tissue-specific deletion of *Egfr* did not initially generate the same large tissue mass in response to injury observed in wild-type mice (**Figure 3.6C, 3.1B**). The day 3 timepoint showed no gross changes from the earlier timepoints. By day 14, when EGFR wild-type TMs had normally grossly repaired, the perforations had failed to close in the EGFR KO mice (**Figure 3.6C**). We examined H&E-stained cross sections of perforated TMs from EGFR KO mice and again observed neither a large build-up of tissue nor closure of the wound by day 7 (**Figure 3.6D**). In order to determine if the EGFR KO mice had a proliferative defect following wounding, we administered EdU 2 hours prior to harvesting of the TM. Whereas wild-type EGFR⁺ TMs showed a robust proliferative response to injury, EGFR KO TMs showed significant reductions in the number of EdU-labeled cells, particularly on days 1 and 3 (**Figure 3.6**). Thus, the initiation of the injury response and tissue mass accumulation appear contingent on the presence of EGFR. Evolutionarily, *Areg* appears to be fairly

conserved across mammals (**Supp. Figure 3.8L**), suggesting a potential role for EGFR signaling via Areg activation in other mammalian species. We conclude that *Gpr15L*+ *Areg*+ cells activate EGFR signaling likely in an autocrine fashion, driving the initiation of the regeneration program of the TM (**Figure 3.6F**).

3.4 Discussion

The data presented here serves to define and provide an initial characterization of adult mammalian regeneration under physiological circumstances without genetic or pharmacologic manipulation. We provide a computational and molecular characterization of epimorphic regeneration of the tympanic membrane after it has suffered a full-thickness injury. We performed single-cell RNA sequencing to provide an unbiased and comprehensive roadmap of this multi-tissue regenerative process. We highlight the populations that have previously been described to exist within the TM at homeostasis (Frumm et al. 2021) and show how these populations are transcriptionally altered throughout regeneration. Moreover, our results show that there are novel cell populations that arise during regeneration, providing us important insight to candidate molecular signals that drive regeneration.

TM wound healing is via epimorphic regeneration

Herein we characterize repair of the adult murine TM and present data supporting our postulation that wound healing of this tissue occurs by epimorphic regeneration.

Epimorphic regeneration is perhaps best-described in the axolotl limb (JD et al. 2016; Kragl

et al. 2009) and is defined by: (1) induction of a unique wounded cell population, (2) creation of a multilineage blastema, and (3) scar-free resolution of injuries. These features are typical of systems in vertebrates more classically defined as having the capacity for epimorphic regeneration (Haas and Whited 2017). The gross and microscopic histological phenomenology that we have described in this work appears to occur similarly in all other mammals previously studied including humans (Lou, Tang, and Yang 2011), rats (Yilmaz et al. 2021), chinchillas, dogs, and guinea pigs (Wang AY et al. 2014). This suggests that this regenerative response is a general phenomenon of mammals, rather than being a peculiarity of an individual mammalian species.

A wounded keratinocyte population is formed during TM healing

TM perforations are distinct from other epidermal wounds because they are full-thickness—i.e. they involve the epidermal, mesenchymal, and mucosal layers of the TM. Additionally, owing to the anatomic position of the TM, no underlying tissue scaffold exists to guide regeneration. Prior histological studies of the healing TM and the data shown here indicate that keratinocytes seem to be the first cell type responding to tissue injury (Chari et al. 2019). This is again unique from other epidermal wounds, where the first steps in repair require coagulation and formation of granulation tissue (containing macrophages, fibroblasts, and extracellular matrix (ECM) components (Sorg et al. 2017)), which is followed by and thought to be a prerequisite for effective epithelialization (Sorg et al. 2017; Rittié 2016). With single-cell RNA sequencing of TMs throughout a wound-healing time course, we confirmed that the earliest transcriptional shifts do indeed occur in the keratinocytes. Furthermore, we discovered that there is a unique population of

keratinocytes that emerges only after tissue injury, which we have termed the “wounded epithelium.” Based on its transcriptional signature, this population does not appear to be derived from a pre-existing stem cell population, which is remarkably similar to what has been documented in single-cell data of the initial wound response in the axolotl (Gerber et al., n.d.).

A multilineage blastema forms in the healing TM

Epimorphic regeneration in other vertebrates relies on the wounded epidermis to induce multiple lineages of cells to de-differentiate and form a blastema which continues the process of faithfully regenerating the injured tissue (LJ and CM 2008; CS 1957; AL 1976; Stocum 2017). Through our lineage-tracing experiments (**Figure 3.4A, B**), we outlined the migration of cells from the known proliferative centers of the TM (SM et al. 2021) to the perforation site. At day 1 post-injury, computationally and biologically, we validated the appearance of an undifferentiated transient keratinocyte population that only exists on the TM during regeneration, dissipating by day 14 (**Figure 3.4G**). This proposed migration pattern and emergence strongly suggest blastema-driven regeneration in the TM like that of other non-mammals. The volumetric tissue response seen within the TM (**Figure 3.1B, 2B**) coupled with our data that highlights a new wounded epidermis (**Figure 3.4**) shows a strong similarity to the wounded epidermis and resulting blastemal bud seen in axolotl regeneration (Wong AY and JL 2020).

Another tenet of epimorphic regeneration is level-specific replacement of tissue. We show here that the epidermal and mesenchymal cell populations undergo transcriptional shifts

in regeneration of the TM (**Figure 3.3**). How the different layers communicate in TM regeneration is an area for future investigation, particularly within the multi-lineage blastema containing mesenchymal and immune cells.

The TM undergoes scar-free repair

A key aspect of epimorphic regeneration is scar-free repair. In general, mammalian tissues are understood to have an extremely limited capacity to regenerate faithfully (Xia et al. 2018). At the embryonic stage, mammals have the capacity for scar-free healing and regeneration, but this is quickly lost upon maturation (Porrello et al. 2011; Tsonis and Fox 2009). Here, we demonstrate that the murine TM undergoes scar-free repair, as evidenced by the restoration of the organization of collagen fibers in the healed TM (**Figure 3.2G**). This is very unlike what is seen in other reportedly regenerative organs in the adult mammal, like the liver and skin, in which although function restores, the tissues grossly retain a remnant of the injury (Stanger 2015) (KAU and E 2017). Not only does the TM display scar-free repair, but it performs this mechanism under the circumstances of a full-thickness wound and while being suspended in thin air, giving understanding TM regeneration important applications in the field of epithelial pathological scarring.

Recent reports demonstrated in mice that scar-free repair of skin may be possible by mechanical, genetic, or pharmacological manipulations that prevent fibrogenic *Engrailed-1* positive fibroblasts from emerging during healing (S et al. 2021). The work we are reporting here complements and extends that work to demonstrate a tissue where epimorphic regeneration is possible under physiological circumstances even without these

manipulations. Indeed, based upon our scRNA-seq data we did not detect *Engrailed-1* expression in TM fibroblasts throughout the injury time-course. It remains to be seen if circumstances that lead to chronic perforation in humans show scarring and activation of this population.

Egfr signaling is required for TM wound healing

Lastly, we identified the ligand of Egfr, *Areg*, as having a large transcriptional increase in the early stages of TM regeneration with levels restoring back to homeostatic levels by day 14 (**Figure 3.5B**). Interestingly, *Areg* has been shown to be rapidly induced in the wound epidermis of the axolotl post-limb amputation (Bryant et al. 2017). However, in the axolotl limb, *Areg* expression quickly subsides in normal regeneration, and if *Areg* is aberrantly over-expressed, the limb actually does not regenerate properly, exhibiting epithelial thickening and impaired internal proliferation (Bryant et al. 2017). Thus, our findings of a large spike then rapid decrease in *Areg* expression in the post-perforation TM directly aligns with other regenerative processes. We were able to genetically modulate Egfr signaling via a conditional knockout mouse where Egfr was deleted from keratinocytes – this resulted in a complete dissipation of the rapid, robust proliferative response to injury we normally see on the TM as well as an inability for TMs to close the injury at all, which indicates that Egfr activation is necessary for the regeneration of the TM.

Implications and Future Directions

Taken together with this previous work, this work suggests that the potential for epimorphic regeneration is not lost in adult mammals. Our results show that there are

novel cell populations that arise during regeneration, providing us important insight to what molecular signals drive regeneration. We anticipate that a deeper understanding of the process of epimorphic regeneration in the adult mammal TM will permit us to better uncover the critical roadblocks to regeneration in clinical TM conditions, such as chronic TM perforation, as well as in other mammalian tissues. This may ultimately bring us closer to driving whole tissue and organ regeneration in diverse tissues in humans.

Figure 3.1

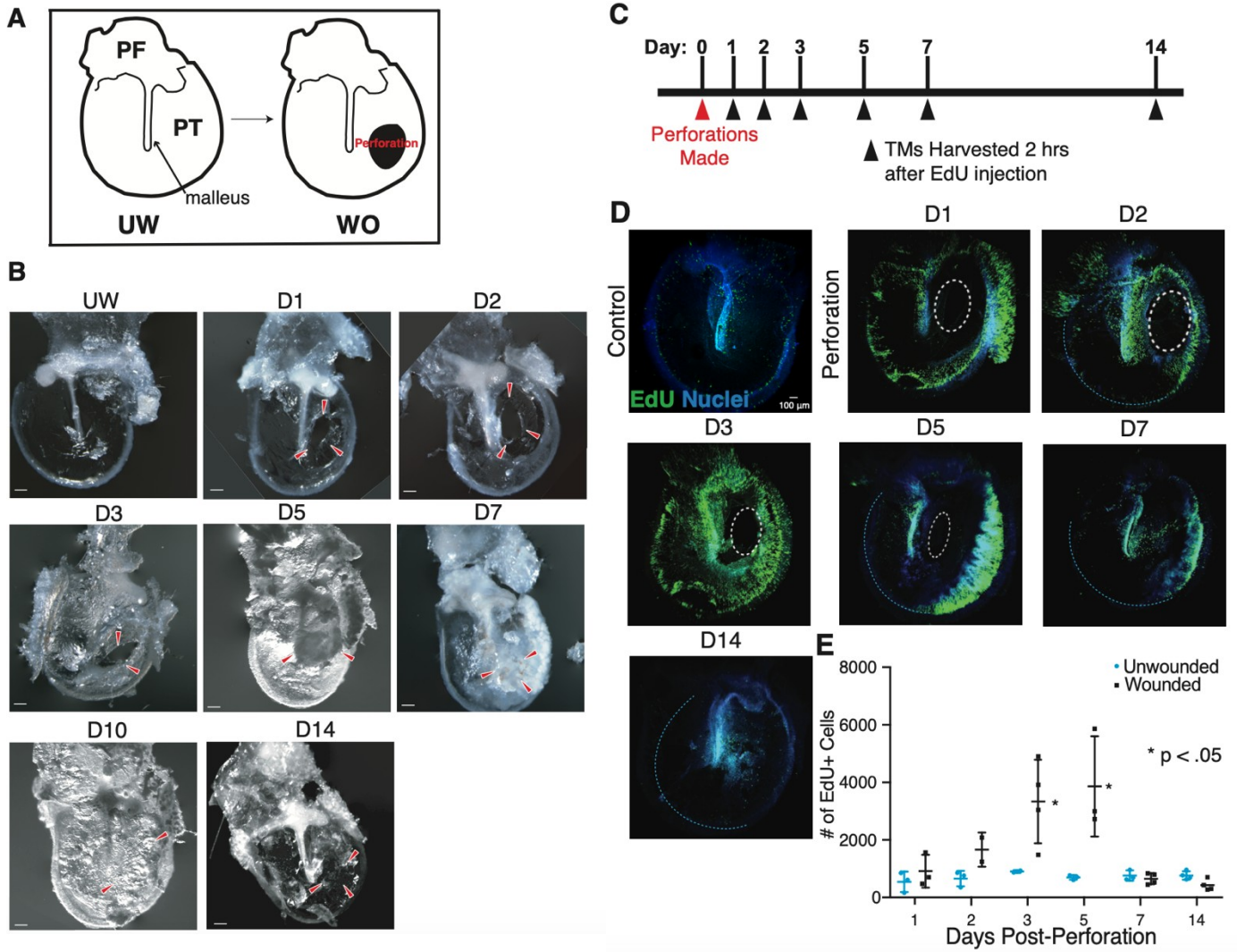


Figure 3.1: The TM displays a rapid and robust proliferative response to injury macroscopically. (A) Representative image of a murine TM dissected en bloc to include the pars flaccida (PF) and pars tensa (PT) (left panel). Perforations were made in the anterior PT (right panel). (B) Representative wild-type murine TMs harvested from different mice at the indicated timepoints post-perforation. Red arrowheads indicate the site of perforation and gross resolution over time. (C) To characterize the proliferative response to injury, perforations were created in the left TMs of mice on day 0. On days 1, 2, 3, 7, and 14, EdU was injected IP 2 hours prior to TM harvest. (D) Edu-labeled whole-mount TMs demonstrate a peak proliferative response 3 days post-injury, with resolution by day 14. White dashed circles indicate the perforation. (E) Graph of number of EdU+ cells in a 400 x 1200 μm area over the malleus in response to injury. Results of t-tests for WO vs UW TMs at a single time-point are indicated with the black bars; * $p < 0.05$. Scale bars: (B) 200 μm (D): 100 μm .

Figure 3.2

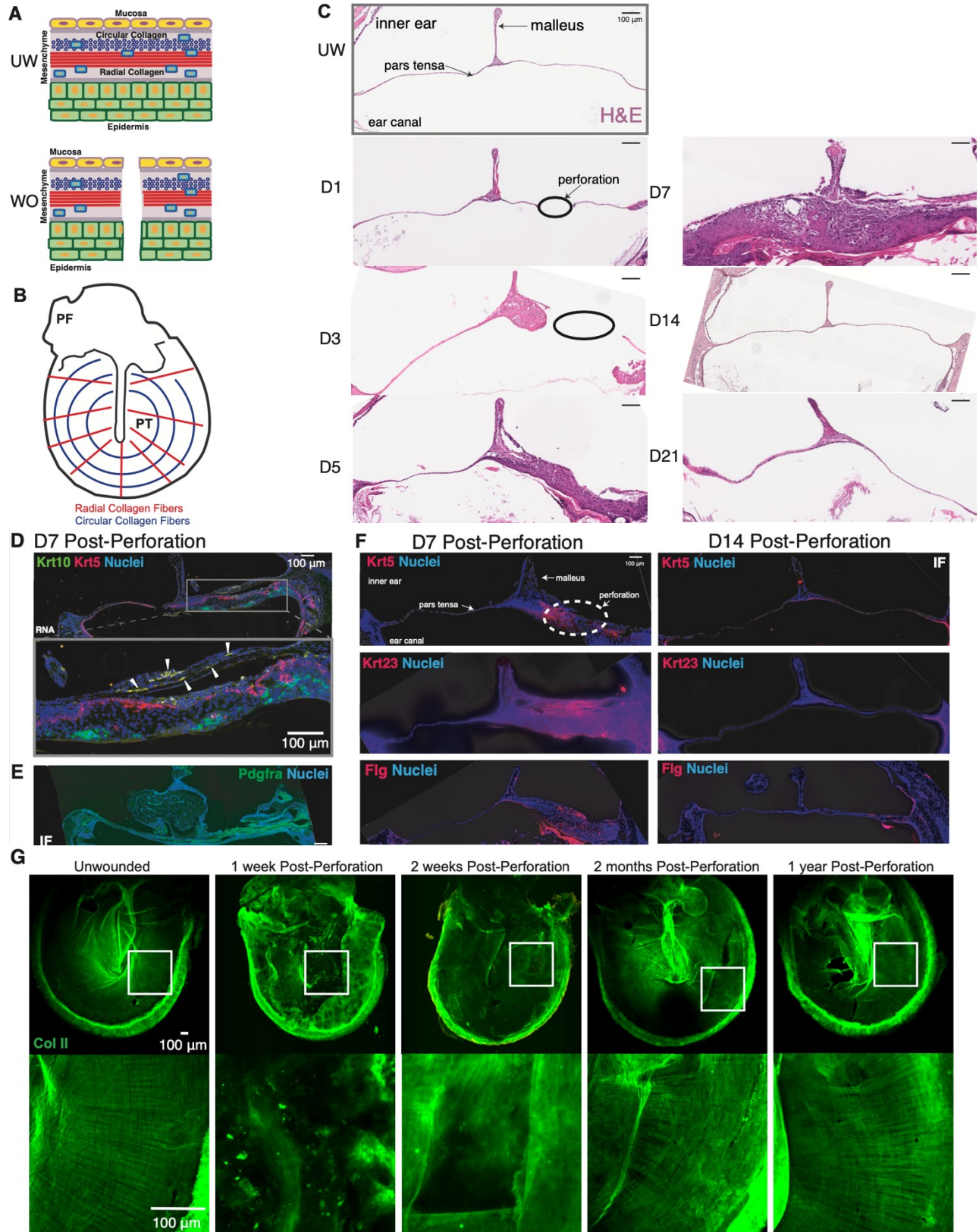
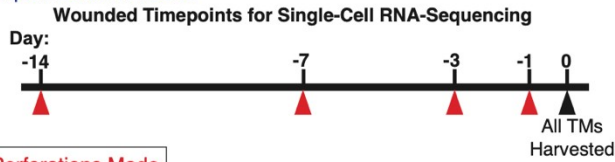


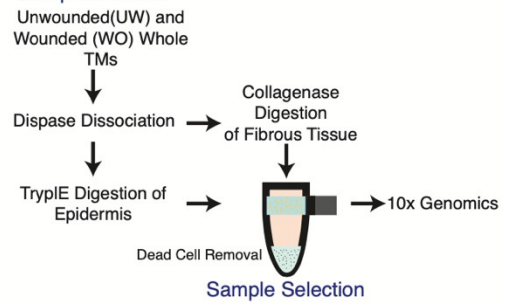
Figure 3.2: The TM regenerates without permanent scarring. (A) A cross-sectional view of the TM demonstrates the three major layers: inner mucosa, middle mesenchyme, and outer epidermis. When wounded, the injury crosses all 3 layers. (B) The mesenchymal layer contains two layers of inner circular and outer radial collagen fibers. (C) Hematoxylin and Eosin (H&E) stained sections of the TM at the level of the perforation mid pars tensa at multiple time points following perforation. Tissue stratification peaks at Day 7 and resolves by Day 21. The epidermal layer is oriented downward, and the black circle indicates the site of the perforation. (D) RNAscope showing expression of *Krt5* (red) and *Krt10* (green) in a cross-section of the TM from day 7 post-injury, illustrating transient mixed stratification within the epidermis. The yellow magnified region highlights an area directly over the wound site. White arrows denote cells co-expressing *Krt5* and *Krt10*. (E) IF for *Pdgfra* in a TM cross-section from day 7, demonstrating the newly formed multi-lineage stratification of the TM. (F) Immunofluorescence (IF) for *Krt5*, *Krt23*, and *Flg* in TM cross-sections from day 7 and day 14 post-injury, demonstrating expansion and quick dissipation of cells positive for these markers. (G) IF for COLII (green) in representative whole-mount TMs harvested at the indicated timepoints post-injury reveals restoration of normal collagen patterning of the TM by year 1 (n=5 mice per timepoint, except n=3 for 1 year). Scale bars: 100 μ m

Figure 3.3

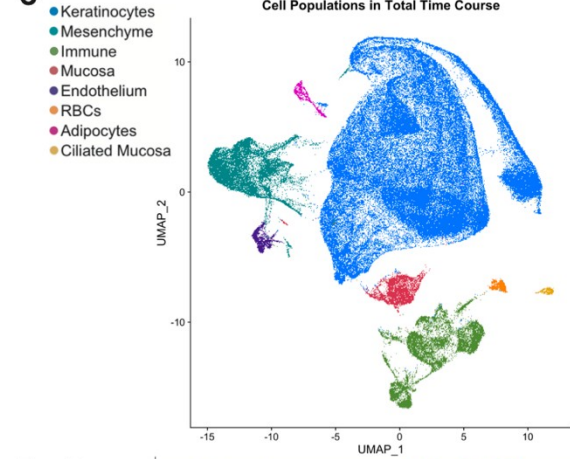
A Experimental Timeline:



B Sample Isolation



C Cell Populations in Total Time Course



E

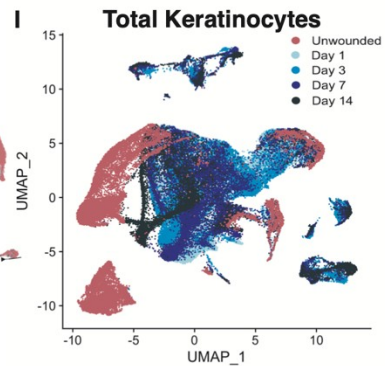
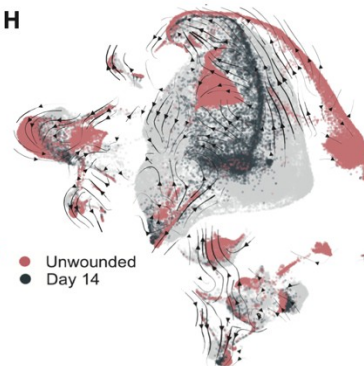
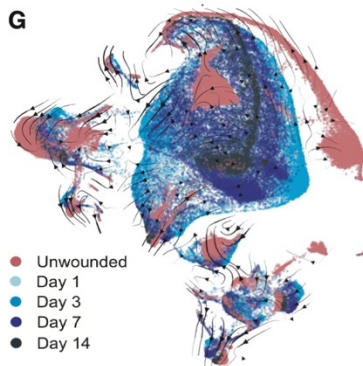
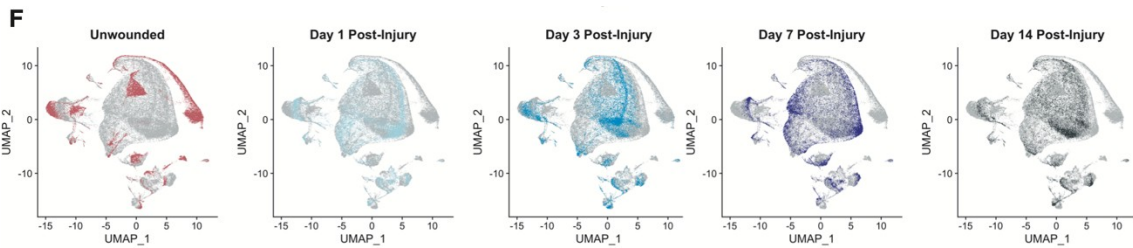
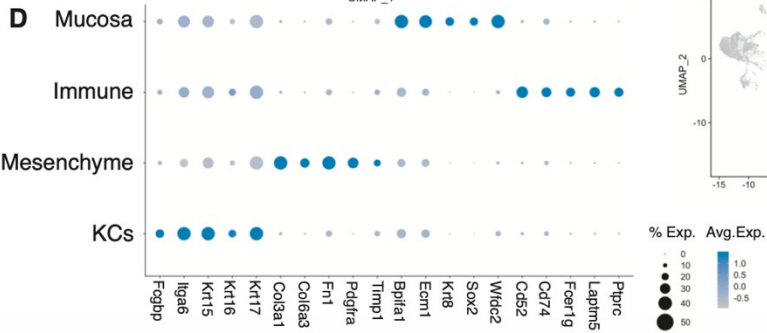
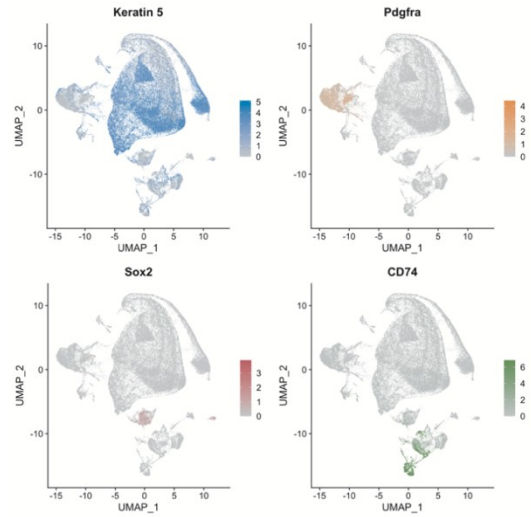


Figure 3.3: Single-cell RNA sequencing (scRNA-seq) reveals the transcriptional shifts of the regenerating TM. (A) TMs at various timepoints post-perforation were harvested and processed at the same timepoint. (B) Single cells were isolated from unwounded and wounded TMs for scRNA-seq. (C) UMAP visualization of all cell clusters in the merged scRNA-seq data, including wounded and unwounded states, compiled and analyzed by Seurat. (D) UMAP plots showing expression of *Krt5* in the KCs, *Pdgfra* in mesenchymal cells, *Sox2* in mucosal cells, and *Cd74* in immune cells. (E) Dot Plot highlighting top marker genes of the KC, mesenchymal, mucosal and immune cell populations. (F) UMAP plots highlighting the cells based on which unwounded/wounded timepoint they originated from. (G-H) Separate UMAP visualizations of all of the unwounded and wounded cells with RNA velocity vectors super-imposed, calculated using the scVelo package with all cells highlighted (G) and with only the unwounded and day 14 cells highlighted (H). (I) Separate UMAP visualization of KCs from all timepoints, which were re-clustered independent of other cell types. Cells are highlighted based on their original injury timepoint.

Figure 3.4

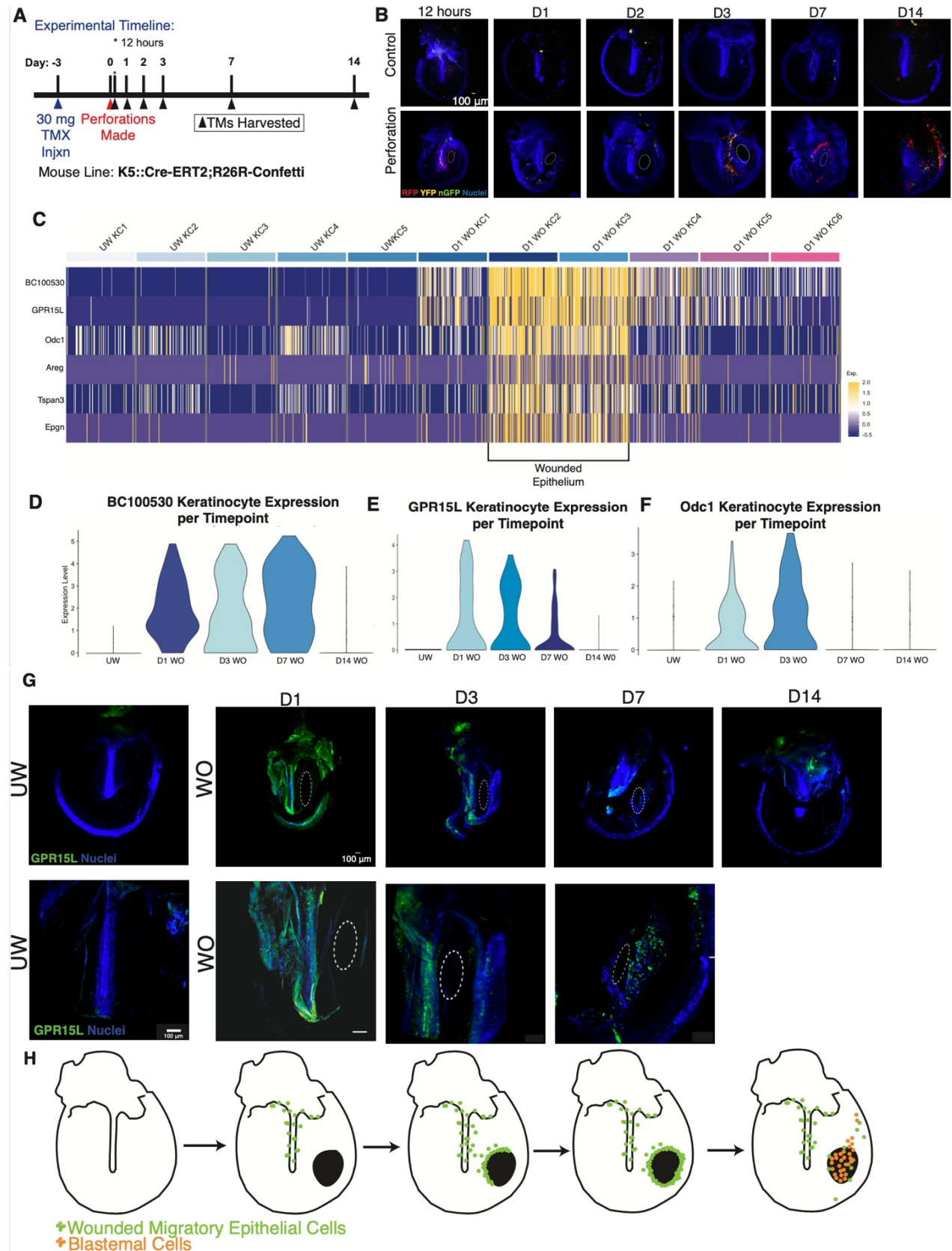


Figure 3.4: A migratory wounded epithelium forms within one day post-injury. (A) *Krt5-CreERT2;R26R-Confetti* mice were injected with a single dose of 30 mg of tamoxifen 3 days prior to TM injury to induce minimal labeling of TM KCs. Perforations were made in the left TMs of mice on day 0, and both TMs were harvested at the indicated timepoints. (B) Control TMs from the right ear (top row) show sparse labeling with the Confetti reporter. Perforated TMs from the left ear (bottom row) show increased labeling over the malleus at early timepoints, with a concentration of labeled cells at the site of injury at later timepoints (n=5 mice per timepoint. White dotted circles indicate the perforation (C) Heat-map showing expression of top genes associated with the wounded epithelial cell state in KC clusters from the unwounded TM and day 1 post-injury. Each column represents a single cell. (D-F) Violin Plots showing expression of *BC100530* (D), *Gpr15L* (E), and *Odc1* (F) in KCs from each timepoint. (G) RNAscope for *Gpr15L* (green) expression on whole-mount TMs throughout the regenerative time course (top row). Higher magnification regions show expression of *Gpr15L* (green) over the malleus at day 1 and near the perforation by day 7 (bottom row), suggesting migration of the wounded epithelium. Scale bars: 100 μ m (H) Cartoon model of the origination and migration of the wounded epithelium on the TM.

Figure 3.5

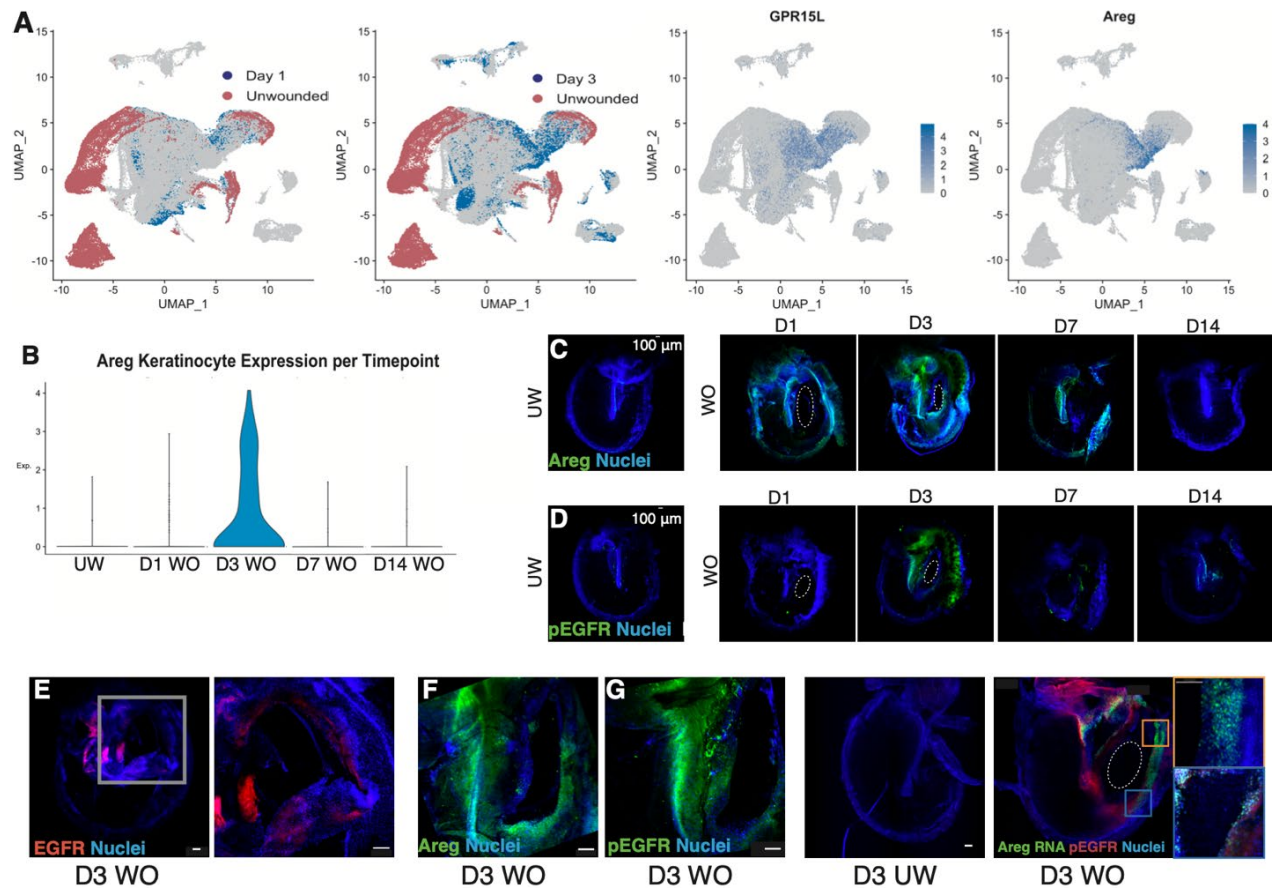


Figure 3.5: A blastema-like structure with activation of the *Egfr* pathway arises at the site of injury. (A) UMAP visualization of the KCs from all timepoints with the unwounded cells highlighted in red and day 1 or day 3 keratinocytes in blue. The right panels highlight cells with the highest expression of *Gpr15L* or *Areg*. (B) Violin plot showing expression of *Areg* in keratinocytes from each timepoint. (C-D) IF for *Areg*(C) and *pEgfr* (D) in unwounded and wounded whole-mount TMs shows peak expression of both at day 3 post-injury. White dotted circles indicate the perforations (E-G) IF for *Egfr* (E), *Areg* (F), and *pEGFR* (G) on representative whole-mount TMs from the day 3 wounded state. Higher magnification shows increased staining around the site of perforation (H-I) IF for *pEgfr* co-stained with *Areg* RNA using RNAscope on a whole-mount TM of the day 3 unwounded(H) and wounded(I) state. Panels (I') and (I'') show zoomed in images of co-localization of *Areg* and *pEgfr* from the D3 WO TM. Scale bars: 100 μ m

Figure 3.6

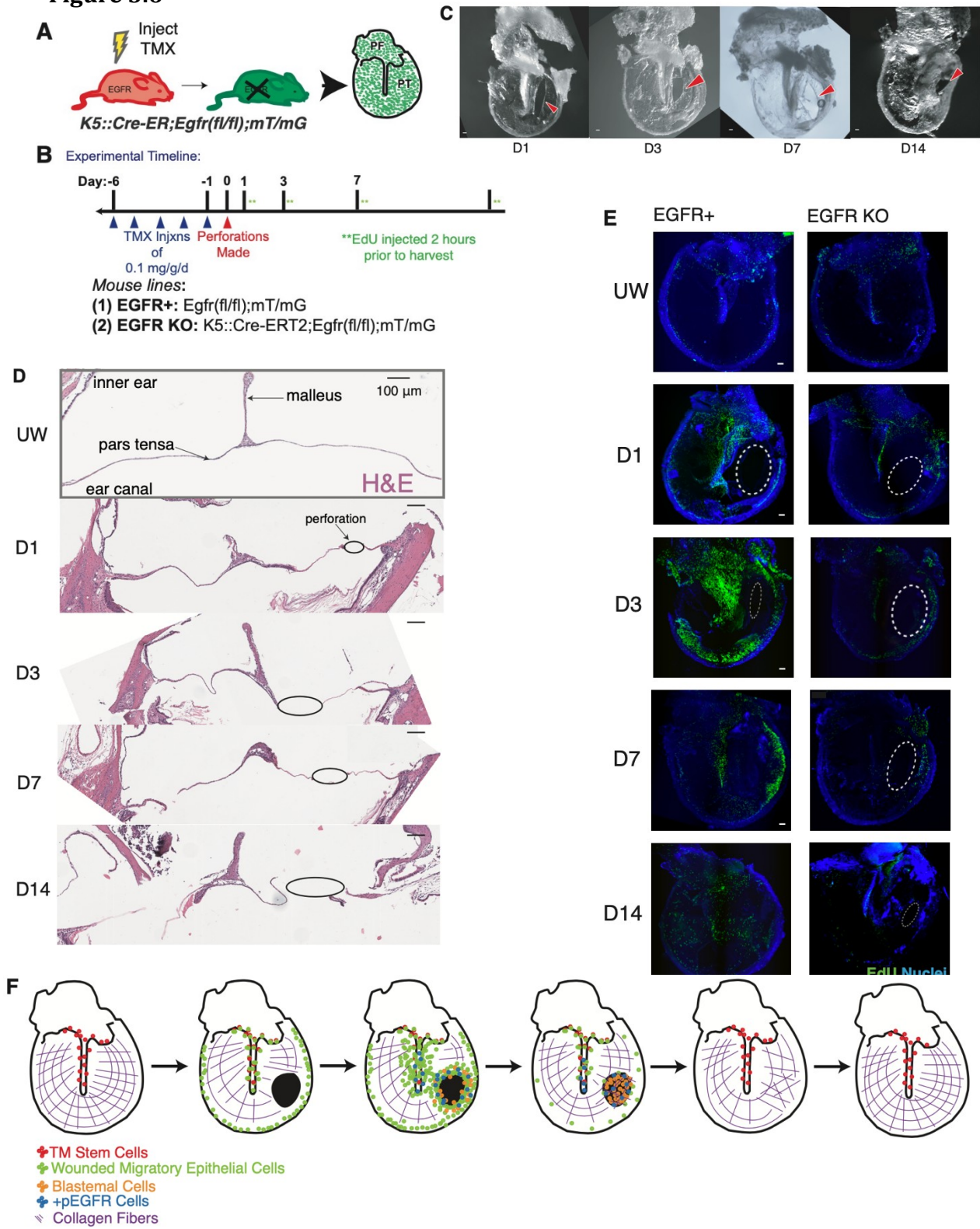


Figure 3.6: Egfr is required for the early TM regenerative response. (A) *EGFR* deletion was induced *in vivo* in adult *K5-CreERT2;Egfr^{fl/fl}; R26^{mTmG/mTmG}* mice via tamoxifen injection. *Egfr^{fl/fl}; R26^{mTmG/mTmG}* mice served as negative controls. (B) Tamoxifen was administered for five consecutive days to induce complete recombination in TM keratinocytes prior to perforation. TMs were then harvested at multiple timepoints post-injury, with EdU injection 2 hours prior to each harvest. (C) Wounded TMs isolated from different EGFR KO mice at multiple timepoints post-injury demonstrate incomplete resolution of injury. Red arrowheads indicate the site of perforation. (D) H&E-stained sections of the TM at the level of the perforation mid pars tensa at multiple time points following perforation in EGFR KO mice, showing that tissue stratification and wound closure is absent. The epidermal layer is oriented downward, and the black circle indicates the site of the perforation. (E) EdU labeling in control EGFR+ mice post-perforation (left) demonstrates peak labeling at day 3 and closure of the perforation by day 14. EdU labeling in EGFR KO mice post-perforation (right) shows a lack of a proliferative response and incomplete wound closure. White dashed circles indicate the perforation. (F) Schematic of our proposed model of TM regeneration. Scale bars: 100 μ m.

Supplementary Figure 3.1

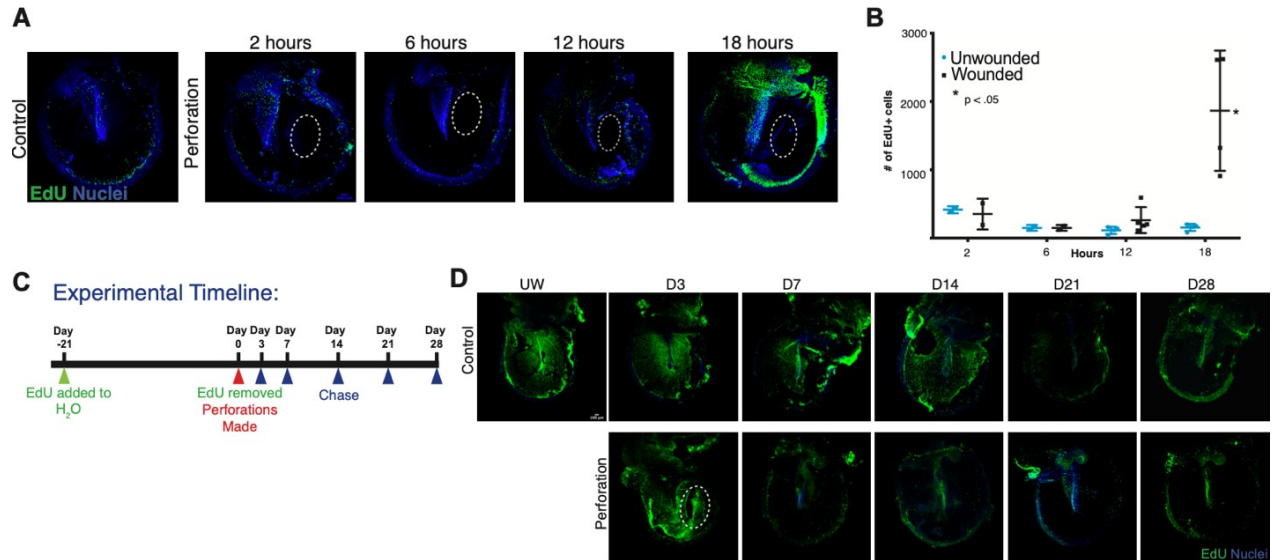


Figure S3.1: The TM undergoes a rapid, patterned response to injury. (A)

Representative whole-mount TMs from perforations created in left TMs of mice at 2, 6, 12, and 18 hours pre-harvest. EdU was injected IP 2 hours prior to the left (perforated) and right (control) TMs being harvested. The perforation is indicated with a dashed white line. (B) Graph of number of EdU+ cells in a 400 x 1200 μm area over the malleus in response to injury over 18 hours. Results of t-tests for WO vs UW TMs at a single time-point are indicated with the black bars; * $p < 0.05$. (C) Timeline describing the pulse-chase experiment. Mice were exposed to EdU continuously for three weeks (pulse), and then the EdU source was removed, the left TMs of the mice were perforated, and the label allowed to dilute for four weeks (chase). (D, E) Representative whole-mount TMs harvested without injury (D) and 3 days, 1 week, 2, 3 and 4 weeks post-injury (E) during the labeling. TMs are stained for EdU (green). Scale bars: 100 μm .

Supplementary Figure 3.2

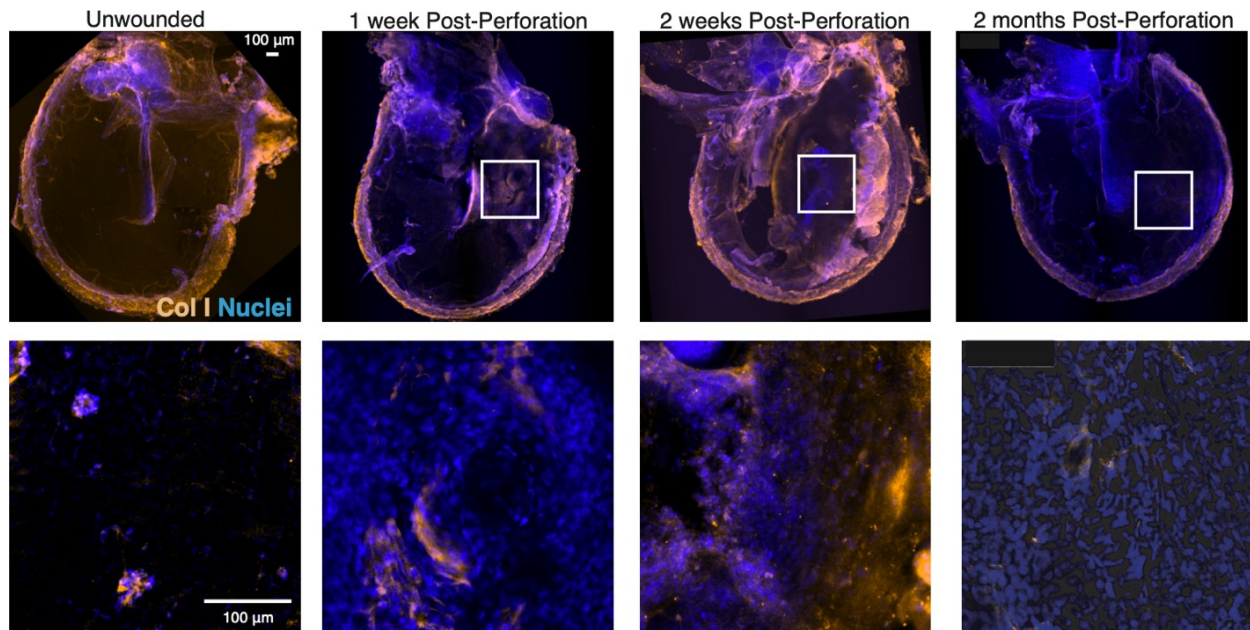


Figure S3.2: Collagen changes in response to wounding dissipate by 2 weeks. IF for Collagen I (orange) in representative whole-mount TMs harvested at the indicated timepoint post-injury to display the return to wildtype architecture (first panel) in collagen patterning of the TM. Each whole-mount represents at least an n=5. Minor artifactual staining is present at both the unwounded and 2-month timepoints. Scale bars: 100 μm.

Supplementary Figure 3.3

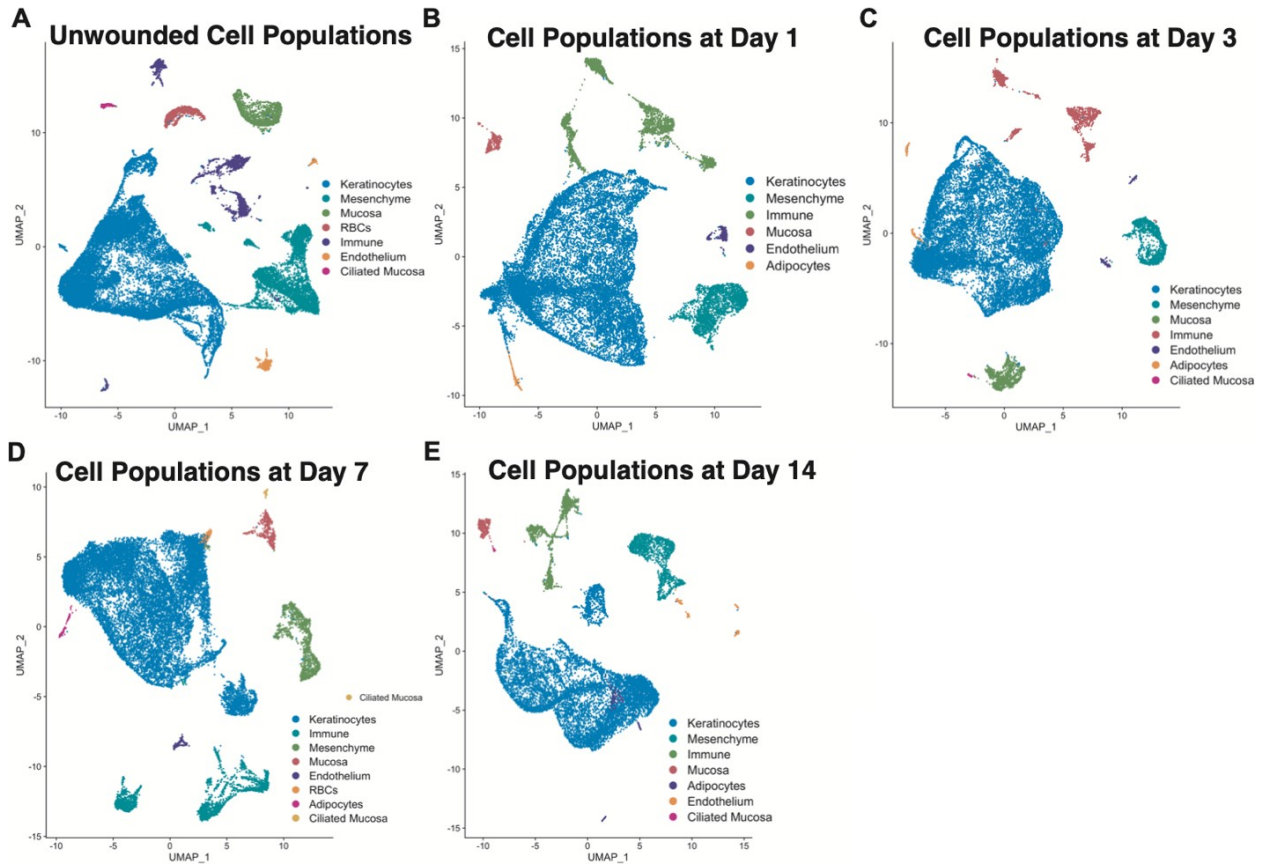


Figure S3.3: ScRNA-seq identifies major populations of cells at each timepoint during the injury response. (A-E) UMAP visualization of all cell clusters in the individual timepoint scRNA-seq data, including the unwounded state (A), day 1(B), day 3 (C), day 7 (D), and day 14(E), compiled and analyzed by Seurat.

Supplementary Figure 3.4

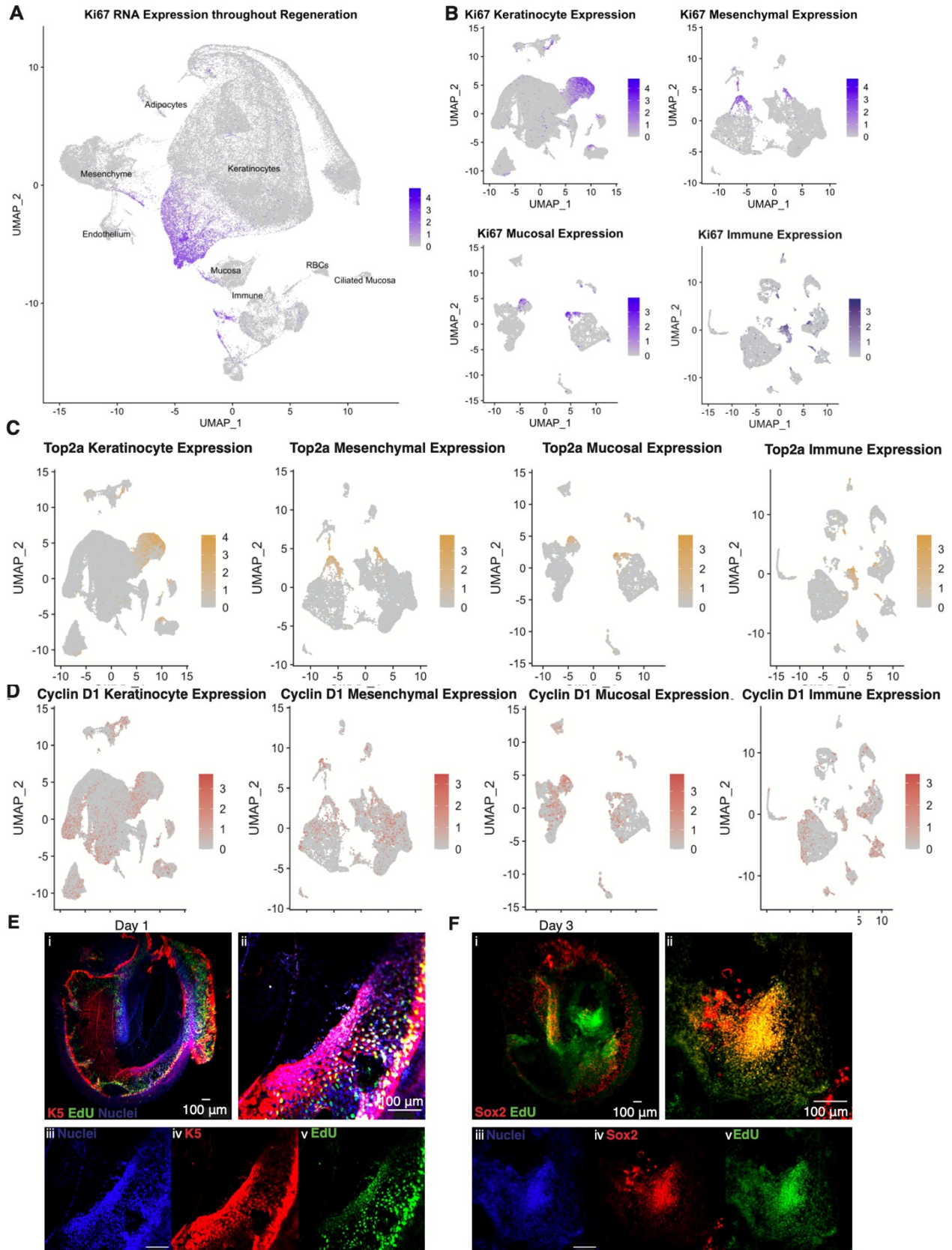


Figure S3.4: Markers of proliferation reveal turnover of all layers of the TM. (A) UMAP plot showing expression of *Mki67* in all the wounded timepoints and unwounded state cells of the murine TM. (B)- (D) UMAP plots showing expression of *Mki67* (B), *Top2a* (C), and *Ccnd1* (D) in the KC fraction, mesenchymal fraction, mucosal fraction, and immune fraction of cells from the total time course. (E) IF for Krt5 (red) co-stained with EdU (Green) in a representative whole-mount TM (i) from one day post-injury. EdU was injected IP 2 hours prior to the TMs being harvested. (ii)-(v) are 4x zoomed in panels of (i). (F) IF for Sox2 (red) co-stained with EdU (Green) in a representative whole-mount TM (i) from 3 days post-injury. (ii)-(v) are 4x zoomed in panels of (i). Scale bars: 100 μ m.

Supplementary Figure 3.5

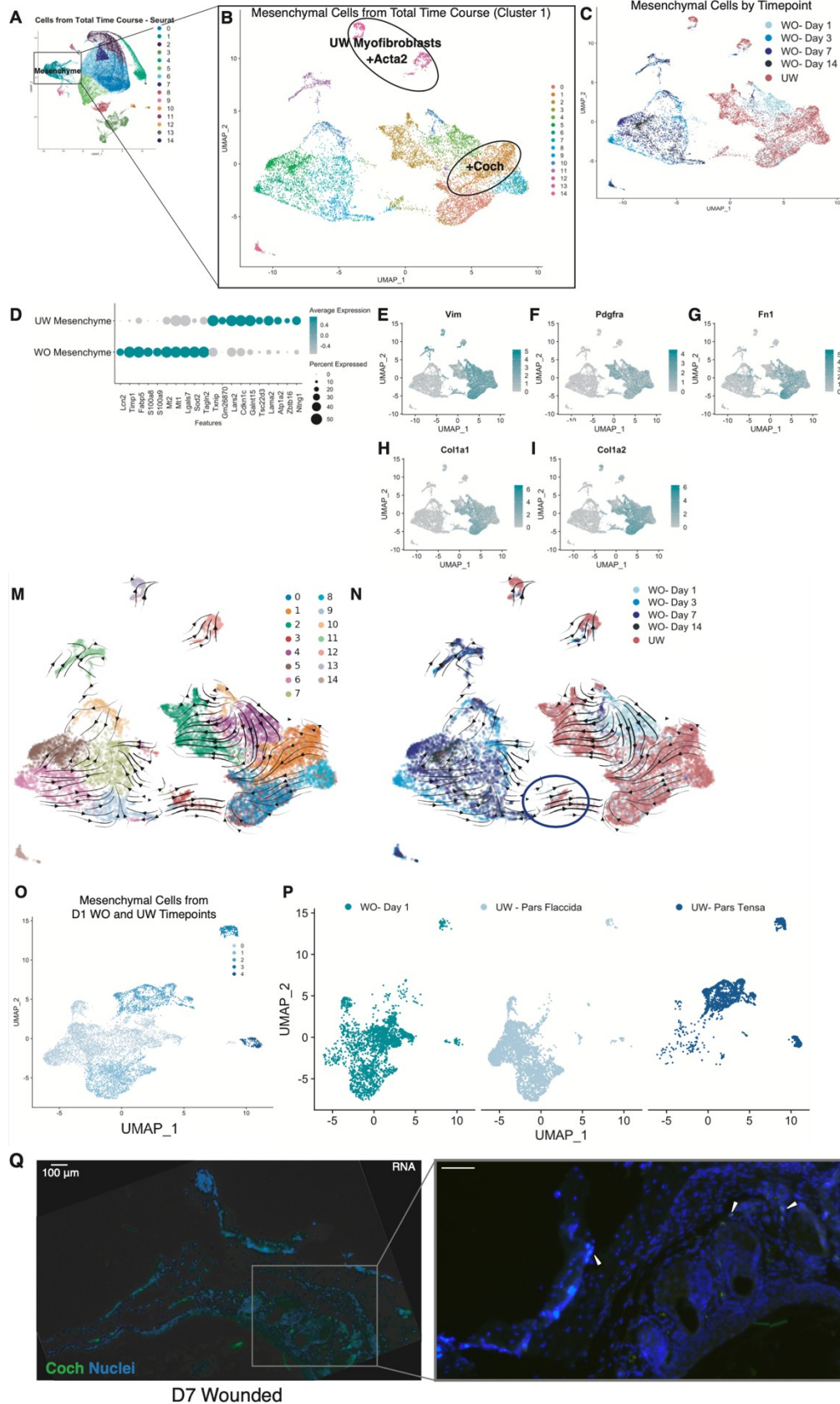


Figure S3.5: Time-course mesenchymal-specific analysis reveals distinct post-injury transitions. (A) UMAP visualization of the cell clusters identified in scRNA-Seq of all the wounded and unwounded state cells of the murine TM, compiled and analyzed by CellFindR. (B) UMAP visualization of mesenchymal cells from the original clustering, containing the mesenchymal cells from all timepoints, which were re-clustered independent from the other cell types. (C) UMAP visualization of mesenchymal cells, with the cells highlighted based on their original injury timepoint. (D) Dot Plot representation of a subset of the genes that have expression differences in the WO mesenchyme vs the UW mesenchyme. (E-I) Mesenchymal fraction UMAP plots indicating expression of (E) *Vimentin*, (F) *Pdgfra*, (G) *Fibronectin 1*, (H) *Collagen 1a1*, (I) *Collagen1a2*. (M-N) UMAP visualizations of the mesenchymal populations with RNA velocity vectors super-imposed, calculated using the scVelo package. (M) has cells clustered by their Seurat identities. (N) has cells clustered by timepoint. Blue circle in (N) highlights vectors moving from the WO to the UW state. (O) UMAP visualization of the Unwounded and Day 1 mesenchymal cells, which were re-clustered independent from the other timepoints. (P) UMAP visualization of the unwounded pars flaccida, unwounded pars tensa, and day 1 timepoints separated into panels to observe overlapping cells across conditions. (Q) RNAscope for *Cochlin* in a TM cross-section from day 7, demonstrating the newly formed multi-lineage blastema of the TM, which includes mesenchymal cells. Scale bar: 100 μ m.

Supplementary Figure 3.6

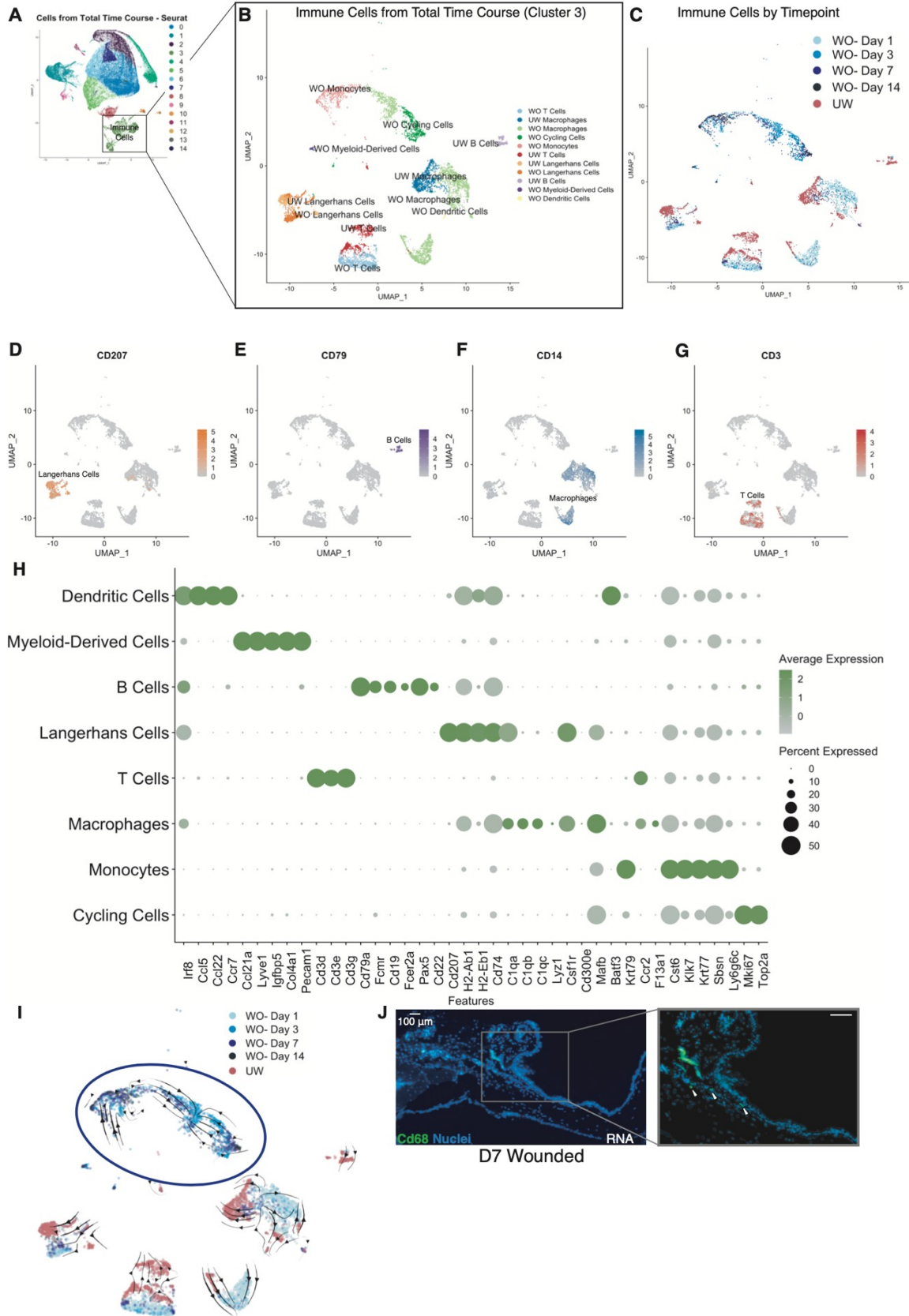


Figure S3.6: Time-course immune-specific analysis reveals distinct immune populations that arise in response to injury. (A) UMAP visualization of the cell clusters identified in scRNA-Seq of all the wounded and unwounded state cells of the murine TM, compiled and analyzed by CellFindR. (B) UMAP visualization of Cluster 3 from the original clustering, containing the immune cells from all timepoints, which were re-clustered independent from the other cell types. (C) UMAP visualization of immune cells, with the cells highlighted based on their original injury timepoint. (D)- (G) UMAP plots showing expression of (D) *Cd207* to identify Langerhans Cells, (E) *Cd79* to identify B cells, (F) *Cd14* to identify Macrophages, and (G) *Cd3* to identify T cells. (E) Dot Plot visualization of top marker genes for each major immune sub-population present in the TM during regeneration. (I) UMAP visualization of the immune populations with RNA velocity vectors super-imposed, calculated using the scVelo package with cells clustered by timepoint. Blue circle indicates wounded immune cells unique to day 3-14. (J) RNAscope for *Cd68* in a TM cross-section from day 7, demonstrating the newly formed multi-lineage blastema of the TM, which includes immune cells. Scale bar: 100 μ m.

Supplementary Figure 3.7

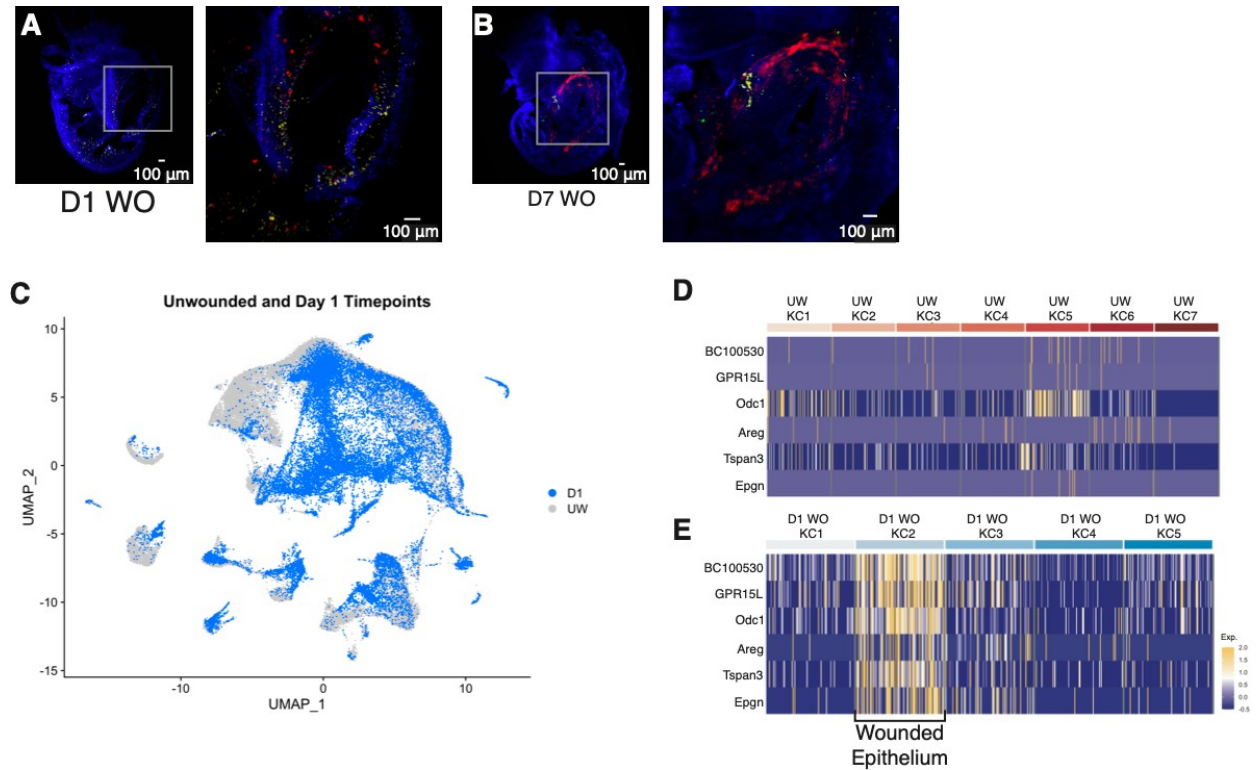


Figure S3.7: Computational analyses of the 1-day post-injury dataset reveal a transcriptional signature for a novel and transient wounded epithelium. (A) Representative whole-mount TM from 1 day post-injury of a *Krt5-CreERT2;R26R-Confetti* mouse injected with a single dose of 30 mg of tamoxifen 3 days prior to injury to induce minimal labeling of cells. Perforations were created in left TMs of mice on day 0, and the right(control) and left(perforated) TMs were harvested at the indicated timepoint. The injury is outlined with the gray box. Right panel is zoomed in view of the TM corresponding to the location of the box. (B) Representative whole-mount TM from 7 days post-injury from experiment described in (A). Each TM represents an n of at least 5. (C) UMAP visualization of the subset of cells from the Day 1 wounded and unwounded state of cells, re-clustered and colored by timepoint to display the transcriptional shift immediately post-perforation. (D-E) Heat-map showing expression of top genes associated with the wounded epithelium state of the TM in the KC clusters from the unwounded TM (D) and day 1 (E) regenerating TM. Yellow indicates high expression and blue low expression. Each column is a single cell. Scale bar: 100 μ m.

Supplementary Figure 3.8

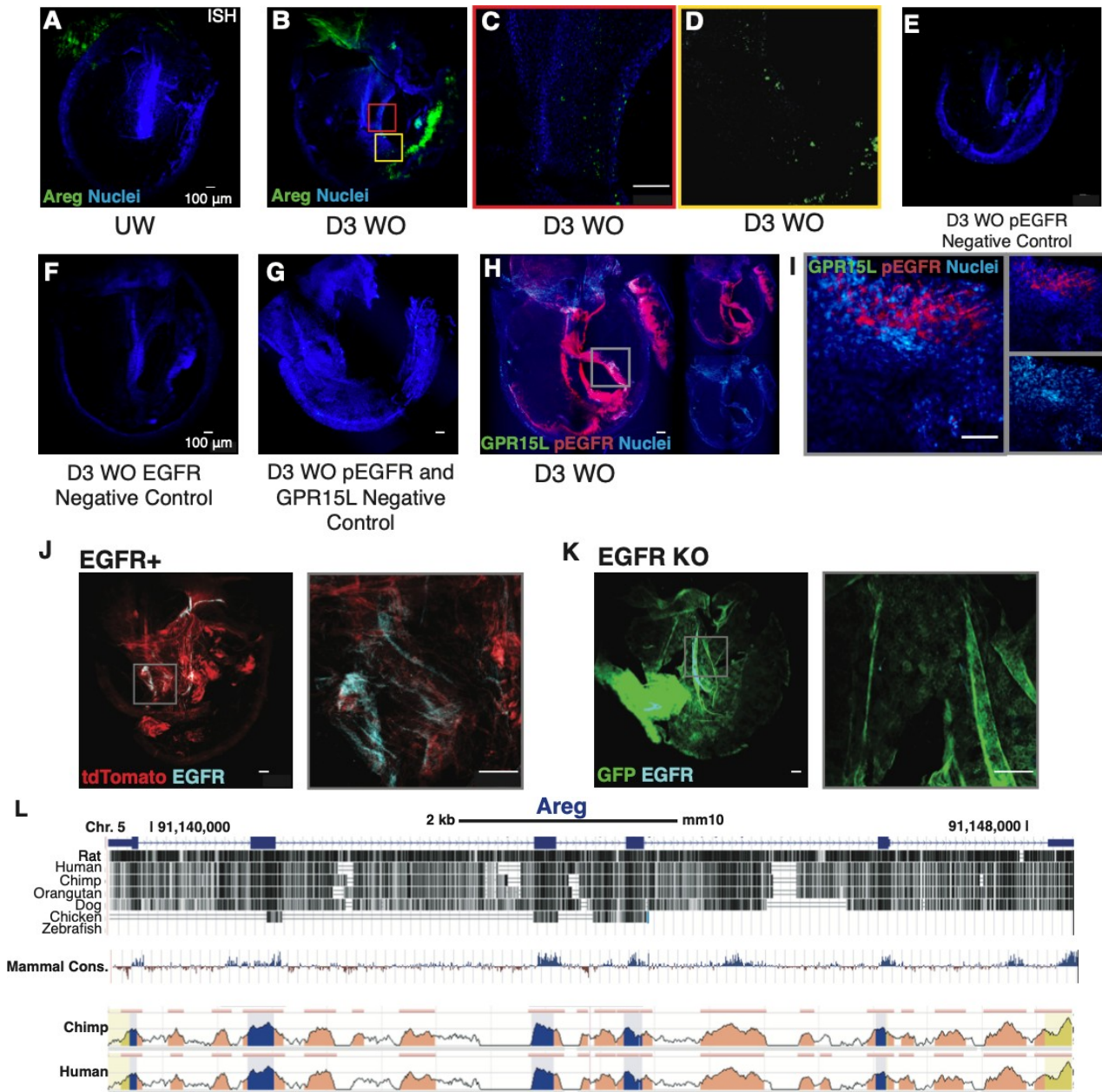


Figure S3.8: Areg RNA expression identifies activated keratinocytes in response to injury. (A-D) RNAscope for *Areg* (green) on representative whole-mount TMs from the unwounded state (A) and day 3 post-injury (B) from wild-type mice. (C-D) represent zoomed in images of the day 3 WO TM corresponding to the gray boxes in (B). (E) Day 3 wounded TM stained with Alexa 488 anti-rabbit secondary to control for artifactual staining for pEGFR experiments. (F) Day 3 wounded TM stained with Alexa 555 anti-rabbit secondary to control for artifactual staining for Egfr experiments. (J-K) IF for Egfr in representative unwounded whole-mount TMs from an *Egfr^{fl/fl}; R26^{mTmG/mTmG}* ('EGFR+') mouse (J) and a *K5^{Cre-ERT2/+}; Egfr^{fl/fl}; R26^{mTmG/mTmG}* ('EGFR KO') mouse (K) injected with tamoxifen. Zoomed in images demonstrate absence of Egfr staining in the KO TM. (L) Mouse *Areg* on chromosome 5 (chr5;mm10). Black bars denote conservation across the listed species; Blue peaks denote areas of high conservation in comparison of the listed species to mouse. Scale bars: 100 μ m.

3.6 Methods

Animals

Mice husbandry and procedures were conducted following the guidelines of the Institutional Animal Care and Use Committee at the University of California, San Francisco (approval number #192822). Experiments using wild-type mice were performed in strain FVB/NJ. *K5-CreERT2*, *Egfr^{fl/fl}* (TC and DW 2009), *R26R-Confetti* (Snippert et al. 2010), and *mTmG* (Muzumdar et al. 2007) mouse lines were acquired from the Jackson Laboratory and maintained on a C57BL/6 background. To generate *Egfr^{fl/fl}; R26^{mTmG/mTmG}* conditional KO mice, *Egfr^{fl/fl}* mice carrying loxP sites flanking exon 3 of *Egfr* were initially crossed with *R26^{mTmG/mTmG}* mice, and then *Egfr^{fl/fl}; R26^{mTmG/mTmG}* were crossed with Keratin5-CreER transgenic mice. For most experiments, adult animals—both male and female—between 6 and 12 weeks of age were used.

Perforations

Perforations in mouse TMs were created as previously described (SM et al. 2021). In brief, animals were anesthetized with isoflurane, and the left TM was visualized under a dissection microscope. Perforations were then created in the left anterior pars tensa, using a 25-gauge needle. The right TM of each mouse was kept uninjured, serving as a control.

TM Dissociations

TMs were dissected from 10 6-week-old FVB/NJ mice (all female) per timepoint (1-, 3-, 7-, and 14-days post-injury), with the contralateral ear to the site of perforation serving as an

unwounded control. TMs were incubated in dispase (Corning) at 37°C for ten minutes and then mechanically separated into epidermal and fibrous/mucosal fractions. The epidermal tissue was dissociated in TrypLE (Life Technologies), and the fibrous/mucosal tissue was dissociated in 0.2 mg/mL collagenase P (Sigma-Aldrich) and 5 µg/mL DNase. Both dissociations were done at 37°C for 10 minutes, with trituration every five minutes. Cells were passed through 40 µm strainers, collected by centrifugation, and subjected to removal of dead cells (Miltenyi Biotec). The cells were resuspended at 1,000 cells/µL in 0.04% BSA in phosphate buffered saline (PBS), and 30,000 cells were loaded for single cell capture.

scRNA-seq Analysis

Isolated cells were run on the Chromium Controller (10X Genomics) with the Single Cell 3' Reagent Kit v2, and the generated libraries were sequenced on an Illumina HiSeq 4000. Mouse data was aligned to mm10. Data was run through CellRanger 2.0.0 (10x Genomics) and then analyzed via R primarily through single cell analysis package Seurat version 4 (Y et al. 2021; R et al. 2015). In order to limit non-biological sources of variation, standard processing steps were conducted to remove cells expressing less than 200 genes and genes expressed in less than three cells. The data matrices were then log-normalized in a sparse data matrix. Principal component analysis was performed, and the first 10 components that emerged were used to cluster the cells via Seurat-implemented Louvain clustering. We implemented dimensionality reduction analysis and unbiased clustering of cell populations based on similar gene expression patterns without using prior knowledge of population markers to drive the clustering. UMAP plots were generated to create a 2D representation of this multidimensional data. The keratinocytes were analyzed both with

and without a linear regression based on cell cycle analysis and assignment of each cell to either S, G1 or G2 phase; no considerable differences were seen between these two analysis modalities, so the data representation used was that of pre-cell cycle regression analysis. Samples from all timepoints following TM injury were harvested and run together in the same batch, so no regression due to batch effects was necessary. All of the individual timepoint read count matrices were combined together and re-clustered via Seurat. This Seurat object was then used for isolating the total keratinocyte, mucosal, immune, and mesenchymal datasets.

Immunofluorescence (IF)

Whole-mount TMs were dissected en bloc, fixed in 4% paraformaldehyde (PFA) at 4°C for four hours, and decalcified in 5% EDTA overnight. For antibody staining, TMs were permeabilized in PBS with 0.5% Triton X-100 for two hours at room temperature (RT), blocked in PBS with 0.5% Triton X-100 and 10% fetal bovine serum (FBS; blocking buffer) for two hours at RT, and incubated in primary antibody diluted in blocking buffer at 4°C overnight. TMs were then washed with PBS, incubated in secondary antibodies in blocking buffer for one hour at RT, and again washed with PBS. For addition of a nuclear stain, TMs were incubated in Hoechst dye diluted 1:1000 in PBS for 30 minutes and washed in PBS. TMs were mounted with Prolong Gold Antifade Mountant (Life Technologies) and sealed with coverslips. Primary antibodies used were rabbit anti-Keratin5 (1:1000) (BioLegend #905501), rabbit anti-Keratin23 (1:100) (LS-Bio #LS-C400571), rabbit anti-Filaggrin (1:100) (LS-Bio #LS-B13455), mouse anti-Collagen II (1:200) (Invitrogen #MA5-12789), rabbit anti-Collagen I (1:100)(Novus #NB600-408), rabbit anti-Areg (1:100) (Invitrogen

#PA5-109404), rabbit anti-EGFR (1:100)(Abcam #ab52894) and rabbit anti-pEGFR (1:350) (CST #2234). Secondary antibodies used in these studies were all Alexa fluor-conjugated antibodies (1:250) (Thermo Fisher Scientific).

To prepare paraffin sections of the TM, auditory bullae were fixed with 4% PFA overnight and decalcified in 5% EDTA for three days with daily solution changes. They were then dehydrated, embedded in paraffin, and sectioned at 7- μ m thickness. To stain the sections, the paraffin was removed in Histo-Clear II (Electron Microscopy Sciences). The tissue was then rehydrated, and slides were sub-boiled in citrate buffer (10 mM citric acid, 2 mM EDTA, 0.05% Tween-20, pH 6.2) for ten minutes on a heating plate to retrieve the antigens. Samples were permeabilized and blocked at RT for one hour in Animal-Free Blocker (Vector Labs SP-5030) mixed with 0.5% Triton X-100 and 2% normal goat serum (Cell Signaling Technology). The slides were stained with primary and secondary antibodies as described above, but nuclear staining with Hoechst dye was performed at 1:500 for 5 minutes at RT.

Imaging

Fluorescent imaging of whole-mount TMs was performed on a Nikon A1R HD confocal microscope with a DU4G filter-based detector, using a Plan Apo Lambda 10x 0.45NA or Super Plan Fluor LWD 20x 0.70NA air objective lens with digital zoom of either 1x or 2x. TMs from *K5-CreERT2*; *R26R-Confetti* mice were acquired using a Nikon AZ100 macro confocal microscope with a DUS spectral detector using a 4x objective and 2x optical zoom, as well as a 1x or 2x digital zoom. Both microscopes used NIS-Elements software for

acquisition. Whole-mount images are displayed as maximum intensity projections of z-stacks. TM sections were imaged on a Leica DM6 B microscope. FIJI (ImageJ) software was used to analyze images, place scale bars, export individual TIFFs, and adjust levels for each channel as needed to maximize image clarity. Imaging of gross anatomy of TMs was performed using a Leica M205 FA stereo microscope and a 2x air objective with the LAS X software.

RNAscope

Mice were euthanized with CO₂ and thoracotomy and perfused with RNase-free PBS followed by 4% paraformaldehyde (PFA) diluted with RNase-free PBS (for isolation of wholemount TMs) or 10% normal buffered formalin (NBF)(for preparation of tissue sections). In preparation for RNAscope in tissue sections, auditory bullae were isolated, incubated in NBF at RT for 24 hours, decalcified, embedded in paraffin, and sectioned at 7- μ m thickness. The RNAscope Multiplex Fluorescent Reagent Kit v2 (Advanced Cell Diagnostics) protocol was adapted with the following conditions: manual target retrieval was performed for 15 minutes, and digestion with Protease Plus was performed for 30 minutes.

To perform RNAscope in wholemount TMs, a protocol for staining of whole-mount zebrafish embryos was adapted (Gross-Thebing, Paksa, and Raz 2014). The TMs were fixed in 4% PFA diluted in RNase-free PBS for 6 hours at RT. They were then washed in PBT (RNase-free PBS with 0.1% Tween 20), dehydrated in increasing concentrations of methanol (25, 50, and 75% in PBT), and stored in 100% methanol at -20°C overnight. The

next day, the TMs were rehydrated using decreasing concentrations of methanol (75, 50, and 25% in PBT), incubated in Protease III at RT for 10 minutes, washed, and incubated with the appropriate probes for hybridization at 50°C overnight. The TMs were then washed in 0.2x SSCT, fixed in 4% PFA at RT for 10 minutes, and washed again. The signal was amplified and developed following the protocol for the RNAscope Multiplex Fluorescent Reagent Kit v2 protocol.

EdU Administration, Detection and Analysis

To label proliferating cells in the TM at the time of tissue harvest, mice were injected 2-hours prior to takedown with EdU (Carbosynth Limited) was resuspended at 5 mg/mL in saline and passed through a 0.22 µm filter. Mice were each injected with 1 mg (200 µL) by intraperitoneal (IP) injection. To fully label and track the proliferating cell population in the TM over time, EdU was administered continuously, first by IP injection at the start of the experiment and then via supplementation in the drinking water at a concentration of 0.5 mg/mL with 1% sucrose that had been filtered using a 0.2-µm filter. The water supply was changed every three days with care taken to protect the water bottles from light. TMs were dissected and processed as described for IF. The Click-iT EdU Alexa Fluor 488 or 647 Imaging Kit (ThermoFisher Scientific) was used for EdU detection. For combined EdU and protein detection, the IF protocol was followed after EdU detection, starting from the blocking step. Quantification of EdU-labeled cells was performed using Fiji (ImageJ).

Lineage tracing with the R26R-Confetti Reporter

To perform minimal labeling of TM keratinocytes, *K5-CreERT2;R26R-Confetti* mice were given a single IP injection of 30 mg tamoxifen 3 days prior to perforation. At the specified time-points post-injury, whole-mount TMs were dissected en bloc, fixed in 4% PFA at 4°C for 4 hours shielded from light, and decalcified in 5% EDTA at 4°C overnight. Prior to mounting, TMs were permeabilized in 0.5% Triton X-100 in PBS at RT for 2 hours, and nuclei were stained with Hoechst as above.

Egfr Deletion

To induce *Egfr* deletion *in vivo*, *K5-CreERT2;Egfr^{fl/fl}; R26R^{mTmG/mTmG}* mice received IP injections of tamoxifen (0.1 mg/g body weight) dissolved in corn oil at a concentration of 25 mg/mL for 6 days consecutively. Loss of *Egfr* protein was validated by immunofluorescence for Egfr.

Statistics

Analyses for scRNA-seq data were done using Seurat functions, and GraphPad Prism was used to analyze all other data. Statistical significance was determined by t-test when comparing two groups. All representative wholemount images of IF or RNAscope represent an n of at least 3, and all EdU images represent an n of at least 5.

3.7 References

- AL, Mescher. 1976. "Effects on Adult Newt Limb Regeneration of Partial and Complete Skin Flaps over the Amputation Surface." *The Journal of Experimental Zoology* 195 (1): 117–27. <https://doi.org/10.1002/JEZ.1401950111>.
- Aragona, Mariaceleste, Sophie Dekoninck, Steffen Rulands, Sandrine Lenglez, Guilhem Mascré, Benjamin D. Simons, and Cédric Blanpain. 2017. "Defining Stem Cell Dynamics and Migration during Wound Healing in Mouse Skin Epidermis." *Nature Communications* 2017 8:1 8 (1): 1–14. <https://doi.org/10.1038/ncomms14684>.
- AW, Seifert, and Muneoka K. 2018. "The Blastema and Epimorphic Regeneration in Mammals." *Developmental Biology* 433 (2): 190–99. <https://doi.org/10.1016/J.YDBIO.2017.08.007>.
- AY, Wang, Shen Y, Wang JT, Friedland PL, Atlas MD, and Dilley RJ. 2014. "Animal Models of Chronic Tympanic Membrane Perforation: A 'time-out' to Review Evidence and Standardize Design." *International Journal of Pediatric Otorhinolaryngology* 78 (12): 2048–55. <https://doi.org/10.1016/J.IJPORL.2014.10.007>.
- AY, Wong, and Whited JL. 2020. "Parallels between Wound Healing, Epimorphic Regeneration and Solid Tumors." *Development (Cambridge, England)* 147 (1). <https://doi.org/10.1242/DEV.181636>.

B, Singh, Carpenter G, and Coffey RJ. 2016. "EGF Receptor Ligands: Recent Advances."

F1000Research 5. <https://doi.org/10.12688/F1000RESEARCH.9025.1>.

Blanpain, Cédric, and Elaine Fuchs. 2009. "Epidermal Homeostasis: A Balancing Act of Stem

Cells in the Skin." *Nature Reviews Molecular Cell Biology* 2009 10:3 10 (3): 207–17.

<https://doi.org/10.1038/nrm2636>.

Bryant, Donald M., Konstantinos Sousounis, Duygu Payzin-Dogru, Sevara Bryant, Aaron

Gabriel W. Sandoval, Jose Martinez Fernandez, Rachelle Mariano, et al. 2017.

"Identification of Regenerative Roadblocks via Repeat Deployment of Limb

Regeneration in Axolotls." *Npj Regenerative Medicine* 2 (1).

<https://doi.org/10.1038/S41536-017-0034-Z>.

Chalkley, Donald Thomas. 1954. "A Quantitative Histological Analysis of Forelimb

Regeneration in *Triturus Viridescens*." *Journal of Morphology* 94 (1): 21–70.

<https://doi.org/10.1002/JMOR.1050940103>.

CM, Chuong, and Noveen A. 1999. "Phenotypic Determination of Epithelial Appendages:

Genes, Developmental Pathways, and Evolution." *The Journal of Investigative*

Dermatology. Symposium Proceedings 4 (3): 307–11.

<https://doi.org/10.1038/SJ.JIDSP.5640235>.

CS, THORNTON. 1957. "The Effect of Apical Cap Removal on Limb Regeneration in Amblystoma Larvae." *The Journal of Experimental Zoology* 134 (2): 357–81.
<https://doi.org/10.1002/JEZ.1401340209>.

DA, Chari, Frumm SM, Akil O, and Tward AD. 2019. "Cellular Dynamics in Early Healing of Mouse Tympanic Membranes." *Otology & Neurotology : Official Publication of the American Otological Society, American Neurotology Society [and] European Academy of Otology and Neurotology* 40 (2): e160–66.
<https://doi.org/10.1097/MAO.0000000000002060>.

Farahani, Ramin M., and Munira Xaymardan. 2015. "Platelet-Derived Growth Factor Receptor Alpha as a Marker of Mesenchymal Stem Cells in Development and Stem Cell Biology." *Stem Cells International* 2015. <https://doi.org/10.1155/2015/362753>.

Gantwerker, Eric A., and David B. Hom. 2011. "Skin: Histology and Physiology of Wound Healing." *Facial Plastic Surgery Clinics of North America* 19 (3): 441–53.
<https://doi.org/10.1016/J.FSC.2011.06.009>.

Gao, Tianxi, Xiaoli Li, Juan Hu, Weijun Ma, Jingjing Li, Na Shao, and Zhenghui Wang. 2017. "Management of Traumatic Tympanic Membrane Perforation: A Comparative Study." *Therapeutics and Clinical Risk Management* 13 (July): 927.
<https://doi.org/10.2147/TCRM.S139631>.

Gerber, Tobias, Prayag Murawala, Dunja Knapp, Wouter Masselink, Maritta Schuez, Sarah Hermann, Malgorzata Gac-Santel, et al. n.d. "Single-Cell Analysis Uncovers Convergence of Cell Identities during Axolotl Limb Regeneration." <https://doi.org/10.1126/science.aaq0681>.

Gil-Yarom, Naama, Lihi Radomir, Lital Sever, Matthias P. Kramer, Hadas Lewinsky, Chamutal Bornstein, Ronnie Blecher-Gonen, et al. 2017. "CD74 Is a Novel Transcription Regulator." *Proceedings of the National Academy of Sciences of the United States of America* 114 (3): 562. <https://doi.org/10.1073/PNAS.1612195114>.

Greig, Michael J., Sherry Niessen, Scott L. Weinrich, Jun Li Feng, Manli Shi, and Ted O. Johnson. 2015. "Effects of Activating Mutations on EGFR Cellular Protein Turnover and Amino Acid Recycling Determined Using SILAC Mass Spectrometry." *International Journal of Cell Biology* 2015. <https://doi.org/10.1155/2015/798936>.

Gross-Thebing, Theresa, Azadeh Paksa, and Erez Raz. 2014. "Simultaneous High-Resolution Detection of Multiple Transcripts Combined with Localization of Proteins in Whole-Mount Embryos." *BMC Biology* 2016 12:1 12 (1): 1–14. <https://doi.org/10.1186/S12915-014-0055-7>.

Haas, Brian J., and Jessica L. Whited. 2017. "Advances in Decoding Axolotl Limb Regeneration." *Trends in Genetics : TIG* 33 (8): 553–65. <https://doi.org/10.1016/J.TIG.2017.05.006>.

- Hall, Margaret J, Alexander Schwartzman, Jin Zhang, and Xiang Liu. 2010. "Ambulatory Surgery Data From Hospitals and Ambulatory Surgery Centers: United States, 2010."
- JD, Currie, Kawaguchi A, Traspas RM, Schuez M, Chara O, and Tanaka EM. 2016. "Live Imaging of Axolotl Digit Regeneration Reveals Spatiotemporal Choreography of Diverse Connective Tissue Progenitor Pools." *Developmental Cell* 39 (4): 411–23. <https://doi.org/10.1016/J.DEVCEL.2016.10.013>.
- JP, Brockes, and Kumar A. 2008. "Comparative Aspects of Animal Regeneration." *Annual Review of Cell and Developmental Biology* 24: 525–49. <https://doi.org/10.1146/ANNUREV.CELLBIO.24.110707.175336>.
- K, Muneoka, Fox WF, and Bryant SV. 1986. "Cellular Contribution from Dermis and Cartilage to the Regenerating Limb Blastema in Axolotls." *Developmental Biology* 116 (1): 256–60. [https://doi.org/10.1016/0012-1606\(86\)90062-X](https://doi.org/10.1016/0012-1606(86)90062-X).
- KAU, Gonzales, and Fuchs E. 2017. "Skin and Its Regenerative Powers: An Alliance between Stem Cells and Their Niche." *Developmental Cell* 43 (4): 387–401. <https://doi.org/10.1016/J.DEVCEL.2017.10.001>.
- Klinge, Uwe, Axel Dievernich, Rene Tolba, Bernd Klosterhalfen, and Luke Davies. 2020. "CD68+ Macrophages as Crucial Components of the Foreign Body Reaction

Demonstrate an Unconventional Pattern of Functional Markers Quantified by Analysis with Double Fluorescence Staining.” *Journal of Biomedical Materials Research Part B: Applied Biomaterials* 108 (8): 3134–46. <https://doi.org/10.1002/JBM.B.34639>.

Kragl, Martin, Dunja Knapp, Eugen Nacu, Shahryar Khattak, Malcolm Maden, Hans Henning Epperlein, and Elly M. Tanaka. 2009. “Cells Keep a Memory of Their Tissue Origin during Axolotl Limb Regeneration.” *Nature* 2009 460:7251 460 (7251): 60–65. <https://doi.org/10.1038/NATURE08152>.

Leigh, Nicholas D, Garrett S Dunlap, Kimberly Johnson, Rachele Mariano, Rachel Oshiro, Alan Y Wong, Donald M Bryant, et al. n.d. “Transcriptomic Landscape of the Blastema Niche in Regenerating Adult Axolotl Limbs at Single-Cell Resolution.” <https://doi.org/10.1038/s41467-018-07604-0>.

LJ, Campbell, and Crews CM. 2008. “Wound Epidermis Formation and Function in Urodele Amphibian Limb Regeneration.” *Cellular and Molecular Life Sciences : CMLS* 65 (1): 73–79. <https://doi.org/10.1007/S00018-007-7433-Z>.

Lou, Z. C., Y. M. Tang, and J. Yang. 2011. “A Prospective Study Evaluating Spontaneous Healing of Aetiology, Size and Type-Different Groups of Traumatic Tympanic Membrane Perforation.” *Clinical Otolaryngology : Official Journal of ENT-UK ; Official Journal of Netherlands Society for Oto-Rhino-Laryngology & Cervico-Facial Surgery* 36 (5): 450–60. <https://doi.org/10.1111/J.1749-4486.2011.02387.X>.

M, Globus, Vethamany-Globus S, and Lee YC. 1980. "Effect of Apical Epidermal Cap on Mitotic Cycle and Cartilage Differentiation in Regeneration Blastemata in the Newt, *Notophthalmus Viridescens*." *Developmental Biology* 75 (2): 358–72.
[https://doi.org/10.1016/0012-1606\(80\)90169-4](https://doi.org/10.1016/0012-1606(80)90169-4).

Maria, Peter Luke Santa, Sharon Leanne Redmond, Marcus David Atlas, and Reza Ghassemifar. 2010. "Histology of the Healing Tympanic Membrane Following Perforation in Rats." *The Laryngoscope* 120 (10): 2061–70.
<https://doi.org/10.1002/LARY.20998>.

McDonald, Timothy M., Agnes S. Pascual, Chandana K. Uppalapati, Kimbal E. Cooper, Kathryn J. Leyva, and Elizabeth E. Hull. 2013. "Zebrafish Keratocyte Explant Cultures as a Wound Healing Model System: Differential Gene Expression & Morphological Changes Support Epithelial–Mesenchymal Transition." *Experimental Cell Research* 319 (12): 1815–27. <https://doi.org/10.1016/J.YEXCR.2013.03.036>.

Muzumdar, Mandar Deepak, Bosiljka Tasic, Kazunari Miyamichi, Ling Li, and Liqun Luo. 2007. "A Global Double-Fluorescent Cre Reporter Mouse." *Genesis* 45 (9): 593–605.
<https://doi.org/10.1002/DVG.20335>.

Porrello, Enzo R., Ahmed I. Mahmoud, Emma Simpson, Joseph A. Hill, James A. Richardson, Eric N. Olson, and Hesham A. Sadek. 2011. "Transient Regenerative Potential of the

Neonatal Mouse Heart.” *Science* 331 (6020): 1078–80.

<https://doi.org/10.1126/SCIENCE.1200708>.

R, Satija, Farrell JA, Gennert D, Schier AF, and Regev A. 2015. “Spatial Reconstruction of Single-Cell Gene Expression Data.” *Nature Biotechnology* 33 (5): 495–502.

<https://doi.org/10.1038/NBT.3192>.

Ray, Paramita, Yee Sun Tan, Vishal Somnay, Ranjit Mehta, Merna Sitto, Aarif Ahsan, Shyam Nyati, et al. 2016. “Differential Protein Stability of EGFR Mutants Determines Responsiveness to Tyrosine Kinase Inhibitors.” *Oncotarget* 7 (42): 68597.

<https://doi.org/10.18632/ONCOTARGET.11860>.

Rittié, Laure. 2016. “Cellular Mechanisms of Skin Repair in Humans and Other Mammals.” *Journal of Cell Communication and Signaling* 10 (2): 103.

<https://doi.org/10.1007/S12079-016-0330-1>.

RM, Rosenfeld, Schwartz SR, Pynnonen MA, Tunkel DE, Hussey HM, Fichera JS, Grimes AM, et al. 2013. “Clinical Practice Guideline: Tympanostomy Tubes in Children.”

Otolaryngology--Head and Neck Surgery : Official Journal of American Academy of Otolaryngology-Head and Neck Surgery 149 (1 Suppl).

<https://doi.org/10.1177/0194599813487302>.

Rodrigues, Melanie, Nina Kosaric, Clark A. Bonham, and Geoffrey C. Gurtner. 2019. “Wound

Healing: A Cellular Perspective.” *Physiological Reviews* 99 (1): 665.

<https://doi.org/10.1152/PHYSREV.00067.2017>.

S, Mascharak, desJardins-Park HE, Davitt MF, Griffin M, Borrelli MR, Moore AL, Chen K, et al.

2021. “Preventing Engrailed-1 Activation in Fibroblasts Yields Wound Regeneration without Scarring.” *Science (New York, N.Y.)* 372 (6540).

<https://doi.org/10.1126/SCIENCE.ABA2374>.

Seifert, Ashley W., and Malcolm Maden. 2014. “New Insights into Vertebrate Skin

Regeneration.” *International Review of Cell and Molecular Biology* 310 (January): 129–69. <https://doi.org/10.1016/B978-0-12-800180-6.00004-9>.

SM, Frumm, Yu SK, Chang J, Artichoker JA, Scaria SM, Lee KP, Byrnes LE, Sneddon JB, and

Tward AD. 2021. “A Hierarchy of Proliferative and Migratory Keratinocytes Maintains the Tympanic Membrane.” *Cell Stem Cell* 28 (2): 315-330.e5.

<https://doi.org/10.1016/J.STEM.2020.10.006>.

Snippert, Hugo J., Laurens G. van der Flier, Toshiro Sato, Johan H. van Es, Maaïke van den

Born, Carla Kroon-Veenboer, Nick Barker, et al. 2010. “Intestinal Crypt Homeostasis Results from Neutral Competition between Symmetrically Dividing Lgr5 Stem Cells.”

Cell 143 (1): 134–44. <https://doi.org/10.1016/J.CELL.2010.09.016>.

Sorg, Heiko, Daniel J. Tilkorn, Stephan Hager, Jörg Hauser, and Ursula Mirastschijski. 2017.

“Skin Wound Healing: An Update on the Current Knowledge and Concepts.” *European Surgical Research* 58 (1–2): 81–94. <https://doi.org/10.1159/000454919>.

Stanger, Ben Z. 2015. “Cellular Homeostasis and Repair in the Mammalian Liver.” *Annual Review of Physiology* 77 (February): 179. <https://doi.org/10.1146/ANNUREV-PHYSIOL-021113-170255>.

Stocum, David L. 2017. “Mechanisms of Urodele Limb Regeneration.” *Regeneration* 4 (4): 159. <https://doi.org/10.1002/REG2.92>.

Stoll, Stefan W., Philip E. Stuart, Sylviane Lambert, Alberto Gandarillas, Laure Rittié, Andrew Johnston, and James T. Elder. 2016. “Membrane-Tethered Intracellular Domain of Amphiregulin Promotes Keratinocyte Proliferation.” *The Journal of Investigative Dermatology* 136 (2): 444. <https://doi.org/10.1016/J.JID.2015.10.061>.

Stone, Rivka C., Irena Pastar, Nkemcho Ojeh, Vivien Chen, Sophia Liu, Karen I. Garzon, and Marjana Tomic-Canic. 2016. “Epithelial-Mesenchymal Transition in Tissue Repair and Fibrosis.” *Cell and Tissue Research* 365 (3): 495. <https://doi.org/10.1007/S00441-016-2464-0>.

T, Mehrel, Hohl D, Rothnagel JA, Longley MA, Bundman D, Cheng C, Lichti U, Bisher ME, Steven AC, and Steinert PM. 1990. “Identification of a Major Keratinocyte Cell Envelope Protein, Loricrin.” *Cell* 61 (6): 1103–12. <https://doi.org/10.1016/0092->

8674(90)90073-N.

T, Velnar, Bailey T, and Smrkolj V. 2009. "The Wound Healing Process: An Overview of the Cellular and Molecular Mechanisms." *The Journal of International Medical Research* 37 (5): 1528–42. <https://doi.org/10.1177/147323000903700531>.

TC, Lee, and Threadgill DW. 2009. "Generation and Validation of Mice Carrying a Conditional Allele of the Epidermal Growth Factor Receptor." *Genesis (New York, N.Y. : 2000)* 47 (2): 85–92. <https://doi.org/10.1002/DVG.20464>.

TR, Gawriluk, Simkin J, Thompson KL, Biswas SK, Clare-Salzler Z, Kimani JM, Kiama SG, Smith JJ, Ezenwa VO, and Seifert AW. 2016. "Comparative Analysis of Ear-Hole Closure Identifies Epimorphic Regeneration as a Discrete Trait in Mammals." *Nature Communications* 7 (April). <https://doi.org/10.1038/NCOMMS11164>.

Tsonis, Panagiotis A., and Timothy P. Fox. 2009. "Regeneration According to Spallanzani." *Developmental Dynamics* 238 (9): 2357–63. <https://doi.org/10.1002/DVDY.22057>.

U, Kierdorf, Li C, and Price JS. 2009. "Improbable Appendages: Deer Antler Renewal as a Unique Case of Mammalian Regeneration." *Seminars in Cell & Developmental Biology* 20 (5): 535–42. <https://doi.org/10.1016/J.SEMCDB.2008.11.011>.

Whited, Jessica L, and Clifford J Tabin. 2009. "Limb Regeneration Revisited." *Journal of*

Biology 8 (1): 5. <https://doi.org/10.1186/JBIOL105>.

Xia, Huimin, Xin Li, Weiwei Gao, Xin Fu, Ronnie H. Fang, Liangfang Zhang, and Kang Zhang. 2018. "Tissue Repair and Regeneration with Endogenous Stem Cells." *Nature Reviews Materials* 2018 3:7 3 (7): 174–93. <https://doi.org/10.1038/s41578-018-0027-6>.

Y, Hao, Hao S, Andersen-Nissen E, Mauck WM, Zheng S, Butler A, Lee MJ, et al. 2021. "Integrated Analysis of Multimodal Single-Cell Data." *Cell* 184 (13): 3573-3587.e29. <https://doi.org/10.1016/J.CELL.2021.04.048>.

Yilmaz, Mahmut Sinan, Elvan Sahin, Recep Kaymaz, Berrin Zuhul Altunkaynak, Ayse Oznur Akidil, Sevinc Yanar, Deniz Demir, and Mehmet Guven. 2021. "Histological Study of The Healing of Traumatic Tympanic Membrane Perforation After Vivosorb and Epifilm Application." *Ear, Nose, & Throat Journal* 100 (2): 90–96. <https://doi.org/10.1177/0145561319854320>.

Yu, Kevin Shengyang, Stacey M. Frumm, Jason S. Park, Katharine Lee, Daniel M. Wong, Lauren Byrnes, Sarah M. Knox, Julie B. Sneddon, and Aaron D. Tward. 2019. "Development of the Mouse and Human Cochlea at Single Cell Resolution." *BioRxiv*, August, 739680. <https://doi.org/10.1101/739680>.

ZC, Lou, Lou ZH, and Zhang QP. 2012. "Traumatic Tympanic Membrane Perforations: A Study of Etiology and Factors Affecting Outcome." *American Journal of Otolaryngology*

33 (5): 549–55. <https://doi.org/10.1016/J.AMJOTO.2012.01.010>.

Chapter 4:

Effects of Topical Stimulation on the Tympanic Membrane

4.1 Introduction and Project Goals

A main goal of understanding the molecular mechanisms of tympanic membrane regeneration is because of the clinical need for improved therapeutics for chronic tympanic membrane injuries. Faithful repair of TM perforations is of great clinical importance since unrepaired perforations can lead to conductive hearing loss and result in recurrent ear infections. Though most perforations close within days to weeks without intervention, 6-20% of cases become chronic (Kristensen 1992). The current gold standard when it comes to repair of chronic perforations is surgical myringoplasty or tympanoplasty, in which the graft is successful only 80% of the time (Indorewala et al. 2015). With surgery, there is always the risk of general anesthesia and a high-cost burden. Moreover, some patients are unable to undergo surgical repair due to other comorbidities and thus are subject to conductive hearing loss and the potential infections that could ensue.

There are non-surgical repair tactics for chronic TM perforations as well, but they are very limited. There has been variable success with patch scaffolds made of other materials, like collagen, silk, chitosan, and calcium alginate (Bonzon et al. 1995; Weber et al. 2006; Kim et al. 2013) Moreover, there has been growing interest in harnessing the power of embryonic stem cells to enhance healing capacity but again with limited success (Rahman et al. 2008; Goncalves et al. 2017; 2016). At this point, researchers have been unable to restart the native healing process in chronically patent wounds.

The tympanic membrane, however, is indeed ideally placed for a non-surgical intervention. Because the tympanic membrane is positioned at the end of the external auditory canal, it

is easily accessible endoscopically. A series of clinical trials tried to take advantage of this fact to easily administer therapies to the tympanic membrane down the EAC. One trial of acute TM perforation patients randomized observational treatment versus placing a Gelfoam patch endoscopically on the TM surface and found that the time to closure was 14.7 +/- 9.1 days in the Gelfoam group versus 26.8 +/- 9.1 days in the observation group (Huang et al. 2018). In a different study that compared observation, Gelfoam patching, and Gelfoam soaked in FGF-2, they found that both interventions (the plain Gelfoam and soaked Gelfoam) had shorter times to closure, but there was no statistical difference between the two interventions (Jin, Dong, and Lou 2017). Lastly, there was a study that compared interventions of liquid drops of EGF, FGF-2 or ofloxacin applied directly to the TM down the ear canal, and again, the time to closure was shorter than no intervention, but there was no statistical difference between the interventions (Lou and Lou 2017). Therefore, these trials gave uncertain results of what specific therapies could be potentially utilized for chronic therapies, and at the time, the molecular mechanisms of wound closure were still a mystery with the placebo giving the more or less the exact same response as the treatment.

Based on these clinical trial results, however, we were keen to understand what was driving this shorter closure time they were observing, particularly because they seemed to be observing it with many different types of conditions, particularly ones we would have thought to be inert. We hypothesized that topical stimulation could lead to increased cell turnover in the TM. The goal of our project was to rigorously characterize the effects of different types of topical stimulation to the tympanic membrane and to elucidate by what mechanism topical stimulation was leading to these increased closure rates. Moreover, we

were curious as to what parallels existed between the response to topical stimulation and the response to injury we had previously observed in the TM. Therefore, we aimed to fully characterize the response of the tympanic membrane to topical stimulation and compare the mechanisms by which proliferation is activated to the mechanisms we had elucidated in wound repair, documented in Chapter 3.

4.2 Results

We first set out to definitively answer if contact of any substance on the tympanic membrane would indeed stimulate turnover in the epithelium. We delivered saline (PBS) endoscopically to the surface of murine tympanic membranes, sacrificed the mice at various timepoints over 24 hours and harvested their tympanic membranes (**Figure 4.1A**). We injected the mice with EdU 2 hours prior to takedown to capture which cells were actively proliferating at these time points. Remarkably, by 18-24 hours, we could see a significant increase in EdU-labeled cells compared to wildtype unstimulated tympanic membranes (**Figure 4.1B-C**). Notably, the proliferative response appears to be in the same stem cell/progenitor niche regions of the tympanic membrane that we saw proliferation induced after injury. Therefore, even without an injury, the presence of an inert liquid on the tympanic membrane stimulates proliferation.

Based on clinical trial data that showed both solid and liquid drug stimulation resulting in shorter closure times (Huang et al. 2018), we decided to test out different types of topical stimulation. We tested three conditions of topical stimulation: PBS, corn oil, and mouse

food pellets. Mice were sacrificed at 24 hours after the topical stimulation with EdU injected 2 hours prior to sacrifice. Once again, we found that all of these conditions were able to trigger statistically significant increases in proliferation on the surface of the tympanic membrane when compared to the control opposite ear (**Figure 4.2**). Moreover, the proliferative response again seemed to be globally throughout the tympanic membrane, not localized to one particular region where the topical stimulation occurred. Thus, both liquids and solids were able to trigger this rapid and robust proliferative response.

We were then curious to understand the similarities in the process of induction of proliferation in injury versus the process in topical stimulation. As discussed in chapter 3, when the tympanic membrane is injured, a wounded epithelium forms 24-hours post-injury and continues to expand through day 3. Therefore, we applied PBS to tympanic membranes 3 days prior to sacrifice, and with the harvested TMs, we stained for markers of the injured tympanic membrane's wounded epithelium. In particular, we performed immunofluorescence for Amphiregulin (Areg), a ligand of EGFR, and for pEGFR, as well as RNAscope for *GPR15L*, one of the highest differentially expressed genes in the wounded keratinocyte population (**Figure 4.3**). We found that though the proliferative response to wounding and the response to topical stimulation seem to exist in the same regions and be comparable in size, we do not see the presence of Areg at day 3 (**Figure 4.3B**) or an increase in pEGFR signal (**Figure 4.3C**). However, we do see an increase in *GPR15L* signaling after day 3 (**Figure 4.3A**). Therefore, there are some similarities in signal induction between wounded tympanic membranes and tympanic membranes with topical

stimulation, but the downstream mechanisms in topical stimulation are likely not dependent on EGFR activation via Areg.

4.3 Discussion and Future Directions

Overall, we have shown that topical stimulation, both solid and liquid, induces a rapid and robust proliferative response on the tympanic membrane after 24 hours. This response validates earlier clinical trial data for TM perforation treatments that found that treatment groups versus non-treatment controls were showing similar increases in closure despite the control treatment having no actual drug. Work in Chapter 3 discusses the tympanic membrane as the closest adult mammalian example of regeneration. This data opens the discussion of what exactly does the tympanic membrane need to sense in order to induce a proliferative response. In the case of injury, there is a break in the surface of the pars tensa being made. Therefore, there is also a decrease in tension across the surface and a break in cell-to-cell contact in the region of the injury. Moreover, there is a break in not only the epithelial layer, but also the mesenchymal and mucosal layers of the tympanic membrane when it is injured, and the tympanic membrane is then tasked with repairing all three layers. However, in the case of topical stimulation, the liquid or solid is interacting primarily with just the keratinocytes, so this suggests that the initial rapid and robust proliferative response of the tympanic membrane to both injury and topical stimulation might be only reliant on the keratinocytes sensing the perturbation.

Moreover, RNAscope for *GPR15L*, a marker of the wounded epithelium found in tympanic membrane injury, revealed that this population may also be present after topical stimulation of the tympanic membrane. This suggests that perhaps the induction of proliferation in these two situations are overlapping in mechanism. However, we found that the downstream signaling in topical stimulation versus injury does not appear to be the same. RNAscope for *Areg* and IF for pEGFR did not show the typical increase seen in response to injury by day 3. Our previous work (Chapter 3) showed that EGFR is required for wound closure. However, here EGFR signaling does not appear activated. This suggests that perhaps the decision point for repair of an injury versus generic epithelial proliferation comes downstream of the formation of a wounded epithelium. Moreover, this could also suggest that EGFR signaling is not necessary for the induction of the regeneration response of the TM, but rather is necessary for the resolution of the regeneration response.

The deviation in downstream signaling in topical stimulation versus regeneration of the tympanic membrane could have many explanations. Firstly, since injury perturbs all layers of the tympanic membrane and topical stimulation only perturbs keratinocytes, we could hypothesize that it is signaling of one of the other layers of the tympanic membrane or general cross-talk between the layers that leads to the activation of EGFR signaling. Indeed, the wounded epithelium is activated in both conditions, but this epithelium may be in communication with the injured mesenchyme or mucosa and therefore, receiving different cellular signals than this population of keratinocytes in topical stimulation.

Another possibility for why these tissues differ in their downstream signaling may be due to a difference in tension signaling. Perforation breaks the tension, and thus lowers it, in the tympanic membrane. Topical Stimulation likely increases the tension as a weight is placed on the surface of the tympanic membrane, which has to remain taut to support it. Therefore, the two perturbations to the TM have opposite effects on tension of the organ. Thus, the release of tension may be critical to activating EGFR signaling, which then leads to regeneration of the TM, while the increase in tension could inhibit this signaling. There is evidence that increases in cell contractility due to increased tension leads to an increase in stem cell proliferation and inhibits migration (Ning et al. 2021). Moreover, the force on adherens junctions alone have been reported to induce proliferation via beta-catenin- and Yap1-dependent pathways (Benham-Pyle, Pruitt, and Nelson 2015). Future experiments measuring contractility of cells in the tympanic membrane under these two conditions and staining for pathways involved in tension signaling could help us determine what the changes in tension are and how the epithelial layer of the tympanic membrane is reacting to them.

Lastly, another reason for the difference in downstream response to injury versus topical stimulation could be a response to changes in cell density. One of the known regulators of cell density in epithelial cells is Piezo1. When cells are “stretched” or in lower density, Piezo1 activation leads to an increase in proliferation. When cells are too dense, Piezo1 triggers extrusion and apoptosis (Gudipaty et al. 2017). In the case of TM injury, cells experience a temporary state of lower density due to the hole in the tissue. This density change does not occur in the case of topical stimulation. We could hypothesize that the

decrease in cell density triggers Piezo1 signaling in the injured tympanic membrane, which contributes to regeneration, while the lack of Piezo1 activation in topical stimulation halts the downstream regenerative response after the wounded epithelium forms.

Overall, the crucial next step in this project is to conduct a single-cell experiment similar to what we performed for the injured tympanic membrane (Chapter 3), in which we perturb the TM with the conditions tested in this chapter (PBS, corn oil, murine food pellets), harvest the TMs and submit the cells for single-cell RNA sequencing at days 1, 3, 7 and 14. This will allow us to directly compare the cell populations after topical stimulation to those after wounding and to properly decipher the signaling pathways that contribute to the proliferative response we observe when the TM is topically stimulated.

Figure 4.1

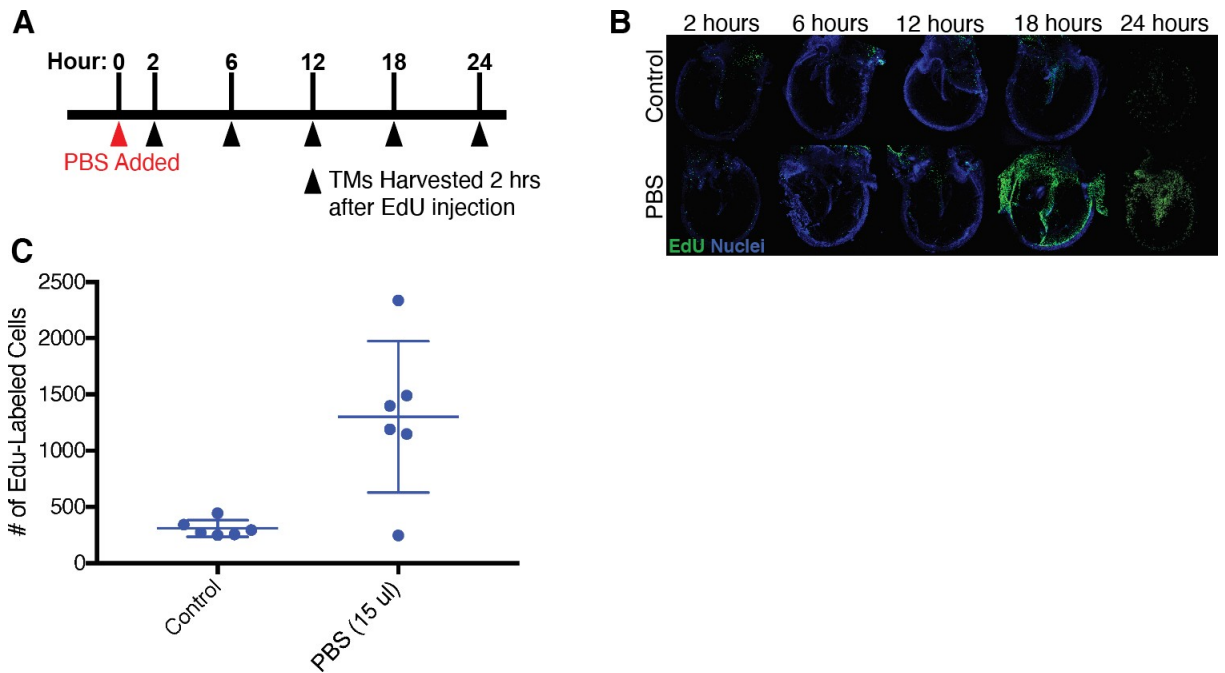


Figure 4.1: Topical PBS induces proliferation on the tympanic membrane. (A) TMs at various timepoints post-addition of PBS were harvested and processed using the Click-it EdU Detection Kit (B) Edu-labeled whole-mount TMs demonstrate a peak proliferative response 18 hours post-addition of PBS. (C) Graph of number of EdU+ cells in a 400 x 1200 μm area over the malleus in response to topical stimulation via PBS. Results of t-tests for PBS vs control TMs at a single time-point were significant with a p-value < 0.05.

Figure 4.2

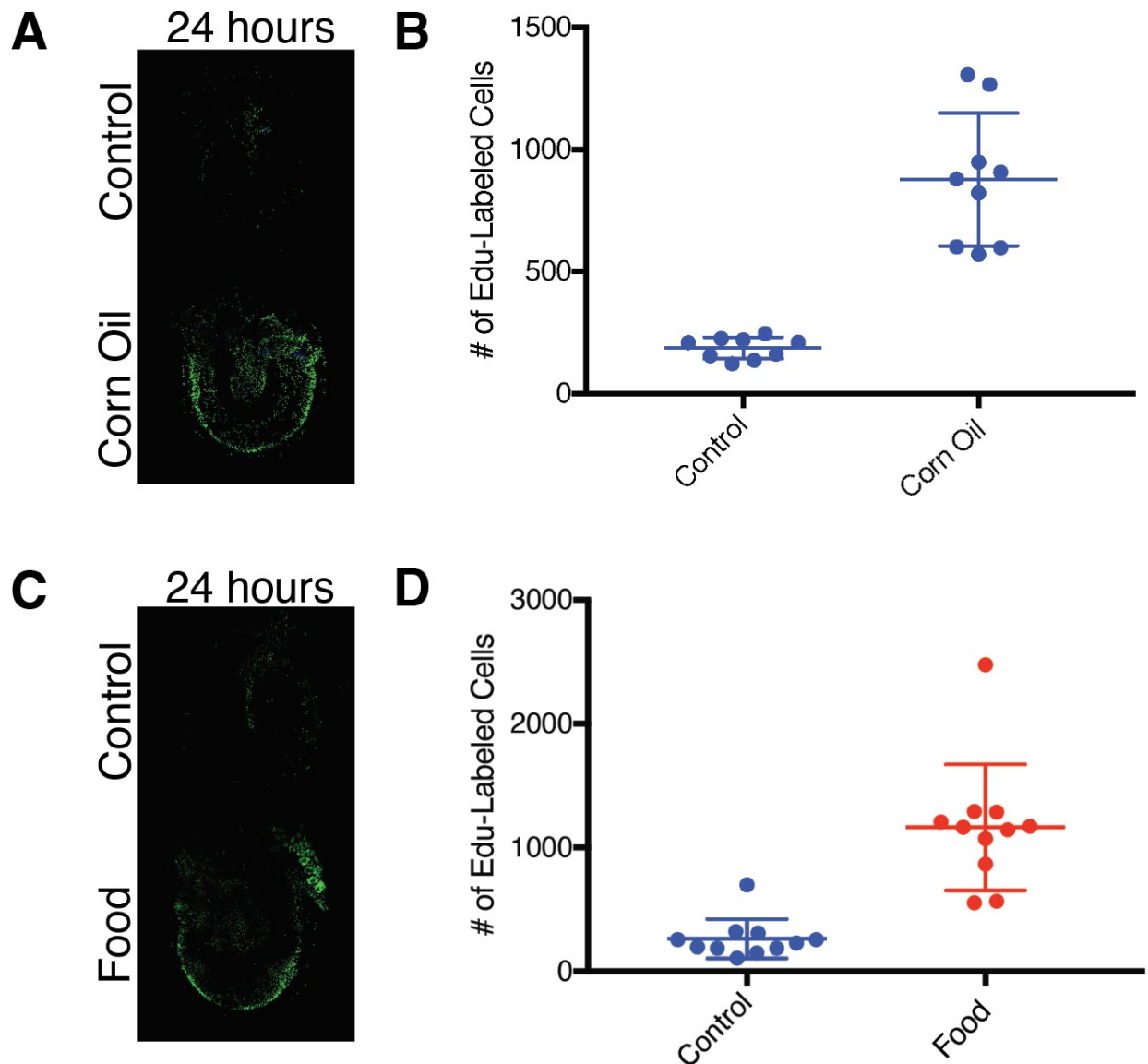


Figure 4.2: Different forms of topical stimulation all induce proliferation. (A, C) Representative wild-type murine TMs harvested from mice 24 hours after either (A) corn oil or (C) murine food pellets were added to the surface of the TM. (B, D) Graph of number of EdU+ cells in a 400 x 1200 μm area over the malleus in response to topical stimulation via (B) corn oil or (D) murine food pellets. Results of t-tests for Stimulation vs control TMs at 24 hours was significant with a p-value < 0.05.

Figure 4.3

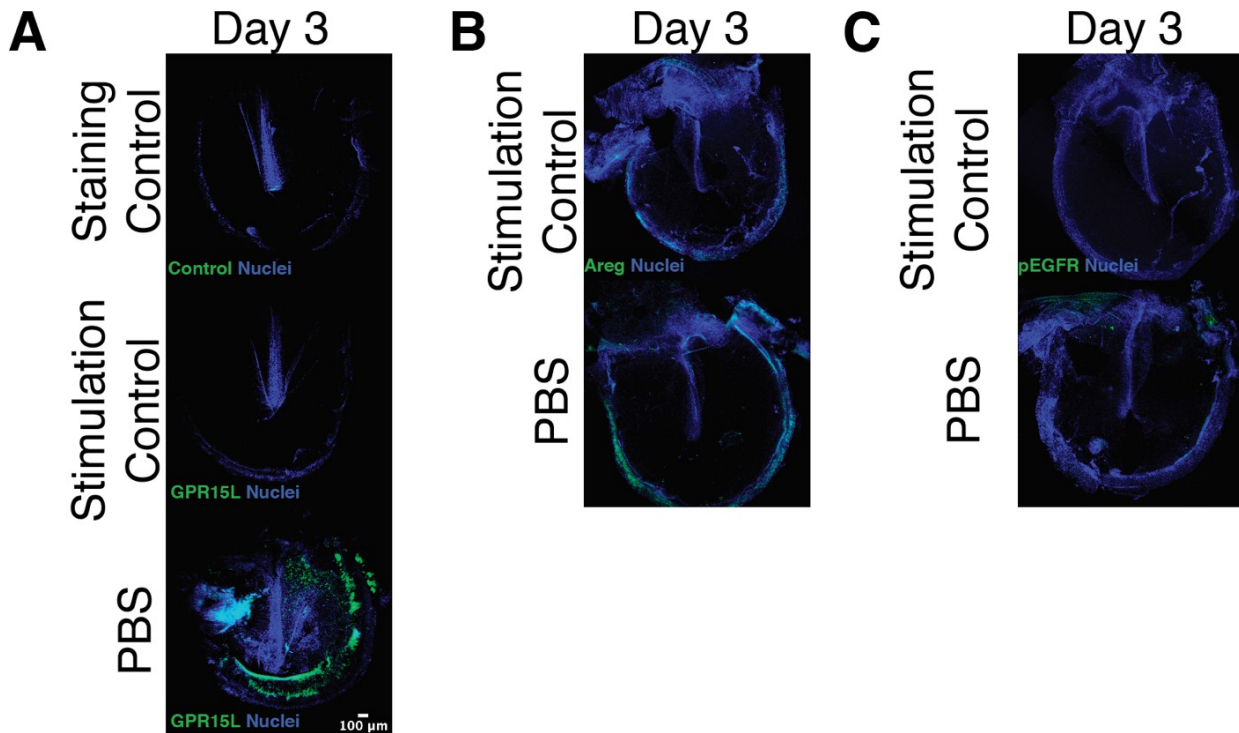


Figure 4.3: Topical stimulation of the TM induces wounded epithelium markers. (A) RNAscope for *Gpr15L* (green) expression on whole-mount TMs 3 days after topical stimulation with PBS. (B) IF for Amphiregulin on whole-mount TMs 3 days after topical stimulation with PBS. (C) IF for pEGFR on whole-mount TMs 3 days after topical stimulation with PBS.

4.5 References

- Benham-Pyle, Blair W, Beth L Pruitt, and W James Nelson. n.d. "Mechanical Strain Induces E-Cadherin-Dependent Yap1 and β -Catenin Activation to Drive Cell Cycle Entry." Accessed January 31, 2022. <https://www.science.org>.
- Bonzon, N., X. Carrat, C. Deminière, G. Daculsi, F. Lefebvre, and M. Rabaud. 1995. "New Artificial Connective Matrix Made of Fibrin Monomers, Elastin Peptides and Type I + III Collagens: Structural Study, Biocompatibility and Use as Tympanic Membranes in Rabbit." *Biomaterials* 16 (11): 881–85. [https://doi.org/10.1016/0142-9612\(95\)94151-A](https://doi.org/10.1016/0142-9612(95)94151-A).
- Goncalves, Stefania, Esperanza Bas, Bradley J. Goldstein, and Simon Angeli. 2016. "Effects of Cell-Based Therapy for Treating Tympanic Membrane Perforations in Mice." *Otolaryngology--Head and Neck Surgery : Official Journal of American Academy of Otolaryngology-Head and Neck Surgery* 154 (6): 1106–14. <https://doi.org/10.1177/0194599816636845>.
- Goncalves, Stefania, Esperanza Bas, Michael Langston, Ariel Grobman, Bradley J. Goldstein, and Simon Angeli. 2017. "Histologic Changes of Mesenchymal Stem Cell Repair of Tympanic Membrane Perforation." *Acta Oto-Laryngologica* 137 (4): 411–16. <https://doi.org/10.1080/00016489.2016.1261411>.

Gudipaty, S. A., J. Lindblom, P. D. Loftus, M. J. Redd, K. Edes, C. F. Davey, V. Krishnegowda, and J. Rosenblatt. 2017. "Mechanical Stretch Triggers Rapid Epithelial Cell Division through Piezo1." *Nature* 2017 543:7643 543 (7643): 118–21.
<https://doi.org/10.1038/nature21407>.

H, Seonwoo, Kim SW, Kim J, Chunjie T, Lim KT, Kim YJ, Pandey S, Choung PH, Choung YH, and Chung JH. 2013. "Regeneration of Chronic Tympanic Membrane Perforation Using an EGF-Releasing Chitosan Patch." *Tissue Engineering. Part A* 19 (17–18): 2097–2107.
<https://doi.org/10.1089/TEN.TEA.2012.0617>.

Huang, Peng, Shujun Zhang, Xinhong Gong, Xuesong Wang, and Zi Han Lou. 2018. "Endoscopic Observation of Different Repair Patterns in Human Traumatic Tympanic Membrane Perforations." *Brazilian Journal of Otorhinolaryngology* 84 (5): 545–52.
<https://doi.org/10.1016/J.BJORL.2017.06.011>.

Indorewala, Shabbir, Taiwo Olugbemiga Adedeji, Abuzar Indorewala, and Gaurav Nemade. 2015. "Tympanoplasty Outcomes: A Review of 789 Cases." *Iranian Journal of Otorhinolaryngology* 27 (79): 101. <https://doi.org/10.22038/ijorl.2015.3641>.

Jin, Zhong hai, Yi Han Dong, and Zi Han Lou. 2017. "The Effects of Fibroblast Growth Factor-

2 Delivered via a Gelfoam Patch on the Regeneration of Myringosclerotic Traumatic Eardrum Perforations Lying Close to the Malleus." *American Journal of Otolaryngology* 38 (5): 582–87. <https://doi.org/10.1016/J.AMJOTO.2017.06.005>.

Kristensen, Søren. 1992. "Spontaneous Healing of Traumatic Tympanic Membrane Perforations in Man: A Century of Experience." *The Journal of Laryngology and Otology* 106 (12): 1037–50. <https://doi.org/10.1017/S0022215100121723>.

Lou, Zhengcai, and Zihan Lou. 2017. "A Comparative Study to Evaluate the Efficacy of EGF, FGF-2, and 0.3% (w/v) Ofloxacin Drops on Eardrum Regeneration." *Medicine* 96 (30). <https://doi.org/10.1097/MD.00000000000007654>.

Ning, Wenxiu, Andrew Muroyama, Hua Li, and Terry Lechler. 2021. "Differentiated Daughter Cells Regulate Stem Cell Proliferation and Fate through Intra-Tissue Tension." *Cell Stem Cell* 28 (3): 436-452.e5. <https://doi.org/10.1016/J.STEM.2020.11.002>.

Rahman, Anisur, Petri Olivius, Joris Dirckx, Magnus Von Unge, and Malou Hultcrantz. 2008. "Stem Cells and Enhanced Healing of Chronic Tympanic Membrane Perforation." *Acta Oto-Laryngologica* 128 (4): 352–59. <https://doi.org/10.1080/00016480701762508>.

Weber, David E., Maroun T. Semaan, Jay K. Wasman, Richard Beane, Lawrence J. Bonassar, and Cliff A. Megerian. 2006. "Tissue-Engineered Calcium Alginate Patches in the Repair of Chronic Chinchilla Tympanic Membrane Perforations." *The Laryngoscope* 116 (5): 700–704. <https://doi.org/10.1097/01.MLG.0000208549.44462.FA>.

Chapter 5:
Future Directions

5.1 Overall Conclusion of this Thesis and Next Steps

This thesis work was undertaken on the tail end of conclusions being drawn from the previous tympanic membrane-focused project in the lab, in which I participated in the finishing up of. This project undertook the gargantuan task of thoroughly characterizing the biology of the tympanic membrane at **homeostasis**. This study used single-cell RNA sequencing (scRNA-seq) to identify the populations at homeostasis with biological validation. It proved that it is predominantly the keratinocytes that are proliferating in the TM, and the entire epidermal layer turns over in approximately three weeks. It identified a stem cell population for the tympanic membrane located primarily at the pars flaccida/pars tensa junction with the committed progenitor cells being concentrated over the malleus. Lastly, this work identified *Pdgfra* as a candidate for promoting cell turnover. During the course of this project, a good amount of work went into optimizing strategies to study the tympanic membrane, including developing dissection methods, creating an explant culture system, live-cell imaging of TMs, staining via IF and ISH, and a method for dissociating cells for single-cell RNA sequencing.

With these interesting discoveries and these tools in our arsenal, we were able to ask and answer a variety of questions about the tympanic membrane no longer under homeostasis, but now under the state of injury when I began this project. Overall, what began as a simple question of how the tympanic membrane heals wounds morphed into a much more complex story defining the tympanic membrane as potentially the most regenerative organ in the adult mammal. This thesis served to prove that the TM can indeed regenerate and

that the tympanic membrane displays the key tenets of epimorphic regeneration in this process, which are (1) rapid development of a wound epidermis, (2) blastema formation, (3) activation of major developmental signaling pathways (in this case, EGFR), and (4) scar-free repair.

The first conclusion made from this work was that the tympanic membrane displays a rapid and robust proliferative response to injury, far faster than we would have anticipated for an epithelial tissue. This was quantified and validated using a variety of techniques. We showed in both whole-mount and cross-sectional views that the TM displays a rapid covering of the wound with thickened tissue that rapidly remodels down to its original shape by two weeks. We were able to quantify this gross response using an EdU pulse 2 hours prior to sacrifice on a time-course of injuries, which revealed that the TM shows a statistically significant increase in proliferation as early as 18 hours. Macroscopically, we could conclude that the TM had repaired the wound site by 2 weeks from both whole-mount and cross-sectional views, but we wanted to further characterize this response at the microscopic level.

We investigated the wound sites of the TM at the microscopic level by staining for Collagen II, the primary collagen of the tympanic membrane at homeostasis. We found that by 2-months post-injury, the collagen fibers had almost perfectly restored the radial and circular collagen matrix unique to the TM, and that by 1 year out, a wounded versus unwounded tympanic membrane were indistinguishable in their collagen patterning. Thus, the tympanic membrane displays scar-free repair, a key principle of epimorphic regeneration.

We then used single-cell RNA sequencing to understand the transcriptional shifts of all three layers of the tympanic membrane throughout the regeneration time course, similarly to how we had characterized the homeostatic TM. This experiment was informative for a number of reasons but notably because it allowed us to define a wounded epidermis that emerges in response to injury of the TM by 24 hours. This wounded epidermis exists through day 3 and disappears at the day 7 and day 14 timepoints. This wounded epidermis was validated using two markers among the highest differentially expressed markers, *GPR15L* and *Areg*. Since *Areg* is also a ligand of EGFR, this led to us investigating EGFR signaling in the repair of the TM. What we found was that pEGFR was greatly increased by day 3 in response to injury, and when we deleted EGFR in *K5-CreERT2;Egfr^{fl/fl};R26^{mTmG/mTmG}* mice, the tympanic membranes were no longer able to close the holes, and the rapid, robust proliferative response we had previously observed was completely abrogated. Thus, we showed that EGFR is required for wound closure of the TM.

The data indicated to us that all layers of the TM display markers of proliferation at some point during regeneration (i.e. *Ki67*, *Top2a*); thus, the TM displays level-specific replacement of the organ, a tenet of epimorphic regeneration (Seifert and Muneoka 2018). The single-cell data also allowed us to define time-dependent shifts in the layers of the TM, with the keratinocytes showing early changes (day 1), and the immune, mesenchymal, and mucosal populations showing a more delayed effect post-injury (day 3 or after). The single-cell data indicated to us that the cells had not completely restored their transcriptional state by day 14, the final time point we collected for sequencing, though TMs appear

grossly resolved at this time. Therefore, at what timepoint the TM fully restores is still necessary to explore. A future single-cell RNA sequencing experiment that looks at later timepoints post-injury of the tympanic membrane, such as 2 months and 6 months out, will be extremely important in defining the fully regenerated transcriptional state of the tympanic membrane and to understanding if the transcriptional state of the TM and the cell populations present at these later time points do fully recapitulate the unwounded TM and maintain the same ratios of cell populations. Once this experiment is conducted, we can then use packages like scVelo to draw trajectories of cells from the unwounded state to the fully regenerated state to prove restoration.

From the validation of the single-cell data that included staining for pEGFR signaling, we saw that it appeared that the wounded epidermis was leading to the activation of cells in a large mass of tissue that developed by day 3 on the regenerating tympanic membrane. This, along with the single-cell data indicating layer-specific turnover, led us to ask the question if this mass of tissue could be a blastema, defined as a multi-lineage tissue responsible for giving rise to the new organ. We validated that the mass was indeed a multi-lineage tissue and used a *Krt5-CreERT2;R26R-Confetti* mouse model to track individual clones showing the migration and growth of these cells throughout regeneration with serial imaging. However, this was only shown in isolated timepoints, not continuously over time, so it is high priority for us to be able to develop a system to watch the transformation of the blastemal tissue throughout regeneration to visualize how the tissue reorganizes to the original structure of an unwounded tympanic membrane. One hypothesis is that the majority of this tissue is lost due to apoptosis and that the natural homeostatic

proliferation of cells fills the wound space. Another hypothesis could be that this tissue loses some of its structure due to apoptosis, but also that the mass remodels and cells migrate into the wound space to restore the original architecture. Live-cell imaging as well as staining for markers of apoptosis, like cleaved Caspase-3, will allow for more definitive answers to these questions. In general, the rate of apoptosis on the TM even at homeostasis has not been studied, so studies focused on defining the homeostatic apoptotic rate and post-injury will be extremely informative.

Lastly, this work provided conclusive evidence that topical stimulation to the tympanic membrane results in a robust proliferative response not dissimilar to the initial rapid proliferative response seen after injury. However, through further characterization of the effects of topical stimulation, we found that the proliferating populations do not seem to retain all of the same markers as the wounded epithelial population in TM injury, so we believe that these processes might have similar inductions but deviate in downstream signaling. Further studies should investigate what major signaling pathways are activated in this response via single-cell RNA sequencing and staining. If we can pinpoint pathways critical for this response, it could help inform ways to keep holes patent in the tympanic membrane, which is often necessary for many surgeries accessing the inner ear. Currently, ENT surgeons encounter great difficulty in trying to keep the TM open when necessary, and it could be due to this proliferative response that is initiated when anything makes contact with the surface of the membrane. The knowledge of this response will help in the development of many future therapies for the inner and middle ear because we can be

cognizant that this effect can happen with any treatments coming in to contact with the TM surface.

5.2 Manipulating Regenerative Mechanisms of the Tympanic Membrane for Therapeutic Development

For a long time now, there has been interest amongst the Otolaryngology community in developing a targeted molecular therapy for tympanic membrane perforation repair. Many clinical trials have tried and failed to harness the mechanisms of repair of the tympanic membrane in a treatment, via manipulation of pathways like FGF, PDGF and KGF (Ma, Zhao, and Zhou 2002). However, these studies lacked a high-level understanding of the actual mechanisms they were trying to manipulate. Without true understanding of what pathways the tympanic membrane *needs* to utilize for regeneration, not just what is sufficient, it is difficult to create a targeted therapy. Some transcriptional profiling attempts had been made (Santa Maria et al. 2011; Hassmann-Poznańska et al. 2013), but these studies did not provide functional validation or staining of tissues like our study did in highlighting the requirement of EGFR signaling for tympanic membrane repair.

Thus, with our ability to display the necessity of EGFR signaling to tympanic membrane repair, we can now test much more targeted strategies for molecular treatments of TM perforation. In particular, future studies should center on showing if EGFR signaling that is specifically dependent on Areg is required for TM perforations to close because this could create an avenue for a highly targeted therapy that mimics the structure and function of

Areg to be administered endoscopically to the perforation and have effects very specific to regeneration of the tympanic membrane. The power to induce scar-free repair in a tympanic membrane would be a huge advance for the field of regenerative medicine.

We already showed with our work that perforation closure is EGFR-dependent, but EGFR signaling has widespread downstream effects and multiple upstream inputs, so a more specific approach would likely have a better result with minimal off-target effects. We can explore this necessity of Areg with the development of mouse models with *Areg* conditionally knocked out of the mouse genome, similar to what we developed for *Egfr*. This can be accomplished using a novel technique called i-GONAD. I-GONAD is a novel CRISPR *in vivo* system, in which the acronym stands for improved-Genome editing via Oviductal Nucleic Acids Delivery (Ohtsuka et al. 2018). This method allows the development of a mouse with a knock-out of a gene after one generation of mating by editing out the gene at the single-cell level of an embryo immediately after fertilization. Thus, we could introduce CRISPR guides to a newly impregnated wildtype female and potentially get a pup that is a heterozygote or homozygote knockout for *Areg*. Though there is a chance none of the pups will have the knockout, when done in multiple pregnant females, the odds are high you can generate a mouse with your genotype of choice.

The mode of delivery for a treatment for tympanic membrane perforation will also be important to optimize going forward. Given our results that simple contact of numerous inert solutions or solids with the TM result in aberrant proliferation, we will have to test different forms of delivery. Making a soluble EGFR agonist or Areg-mimicking molecule

that could be delivered in a droplet manner down the ear canal is one approach. Another approach could involve endoscopically placing small pieces of gel foam soaked in the drug of choice on the rim of the injury. Which method would be the most effective and show actual clinical significance in closure times over placebo is uncertain, but if we can show the ability to potentially regenerate chronically perforated tympanic membranes with an EGFR-based therapy, this could hold powerful significance for the field of regenerative medicine on the whole. Moreover, it would allow for patients with this ailment to avoid having to undergo invasive surgery, relieving a burden on the patient and the healthcare system. Additionally, studies to see if the regenerative mechanisms that govern the tympanic membrane apply to other epithelial tissues could unlock powerful tools to treat chronic injuries throughout the body.

5.3 Single-Cell Resolution of Initiating Steps of Regeneration prior to 24 hours

We showed in our data that there is a statistically significant increase in proliferation as early as 18 hours after injury via EdU studies. However, in our scRNA-seq database we produced of the regenerating TM, the earliest time point that we queried was 24 hours post-injury. This 1-day timepoint revealed very interesting patterns, including a wounded keratinocyte population that only exists in the early regenerative state of the tympanic membrane. However, given that we know that proliferation increases even earlier than 1-day post-injury, it is important to study the transcriptional shifts at these shorter timepoints. In particular, identifying if there are certain triggers for proliferation that can be identified from the transcriptional profile at these shorter timepoints could be powerful

information for understanding the initiation of regeneration in epithelial tissues on the whole. Moreover, sequencing of these earlier timepoints could help define when the wounded epidermis of the tympanic membrane is first initiated. Lastly, the inflammation response post-injury should be triggered almost instantaneously, so these shorter time points could help us further elucidate the migration of inflammatory immune cells onto the tympanic membrane.

Thus, we plan to conduct a scRNA-seq experiment that captures the TM 6, 12 and 18 hours after injury in order to: (1) define the timepoint at which the wounded epidermis first appears, (2) identify new activators of proliferation sub-24 hours after injury, and (3) characterize the earliest inflammation response to injury on the tympanic membrane. The original experiments we conducted looking at regeneration over the course of two weeks were critical to our general understanding and characterization of tympanic membrane regeneration on the whole, but now we are curious to understand the details of the very earliest response to injury within the tympanic membrane, and we believe that what we learn here can help define principles for crucial steps necessary in determining if an epithelial organ will generate or simply undergo wound healing. Moreover, a deeper understanding of the initial molecular sensing in the wound response can help us to understand what triggers might be absent in the case of chronic perforations of the TM. It is unclear currently if chronic tympanic membrane perforations are able to undergo the first steps of regeneration and then get stalled later on in the proliferation stages or if the process is halted prior to initiation of proliferation altogether. Before this thesis work, there was close to no understanding of what biological decisions create the separation

between a fully regenerative and chronically injured TM, but these future experiments coupled with our newly documented discoveries will greatly elucidate this fork in the road.

5.4 Single-Cell Resolution and Validation of Fully Regenerated Tympanic Membranes

As mentioned earlier, we learned from our initial single-cell RNA sequencing experiment that though the TM looks grossly resolved at two weeks post-injury, it is actually not fully resolved from a microscopic point of view. The transcriptional profiles of the cells have begun to more closely resemble the unwounded state but are not entirely restored yet. Therefore, there is a need to sequence time-points that are further out than 2 weeks, such as 2 months and 6 months post-perforation. At these time points, we can see via Collagen II staining that the microstructure of the tympanic membrane appears more or less identical to the unwounded state; therefore, it will be interesting to see if at these later time points, the transcriptional profiles of the cells have also fully restored to the unwounded profile. Therefore, we will perform scRNA-seq on unwounded, 2-month and 6-month post-injury wildtype tympanic membranes. We will run scVelo on the data generated in order to create trajectories through the cells to see if the trajectories map from the unwounded state through the intermediate timepoints and then 2 and 6 months to see if the trajectories lead directly back to the unwounded state. Moreover, using UMAP representations of the cells, we will be able to determine if the 2-month and 6-month cells are overlapping in transcriptional space with the unwounded cells.

Defining a timepoint in which the unwounded and regenerated tympanic membrane are microscopically identical is crucial to fully defining the TM repair process as epimorphic regeneration. Moreover, it is often asked how the actual fibers of the regenerated tympanic membrane compare to the unwounded state, so an important future direction of characterizing a regenerated TM is to develop a system to measure the tensile strength of the tissue. When scarring occurs, there is usually a deposition of fibrous tissue that leads to an overall stiffer and more disorganized tissue. However, based on our Collagen II validation experiments, this is not the case in the tympanic membrane; instead, the TM restores to a structure that recapitulates the original collagen fiber meshwork. However, we need to create a protocol that is able to measure the stress load of the tympanic membrane both pre- and post-injury in order to compare the tensile strength of these tissues since currently, there is no commonly used way to do this. Some protocols that exist in the field of tension and stress measurements of other organs are atomic force microscopy (AFM) and scanning electron microscopy (SEM) (Lee et al. 2017). We have conducted some pilot experiments with SEM to assess the rigidity of the TM two months after injury (**Figure 5.1**), but currently, we are running into issues with the protocol due to an inability to have the tympanic membrane lie flat since the TM naturally has a curvature to it. Thus, it is hard to get clear readings from the tissue, particularly since it has a proclivity for folding in on itself as well. These are issues we hope to trouble-shoot in the near future. By being able to gather quantitative data about the tensile strength of the tissue both pre- and post-injury, we will be able to answer if the tympanic membrane definitively restores all structure and function when regenerating after perforation.

5.5 Live-Cell and Live-Animal Imaging of the healing murine Tympanic Membrane

Via the use of inducible fluorescent mouse models and minimal dosing of tamoxifen, we are able to visualize individual cell clones on the tympanic membrane. From this visualization, we have made educated hypotheses about the trajectories of cells based on isolating numerous timepoints post-injury with a high number of samples per timepoint and observing the patterns of the areas with the majority of fluorescent clones at each time point. In our studies, we used a *Krt5-CreERT2;R26R-Confetti* mouse model to track individual clones after perforation and used this data to define a migratory wounded epidermis present in early tympanic membrane regeneration. However, we want to be able to visualize these clones actually migrating in order to definitively state how these cells arrive at the wound site outside of our conjectures. Thus, we are working on optimizing the live-imaging of fluorescent TMs *in situ*.

In our most recent experiments developing a method for this, we have been able to visualize the homeostatic movement of keratinocytes on an unwounded tympanic membrane floating in media immediately after being dissected from a mouse (**Figure 5.2**). We can watch in real-time as the cells move downwards and outwards from the malleus and from the pars tensa/pars flaccida junction, using a *K5-CreERT2;R26^{mTmG/mTmG}* mouse injected with a minimal dose of tamoxifen to be able to track individual GFP-expressing cells. Now, future directions for this project focus on optimizing this protocol for visualizing live cells in a wounded tympanic membrane. However, we ran pilot experiments to grossly visualize the process of TM regeneration *ex vivo* and found that the mechanical

process did not seem to exactly replicate what we were observing *in vivo*. Rather, it appeared that the TM was able to cover the wound with a new epithelial layer, but it was not actually regenerating and repairing the wound site with all three layers of tissue. Thus, there are two approaches we are working on moving forward. We have been testing different medias with different proportions of serum and supplements for floating the tympanic membrane in after being dissected out of the mouse that may help recapitulate the environment necessary for the TM to undergo regeneration. Along with that, we have piloted making the perforation both immediately before sacrificing the mouse and one day before sacrificing the mouse to see if we can pinpoint an optimal time post-injury to observe cell migration, and these studies are ongoing. Utilizing our single-cell RNA sequencing data and the necessity of EGFR signaling may help us optimize the media conditions to trigger the regenerative mechanism instead of simple re-epithelization as well.

The other approach that could help us capture the entire regenerative process of the tympanic membrane in real-time would be to conduct live-animal imaging. Technically, the TM visualization is accessible without incision via direct visualization down the external auditory ear canal. However, some clear issues arise with this type of imaging. First off, visualization of the entire tissue would be required to characterize this phenomenon, so any objective over 10x magnification makes it difficult to do this. If we use a higher objective, it becomes nearly impossible to orient oneself to the area being imaged, so the data becomes hard to interpret, but a higher magnification gives us better resolution of the cells themselves. Another issue that arises is that the EAC must be held open by forceps or a

speculum normally to be able to visualize the TM. To do this in the context of a microscope visualizing down the ear canal, a significant amount of tissue around the TM has to be removed, which does not allow for the mouse to stay alive for the long time-course of days to weeks necessary to be able to observe full regeneration. Lastly, if the mouse is kept alive, the breathing of the mouse moves the plane of focus of the microscope and obscures the images we can take. Overall, these challenges will all have to be addressed in order to accurately capture TM regeneration in a live mouse. There have been microscopic cameras developed now that can attach onto a live mouse, so the mouse can be followed over time and kept in its normal habitat. This could solve many of the above problems, but the issues around getting a clear visualization down the ear canal without performing surgery on the mouse is still something we will have to work on optimizing.

Figure 5.1

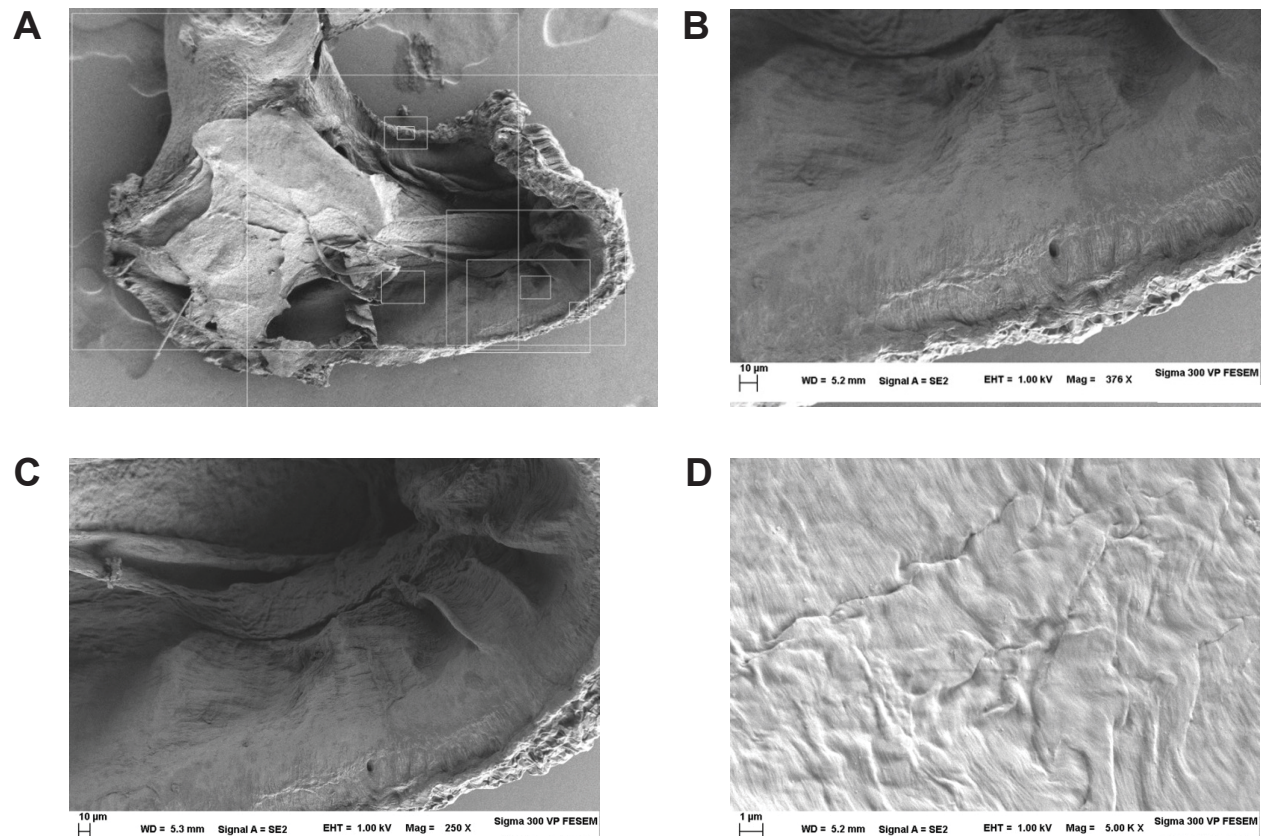


Figure 5.1: Scanning Electron Microscopy struggles to elucidate the structure of the tympanic membrane. (A) Image of whole-mount tympanic membrane taken using scanning electron microscopy. (B-D) Zoomed in images of (B-C) sites near the annulus and in the (D) center of the pars tensa, resolving some of the collagen fiber patterning of the tympanic membrane.

Figure 5.2

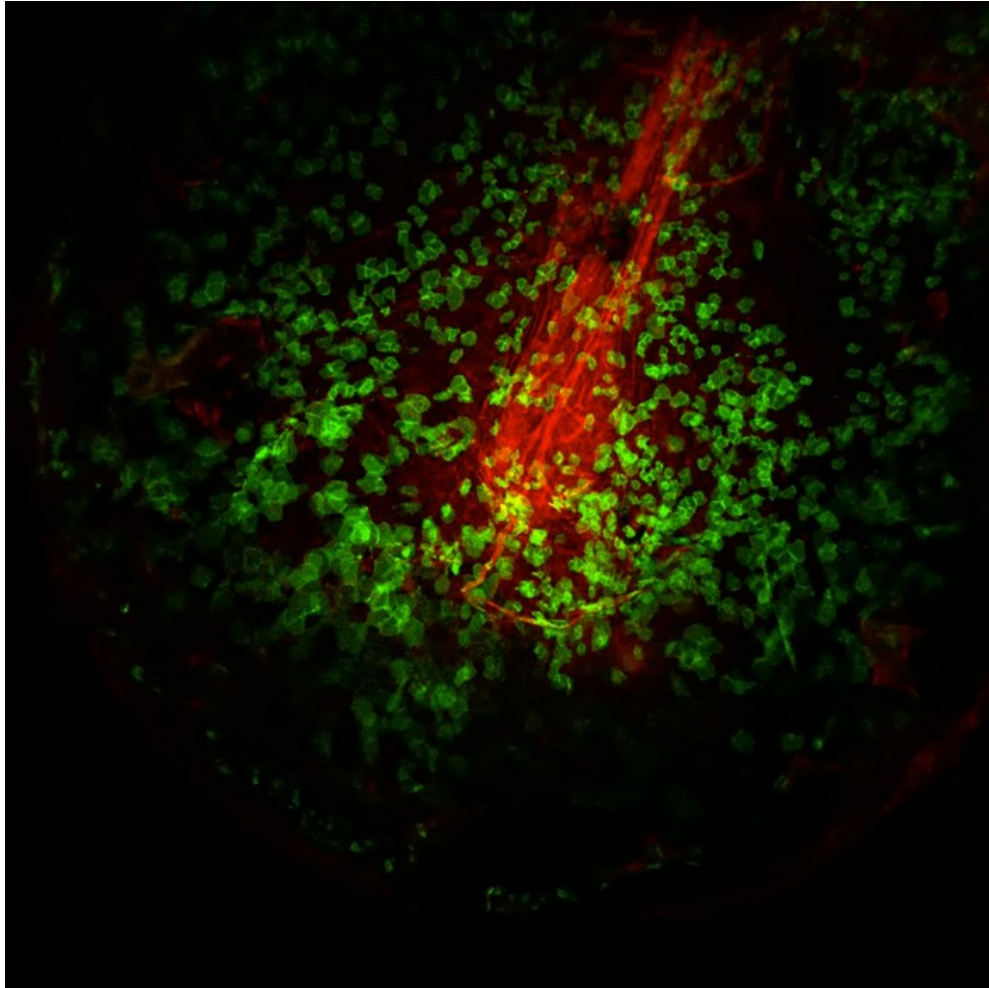


Figure 5.2: Live-cell imaging of the tympanic membrane at homeostasis. TM from a K5-CreERT2;*R26^{mTmG/mTmG}* mouse injected with minimum dose of tamoxifen that was imaged for 24 hours continuously. The GFP expressing cells that are migrating in the superior-to-inferior pattern are keratinocytes.

5.7 References

- AW, Seifert, and Muneoka K. 2018. "The Blastema and Epimorphic Regeneration in Mammals." *Developmental Biology* 433 (2): 190–99.
<https://doi.org/10.1016/J.YDBIO.2017.08.007>.
- Hassmann-Poznańska, Elzbieta, Andrzej Taranta, Izabela Bialuk, Maria Poznańska, Hanna Zajackiewicz, and Maria Małgorzata Winnicka. 2013. "Analysis of Gene Expression Profiles in Tympanic Membrane Following Perforation Using PCR Array in Rats-- Preliminary Investigation." *International Journal of Pediatric Otorhinolaryngology* 77 (10): 1753–59. <https://doi.org/10.1016/J.IJPORL.2013.08.009>.
- Lee, Hansol D., Armando D. Estillore, Holly S. Morris, Kamal K. Ray, Aldair Alejandro, Vicki H. Grassian, and Alexei V. Tivanski. 2017. "Direct Surface Tension Measurements of Individual Sub-Micrometer Particles Using Atomic Force Microscopy." *Journal of Physical Chemistry A* 121 (43): 8296–8305.
https://doi.org/10.1021/ACS.JPCA.7B04041/SUPPL_FILE/JP7B04041_SI_001.PDF.
- Ma, Yuanxui, Hui Zhao, and Xiangning Zhou. 2002. "Topical Treatment with Growth Factors for Tympanic Membrane Perforations: Progress towards Clinical Application." *Acta Oto-Laryngologica* 122 (6): 586–99. <https://doi.org/10.1080/000164802320396259>.
- Ohtsuka, Masato, Masahiro Sato, Hiromi Miura, Shuji Takabayashi, Makoto Matsuyama,

Takayuki Koyano, Naomi Arifin, Shingo Nakamura, Kenta Wada, and Channabasavaiah B. Gurumurthy. 2018. "I-GONAD: A Robust Method for in Situ Germline Genome Engineering Using CRISPR Nucleases." *Genome Biology* 19 (1): 1–15.
<https://doi.org/10.1186/S13059-018-1400-X/TABLES/1>.

Santa Maria, Peter L., Sharon L. Redmond, Russell L. McInnes, Marcus D. Atlas, and Reza Ghassemifar. 2011. "Tympanic Membrane Wound Healing in Rats Assessed by Transcriptome Profiling." *The Laryngoscope* 121 (10): 2199–2213.
<https://doi.org/10.1002/LARY.22150>.

Publishing Agreement

It is the policy of the University to encourage open access and broad distribution of all theses, dissertations, and manuscripts. The Graduate Division will facilitate the distribution of UCSF theses, dissertations, and manuscripts to the UCSF Library for open access and distribution. UCSF will make such theses, dissertations, and manuscripts accessible to the public and will take reasonable steps to preserve these works in perpetuity.

I hereby grant the non-exclusive, perpetual right to The Regents of the University of California to reproduce, publicly display, distribute, preserve, and publish copies of my thesis, dissertation, or manuscript in any form or media, now existing or later derived, including access online for teaching, research, and public service purposes.

DocuSigned by:

3359035DD86491... Author Signature

3/2/2022

Date

Sent: 3/2/2022 7:50:38 AM
Viewed: 3/2/2022 7:56:10 AM
Signed: 3/2/2022 7:56:52 AM